Università degli Studi di Parma

Dipartimento di Ingegneria Civile, dell'Ambiente, del Territorio e Architettura

Dottorato di Ricerca in Ingegneria Civile – XXVII Ciclo
Curriculum: Infrastrutture (ICAR/04)

Alice Bonati

Characterization and modelling of the fire behaviour of asphalt mixtures for applications in highway tunnels

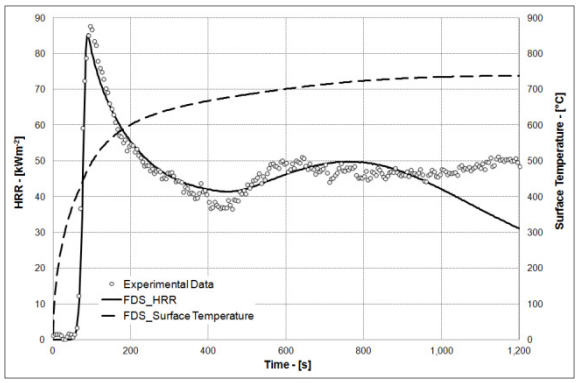

Tutore: Chiar.mo Prof. Felice Giuliani

Coordinatore del Dottorato: Chiar.mo Prof. Gianfranco Forlani

Parma, Gennaio 2015

Università degli Studi di Parma

Dipartimento di Ingegneria Civile, dell'Ambiente, del Territorio e Architettura

Dottorato di Ricerca in Ingegneria Civile – XXVII Ciclo
Curriculum: Infrastrutture (ICAR/04)

Alice Bonati

Characterization and modelling of the fire behaviour of asphalt mixtures for applications in highway tunnels

Tutore: Chiar.mo Prof. Felice Giuliani
Coordinatore del Dottorato: Chiar.mo Prof. Gianfranco Forlani

Parma, Gennaio 2015

Abstract

The importance of defining adequate instruments for improving safety in tunnels has become a pressing necessity since the last few decades. Indeed, several fire incidents happened in highway tunnels all over the world, thus calling into question the effectiveness of the existing safety measurements.

Among the different factors governing the fire safety, an important role is played by a focused selection of the construction products. Indeed, the second basic requirement defined by the European Regulation n. 305/2011 (Construction Products Regulation) is “Safety in case of fire”, which means that:

- the load-bearing capacity of the construction can be assumed for a specific period of time;
- the generation and spread of fire and smoke within the construction works are limited;
- the spread of fire to neighbouring construction works is limited;
- occupants can leave the construction works or be rescued by other means;
- the safety of rescue teams is taken into consideration.

Actually, these concepts were already stated in the Directive 89/106/EEC, and were therefore considered in the European Union Directive 2004/54/EC regarding the minimum safety requirements for tunnels.

In this context, a thorough analysis of the fire behaviour of materials became essential to provide important tools for the design of fire safety in highway tunnels. In fact, the spread of Computational Fluid Dynamics (CFD) codes in the field of the Fire Safety Engineering required the definition of material properties as an input, thus raising the necessity of a proper thermal characterization and description of the fire behaviour.

This work focuses on the characterization of the fire behaviour of asphalt mixture, starting from the analysis of each single component, i.e. asphalt binder, mineral filler, and mineral aggregates. Research methods include:

- literature review and surveys to identify the most common approaches employed for the combustion characterization of materials;
- experimental characterization of the materials by means of thermo-gravimetric analysis, Limiting Oxygen Index (LOI) test and cone calorimeter test;
- modelling the fire behaviour of asphalt concrete by means of a Computational Fluid Dynamics tool: the NIST Fire Dynamics Simulator (FDS). The numerical simulation is initially performed in order to reproduce the cone calorimeter test, thus allowing for the validation of the results derived from the theoretical interpretation of the experimental phase. The later and final stage is dedicated to the implementation of the obtained results in a real-scale application, i.e. in the numerical simulation of a 20 MW fire size, natural ventilation configuration, in the Memorial Tunnel (USA).

The experimental phase outlined the basic material properties that can be used for ranking in terms of susceptibility to ignition. In this perspective, for each component of the asphalt mixture, the main properties were outlined, providing important tools for performance-based mix-design criteria. It is worth noting that the analysis were mainly focused on the ignition process, since the safe egress of the tunnel occupants in case of fire was considered of prevailing importance.

The results highlighted the actual chance of igniting asphalt mixture pavement, but this fact occurs only in case of particularly critical conditions of heat exposure. Moreover, even if the ignition occurs, the contribution of conventional dense-graded asphalt mixture can be considered of relatively small importance if compared to the other fire sources. This basic behaviour can be further improved by a proper selection of the components, i.e. flame retardant fillers and high density aggregates.

The numerical simulation of a real scale tunnel fire highlights that one of the main hazards for tunnel occupants is the smoke spread, which can impede the egress in a few minutes, thus making the ignition of asphalt pavement of secondary importance in this perspective. Furthermore, the limited involvement of asphalt pavement in fire can be considered a further advantage when compared to the thermal degradation undergone by cement concrete pavement due to severe spalling phenomena.

The work of thesis illustrated a possible approach for characterizing the combustion behaviour of asphalt mixture, outlining the most important factors governing such phenomenon. It is worth noting that only this specific aspect was addressed, thus future research should be directed to the mechanical evaluation of specific flame retardant asphalt mixtures in order to achieve not only the adequate fire safety requirement, but also long-lasting quality and a more general durability.

Sommario

I numerosi incidenti verificatisi nei più importanti tunnel alpini negli ultimi decenni hanno evidenziato la necessità di rivisitare i requisiti di sicurezza adottati per i tunnel stradali, rendendo quindi una necessità non più prorogabile la definizione di adeguati strumenti finalizzati al miglioramento della sicurezza.

Tra i diversi fattori che definiscono la sicurezza in caso d'incendio, un ruolo fondamentale è rivestito da una oculata scelta dei materiali e prodotti da costruzione. Infatti, il secondo requisito di base definito dal Regolamento per i Prodotti da Costruzione (CPD n. 305/2011) è proprio la "Sicurezza in caso d'incendio". Tale requisito prescrive che le opere di costruzione debbono essere concepite e realizzate in modo che, in caso di incendio:

- la capacità portante dell'edificio possa essere garantita per un periodo di tempo determinato;
- la generazione e la propagazione del fuoco e del fumo al loro interno siano limitate;
- la propagazione del fuoco a opere di costruzione vicine sia limitata;
- gli occupanti possano abbandonare le opere di costruzione o essere soccorsi in altro modo;
- si tenga conto della sicurezza delle squadre di soccorso.

A onor del vero, tali concetti non sono una vera e propria novità, in quanto già espressi nella Direttiva Comunitaria n. 106 del 1989 e pertanto furono già inseriti e citati nella Direttiva Comunitaria n. 54 del 2004 riguardante i requisiti minimi di sicurezza per le gallerie.

In questo contesto, raggiungere un'approfondita analisi del comportamento al fuoco dei materiali da costruzione assume fondamentale importanza per poter fornire adeguati strumenti per la progettazione della sicurezza in galleria. Nello specifico, la sempre maggiore diffusione di softwares di fluido-dinamica computazionale (CFD) nel campo dell'ingegneria della sicurezza antincendio (Fire Safety Engineering) richiede sempre più dettagliate descrizioni dei materiali impiegati, con conseguente necessità di caratterizzazioni sperimentali sempre più articolate, soprattutto dal punto di vista di analisi termiche.

Il presente lavoro di tesi è dunque orientato principalmente alla caratterizzazione del comportamento al fuoco delle miscele di conglomerato bituminoso, affrontando l'analisi del contributo di ogni singolo componente: leganti bituminosi, filler e aggregati lapidei. Il metodo di ricerca adottato prevede:

- analisi della letteratura esistente e ricerca dei più comuni approcci adottati per la caratterizzazione della combustione dei materiali;
- caratterizzazione sperimentale dei singoli materiali costituenti nonché delle miscele di conglomerato bituminoso tramite analisi termogravimetriche, LOI test e prove mediante cono calorimetrico;
- modellazione dei risultati ottenuti nell'ambito delle prove con cono calorimetrico attraverso il software NIST Fire Dynamics Simulator. La simulazione dei test di prova ha consentito la validazione dei risultati ottenuti mediante rielaborazione teorica dei dati sperimentali.

Successivamente, tali risultati sono stati applicati per la simulazione di un test in vera grandezza realizzato presso il Memorial Tunnel di Boston (USA), in modo da riprodurre un incendio di dimensioni pari a 20 MW in regime di ventilazione naturale.

La fase sperimentale ha consentito di individuare le principali caratteristiche che possono essere impiegate ai fini di una classificazione in termini di infiammabilità. In quest'ottica, per ogni elemento costituente le miscele di conglomerato bituminoso è stato possibile definire le caratteristiche peculiari e ottimali da perseguire per migliorare il comportamento al fuoco della miscela nel suo complesso. Così facendo, è stato possibile definire importanti criteri per un mix-design prestazionale specificatamente orientato alla produzione di conglomerati bituminosi a migliorata reazione al fuoco. Si sottolinea che il lavoro di tesi è stato focalizzato principalmente sulla fase di ignizione del conglomerato, dal momento che si è ritenuto di prioritaria importanza garantire la sicura evacuazione degli occupanti dei mezzi coinvolti.

I risultati sperimentali e le successive modellazioni hanno evidenziato una effettiva possibilità di raggiungere l'ignizione da parte delle pavimentazioni bituminose. Tuttavia, questa condizione si raggiunge solo a seguito di condizioni di esposizione a flussi di calore particolarmente critici. Inoltre, anche in caso di effettiva ignizione della pavimentazione, la potenza termica rilasciata dalla combustione di un conglomerato bituminoso chiuso tradizionale risulta di piccola importanza se confrontata con le altre sorgenti di calore. Ovviamente, questo comportamento già di per sé non particolarmente negativo delle pavimentazioni bituminose può essere ulteriormente migliorato attraverso una scelta oculata dei materiali costituenti, quali filler ritardanti di fiamma e aggregati lapidei ad elevato peso specifico.

La simulazione numerica di un incendio in vera grandezza evidenzia inoltre che uno dei principali fattori di pericolo che incidono negativamente sulla sicurezza dell'evacuazione degli occupanti è rappresentata dalla rapida diffusione del fumo che si sprigiona a seguito della combustione dei materiali coinvolti. Conseguentemente, l'eventuale ignizione della pavimentazione bituminosa può essere riportata ad un secondo livello di importanza, quantomeno nei confronti della sicurezza durante la fase di evacuazione, mentre può assumere un ruolo più rilevante per la sicurezza degli operatori giunti in soccorso per le operazioni di spegnimento. Anche in questo caso, tuttavia, la limitata diffusione delle fiamme alle sole porzioni di pavimentazione immediatamente a ridosso delle sorgenti di calore esclude una facilitazione della diffusione delle fiamme ad altri veicoli, a meno di sversamenti di liquidi combustibili che difficilmente possono essere controllati. Infine, il limitato coinvolgimento della pavimentazione bituminosa rende le operazioni di ripristino sicuramente più agevoli e meno costose, soprattutto in confronto ai danni che si verrebbero a creare per i fenomeni di spalling in pavimentazioni realizzate in conglomerato cementizio.

Il presente lavoro di tesi ha illustrato un possibile approccio finalizzato alla caratterizzazione del comportamento al fuoco del conglomerato bituminoso,

evidenziando i principali fattori che governano tale fenomeno. È comunque bene notare che le soluzioni proposte e definite alla luce di un migliorato comportamento al fuoco devono essere sottoposte ad una mirata caratterizzazione meccanica, qui solo accennata in termini di caratteristiche reologiche dei mastici ritardanti di fiamma. In questo modo sarà possibile pervenire ad una soluzione tecnica che sia in grado di coniugare le esigenze di una migliorata sicurezza in caso d'incendio e le prestazioni meccaniche adeguate alle intense condizioni di traffico previste, oltre ad una generale richiesta di durabilità dell'opera.

List of publications

This thesis is based on the following publications by the author:

- Bonati A., Merusi F., Polacco G., Filippi S., Giuliani F. Ignitability and thermal stability of asphalt binders and mastics for flexible pavements in highway tunnels. *Construction and Building Materials* (2012), Vol. 37, pp. 660-668;
- Bonati A., Bochicchio G., Merusi F., Polacco G., Giuliani F. Fire Behaviour and Heat Release Properties of Asphalt Mixtures. *International Journal of Pavement Research and Technology,* (2013), Vol. 6(2), pp. 100-108*;*
- Bonati A., Merusi F., Bochicchio G., Tessadri B., Polacco G., Filippi S., Giuliani F. Effect of nanoclay and conventional flame retardants on asphalt mixture fire reaction. *Construction and Building Materials* (2013), Vol. 47, pp. 990-1000;
- Bonati A., Merusi F., Bochicchio G., Filippi S., Polacco G., Giuliani F. Experimental research on fire retardancy mechanisms in asphalt-clay nanocomposites. *Conference Proceedings EATA 2013, Braunschweigh 3-5 June 2013;*
- Bonati A., Rainieri S., Bochicchio G., Tessadri B., Giuliani F. Characterization of thermal properties and combustion behaviour of asphalt mixtures in the cone calorimeter. Fire Safety Journal (submitted);

Table of Contents

Nomenclature

Roman Letters

Variable	Description	Units
A	pre-exponential factor	1/s
Bi	Biot number	-
c_p	specific heat capacity	J/kg·K
C	pre-exponential factor (polynomial)	1/s
E	activation energy	J/mol
g	gravity	m/s^2
h_c	convective heat transfer coefficient	$W/m^2 \cdot K$
H	heat	J/g
k	thermal conductivity	W/m·K
L	thickness of the sample	m
m	mass	kg
$\dot{m}''$	mass flow rate per unit area	$kg/m^2 \cdot s$
$\dot{m}'''$	mass flow rate per unit volume	$kg/m^3 \cdot s$
Nu	Nusselt number	-
p	pressure	$kg/m \cdot s^2$
$\dot{q}''$	heat flux per unit area	W/m^2
t	time	s
T	temperature	K
v	velocity	m/s
V	volume	m^3
x	depth	m
Y	mass fraction	g/g

Greek symbols

Variable	Description	Units
α	thermal diffusivity	m/s^2
ε	emissivity	-
kρc	thermal inertia	$W^2 \cdot s/m^4 \cdot K^2$
σ	Stefan–Boltzmann constant	$W/m^2 \cdot K^4$
ρ	density	g/m^3

Main symbols and abbreviations

Variable	Description
CFD	Computational Fluid Dynamics
CHF	Critical Heat Flux
DSC	Differential Scanning Calorimetry
FR	Fire retardant
FDS	Fire Dynamics Simulator
HRR	Heat Release Rate
LOI	Limiting Oxygen Index
NC	Nanocomposite
TGA	Thermo-Gravimetric Analysis
THR	Total heat release
CH	char

1 Introduction

1.1 Road tunnel fire safety: background

In the last few decades the increasing need for faster and more efficient transport infrastructures led to a huge development in the construction of road tunnels. Design of such fundamental infrastructures should aim at the best balance among different design factors like: safety, sustainability, and cost-efficiency both in construction and maintenance.

According to French, German and Italian statistics [1] accidents seem to occur less frequently in road tunnels than in the open road with fatality risk generally lower per vehicle/km. However, some specific events are unique for tunnels, or can lead to much more severe consequences in a tunnel than for an open section. Thus, for tunnels it is of major importance to address events like explosions, release of toxic gases and other dangerous substances, and fires. In fact, during the past decade, a number of tunnel fires with several casualties occurred in Europe: Table 1.1 shows a brief description of the main accidents reporting the estimated energy content developed. A more detailed list of tunnel fire accidents can be found in [1].

Table 1.1 Summary of estimated energy content and peak HRR in tunnel fires involving Heavy Goods Vehicles (HGVs).

Accident	Vehicle Type	Estimated Heat content [GJ]	Estimated peak HRR [MW]	Conseq. for people	Conseq. for tunnel
Eurotunnel	10 HGV	2200	370	30 injured	Damage to ceiling
Mont Blanc	14 HGV 9 cars	5000-7000	380	39 deaths	Closed for 3 years
Tauern	16 HGV 24 cars	4000-4500	300-400	12 deaths	Closed for 3 months
St. Gotthard	13 HGV 10 cars	1400-2700	> 100	11 deaths	Closed for 2 months

Following these catastrophic events, the EU undertook actions to reduce the acceptable risk in tunnels of its rail and road networks. Hence, both prevention and protection strategies attracted serious attention, and two fundamental documents defining minimum safety requirements were published: European Union Directive 2004/54/EC on minimum safety requirements for tunnels in the trans-European road network, and the UN Economical Council Recommendations of the Group of Experts on Safety in Road Tunnels [2,3]. Nevertheless, only few requirements were specified for the construction products in terms of fire resistance, i.e. “the main structure of all tunnels where a local collapse of the structure could have catastrophic consequences, e.g. immersed tunnels or tunnels which can cause the collapse of important neighboring structures, shall ensure a sufficient level of fire resistance”. Also professional groups such as AIPCR (World Road Association) and ITA (International Tunneling Association) fostered the establishment of European thematic networks and research projects such as FIT, Safe-T, and UPTUN [5, 6, 7].

Among the several aspects governing the road tunnel fire safety, the possible contribution of the pavement material to a fire was not addressed to great extent in the past. Indeed, one of the essential requirements mentioned in the Construction Products Regulation [4] is “Safety in case of fire”. This means that the construction works must be designed and built in such a way that, in the event of an outbreak of fire, the construction complies with requirements regarding to the following considerations:

- the load-bearing capacity of the construction can be assumed for a specific period of time;
- the generation and spread of fire and smoke within the works are limited;
- the spread of the fire to neighbouring construction works is limited;
- occupants can leave the works or be rescued by other means;
- safety of rescue teams is taken into consideration.

It is clear that also pavement materials should meet these requirements, as road pavement represents a not negligible surface potentially exposed to fire. For this reason, several countries (Austria, Slovakia, Slovenia and Spain [8,9]) banned asphalt pavement from new motorway tunnels longer than 1000 m and imposed cement concrete pavement, being cement concrete not combustible. Nevertheless, cement concrete is affected by a severe temperature-susceptibility due to spalling phenomena which occur at relatively low temperatures (200 °C) [1].

In addition to the afore-mentioned requirements in terms of fire safety, road tunnels should also be designed in order to provide sufficient safety performance for the normal use conditions. More specifically, the requirements proper to road surface are still valid: skid resistance, safety in use and during accidents, visibility/colour/light reflection, noise reduction capacity, cost-efficiency and durability. In this perspective, thanks to the constant development of sustainable products by means of warm mix asphalt (WMA) technology, use of reclaimed

asphalt pavement (RAP), asphalt pavement represents in most cases a fundamental technical solution, also in road tunnels.

Preliminary research [10,11] on asphalt pavement fire reaction highlighted a very complex fire behavior, significantly dependent on the asphalt mixture composition (mainly asphalt binder and air voids contents) but did not excluded a priori the application of asphalt in road tunnel pavements.

1.2 Aim of the thesis

The present thesis is based on the abovementioned considerations regarding the relationship between tunnel fire safety and asphalt pavements. In fact, due to the presence of asphalt binder, which is obtained from the crude oil, asphalt mixture is a combustible material. Recent catastrophic events, real scale fire tests and CFD simulations outlined extremely high temperatures, far above the flashpoint of asphalt, thus making evident the possible involvement of asphalt in tunnel fires.

The aim of the thesis is the in-depth analysis of asphalt mixtures fire behaviour in order to provide basic guidelines for the mix design of asphalt pavement with proper fire-safety performance, especially in terms of fire reaction. This is achieved by first focusing on the principles of fire dynamics of compartment fires, paying special attention to the first phase of these events, i.e. the ignition. Indeed, great interest is focused on the prevention of asphalt combustion rather than on protection, being asphalt pavement the first way of escape for tunnel's occupants but also the only entry way for rescue teams.

To this aim, the contribution of every single component of asphalt mixture is investigated starting from the combustible portion, i.e. the asphalt binder. Several neat asphalt binders are considered in order to outline a possible correlation between asphalt ignitability and S.A.R.A. fractions. Moreover, nanocomposite (NC) asphalt binders are examined.

The role of mineral filler is then deepened focusing on the particle size, the chemical composition and the filler content in asphalt mastics. This phase of the research is basically based on the principles of fire retardancy technology initially developed for polymers. In this way, Flame-Retardant (FR) asphalt mastics could be produced, reaching sensibly higher thermal stability. Basic rheological analysis is also undertaken in order to verify potential drawbacks of such additives in the mechanical behaviour of mastics.

Fire behaviour of asphalt mixtures is then analysed by means of cone calorimeter tests. The importance of the aggregate distribution, bitumen content and aggregates' physical properties is investigated and the main fire behaviour parameters are outlined (e.g. time to ignition, HRR, THR). Due to the great number of variables, a thorough description of fire behaviour could be achieved only for one specific asphalt mixture, dense graded asphalt mixture, which is one of the most widespread in Italy.

Numerical simulation by means of the Fire Dynamics Simulator (FDS) is then performed in order to reproduce the observed fire behaviour of asphalt in the cone calorimeter test. Even if the combustion characteristics are largely scale-dependent, the numerical simulation outlines basic information useful for the analysis of asphalt pavement in more complex compartment fires, i.e. time to ignition (t_{ig}) and temperature of ignition (T_{ig}).

By comparing the ignition temperature (T_{ig}) with the results of large-scale fire tests performed in past years (e.g. Memorial Tunnel) it is possible to estimate the actual chance of ignition of the asphalt pavement and the flame spread over the surface.

1.3 The outline of the thesis

The present thesis consists of seven chapters where the fundamental aspects to be considered for the analysis of asphalt mixtures fire behaviour are developed.

Chapter 1 – Introduction - provides an overview of the phenomenon and the context in which this work of thesis is founded. The aim of the thesis is also described.

Chapter 2 - Theoretical Principles - aims at describing the basic principles of the combustion theory in order to identify the key-factors which should be addressed in this research work. Fundamental phases of compartment fires are briefly illustrated while an in-depth description of the ignition process in solids is subsequently presented. Thus, specific ignition parameters such as time to ignition, critical heat flux, and temperature of ignition were analytically derived from the literature analysis. The chapter develops with a review of the flame retardant additives mainly used in polymer technology, focusing on the mechanisms of action, benefits and disadvantages.

Chapter 3 – Materials and Methods – describes the materials used in this work of thesis (asphalt binders, mineral fillers, mineral aggregates) and summarizes the asphalt mixes analysed, both mastics and mixtures. Then, the testing methods are thoroughly illustrated.

Chapter 4 – Asphalt Binders and Mastics – reports the results collected by the thermal gravimetric analysis (TGA) and LOI tests performed with asphalt binders and mastics. A preliminary characterization of ignitability and thermal stability is achieved, outlining the most relevant factors for the fire safety performance. Rheological tests complete the asphalt mastics mechanical characterization.

Chapter 5 – Asphalt Mixtures – is entirely focused on the burning behaviour of mixtures by means of the cone calorimeter test. The role of mineral aggregates, particle size distribution and flame retardant fillers is highlighted. Fire behaviour of dense graded mixture is specifically addressed, outlining the most important parameters useful for the subsequent numerical analysis.

Chapter 6 – FDS Numerical Simulation – provides the results collected by the numerical simulation performed by means of the Fire Dynamics Simulator (FDS). In this phase, the burning behaviour of asphalt mixture in cone calorimeter configuration is reproduced by both setting the heat release rate measured in the cone calorimeter tests, and by predicting the heat release rate by modelling the asphalt pyrolysis process. The results obtained in this first step are then used as input data for the subsequent numerical simulation in which a tunnel fire scenario is reproduced. More specifically, the results collected in the Memorial Tunnel Fire Test Ventilation Program are considered, and a 20 MW fire size with natural ventilation is analysed. Being aware that this could be considered only one of the possible fire scenarios, the numerical simulation outlined a limited contribution of asphalt mixture to the overall tunnel fire.

Chapter 7 – Conclusions and Future Research – contains the conclusions of the present work of thesis. This chapter briefly summarizes the most relevant factors governing the fire behaviour of asphalt mixtures and suggestions about future research topics are provided.

References

[1] “Handbook of Tunnel Fire Safety” 2nd ed. Thomas Telford Publishing, London, UK, 2005.

[2] European Union, “Directive 2004/54/EC of the European Parliament and of the Council on minimum safety requirements for tunnels in the trans-European road network”, European Parliament and of the Council, 2004.

[3] UN Economical Council Recommendations of the Group of Experts on Safety in Road Tunnels, Trans. AC, 7/9, 2001.

[4] European Union, “Regulation (EU) No 305/2011 of the European Parliament and of the Council of 9 March 2011 laying down harmonized conditions for the marketing of construction products”, 2011.

[5] World Road Association (PIARC), “Fire and Smoke Control in Road Tunnels”, 1999.

[6] World Road Association (PIARC), “Systems and Equipment for Fire and Smoke Control in Road Tunnels”, 2006.

[7] FIT European Thematic Network, WP3, "Fire Safe Design, Road Tunnels, September 2003, Draft contribution to FIT WP3 report, version 2, issue 1, date 12.09.2003, by WP3 rapporteur Niels Peter Høj. (www.etnfit.net).

[8] Ministerio de Fomento: “Real Decreto 635/2006 de 26 de mayo sobre requisitos mínimos de seguridad en los túneles de carreteras del Estado”. Boletín Oficial del Estado, Madrid, 27 May 2006.

[9] RVS 9.234 “Tunnel/ Bauliche Gestaltung / Innenausbau“. Forschungsgemeinschaft Strasse und Verkehr (FSV), Vienna, 2001.

[10] Colwell, S. et al: “Test Methodologies for Reaction to Fire of Pavement Materials“. Document SAM-04-D20, SAMARIS (Sustainable and Advanced MAterials for Road InfraStructure) Research Project, 2005.

[11] Carvel, R.O. and Torero, J.L.: “The contribution of asphalt road surfaces to fire risk in tunnel fires: preliminary findings”. Proceedings Int. Conf. Risk and Fire Engineering for Tunnels, Stations and Linked Underground Spaces, 19-20 April 2006, Hong Kong. Organized by Tunnel Management International, Tenbury Wells, Worcs., United Kingdom.

2 Theoretical principles

2.1 A qualitative description of compartment fires

Fire is a physical and chemical phenomenon that is greatly interactive by nature. The interactions between the flame, its fuel, and the surroundings can be strongly nonlinear, and quantitative estimation of the processes involved is often complex. The processes of interest in compartment fires mainly involve mass fluxes and heat fluxes to and from the fuel and the surroundings. In order to introduce the most dominant of these processes, this section provides a general and qualitative description of the chemical and physical phenomena associated with fires. A thorough description of these processes can be found in literature [1,2,3]. Particular attention is then dedicated to the ignition process, being the main aim of this thesis the prevention of asphalt combustion.

2.1.1 General description of the combustion process

The study of combustion is a complex subject, being involved a number of disciplines such as: fluid mechanics, heat and mass transport, and chemical kinetics. In order to simplify such a complex phenomenon, the burning of a candle described by Drysdale [3] will be used as an illustration of these natural processes.

Figure 2.1 shows a burning candle and the temperature distribution through the flame. An ignition source, a match for example, heats up the wick and starts melting the solid wax. The wax in the wick vaporizes, and the gases move, by the process of diffusion, out into a region where oxygen is found. The gases are oxidized in a complex series of chemical reactions, in regions where the oxygen–fuel mixture is flammable [3]. The candle flame is then stable; it radiates energy to the solid wax, which melts. Since the wax vaporizes and is removed from the wick, the melted wax moves up the wick, vaporizes, burns, and the result is a steady combustion process.

The mechanisms occurring in the flame involve the flow of energy and the flow of mass. The flow of energy occurs by the processes of radiation, convection, and conduction. The dominant process is that of radiation; it is mainly the soot particles produced by combustion that glow and radiate heat in all

directions. The radiation down toward the solid is the main heat transfer mode, which melts the solid, but convection also plays a role. The convective heat flux is mainly upward, transferring heat up and away from the combustion zone. The larger and more luminous the flame, the quicker the melting process.

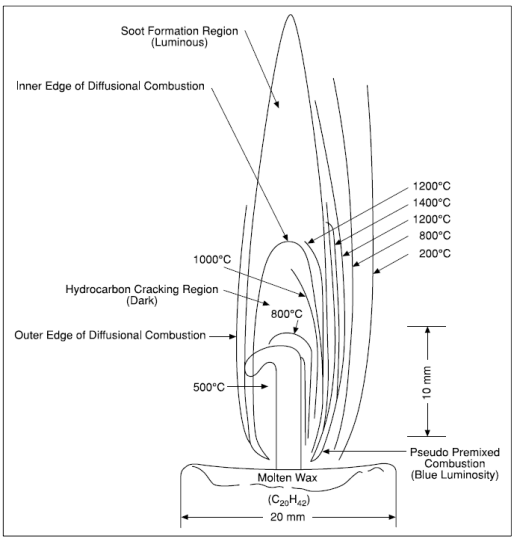

Figure 2.1 A burning candle and the temperature distribution in the flame [1].

The radiative energy reaching the solid is, however, not sufficient to vaporize the wax, only to melt it. The wick is therefore introduced as a way to transport the melted wax up into the hot gases, where the combined processes of radiation, convection, and conduction supply sufficient energy to vaporize the melted wax.

The mass transfer and the phase transformations are also exemplified by the burning candle. The fuel transforms from solid to liquid state. The mass balance requires that the mass that disappears from the wick by vaporization be replaced, and thus the liquid is drawn up into the wick by capillary action. Once there, the heat transfer from the flame causes it to vaporize, and the gases move away from the wick by the process of diffusion. The inner portion of the flame contains insufficient oxygen for full combustion, but some incomplete chemical reactions occur, producing soot and other products of incomplete combustion. These products move upward in the flame due to the convective flow and react there with oxygen. At the top of the flame nearly all the fuel has combusted to produce water and carbon dioxide; the efficiency of the combustion can be seen by observing the absence of smoke emanating from the top of the candle flame. This self-sustained combustion process can most easily be changed by altering the dimensions and properties of the wick, and thereby the shape and size of the flame. A longer and thicker wick will allow more molten wax to vaporize, resulting

in a larger flame and increased heat transfer to the solid. The mass and heat flows will quickly enter a balanced state, with steady burning as a result.

Without the wick, the candle will not sustain a flame, as is true for many other solid fuels. Factors such as the ignition source, the type of fuel, the amount and surface area of the fuel package determine whether the fuel can sustain a flame. A pile of wooden sticks may sustain a flame, while a thick log of wood may not do so. Once these factors are given, the processes of mass and energy transport will determine whether the combustion process will decelerate, remain steady, or accelerate.

Moreover, the phase transformations of other solid fuels may be much more complicated than the melting and vaporizing of the candle wax. The solid fuel may have to go through the process of decomposition before melting or vaporizing and this process may require considerable energy. The chemical structure of the fuel may therefore determine whether the burning is sustained. This is the case of asphalt mixture, which is a non-homogeneous material characterized by the presence of a combustible portion with an extremely complex and variable chemical structure.

The prediction of fire growth can be very difficult, due to the complexity of the physical and chemical processes involved, but also due to the dependence of these processes on the geometric and other abovementioned fuel factors and the great variability in these.

2.1.2 General description of compartment fire growth

Enclosures fires are often discussed in terms of the temperature development in the compartment and divided into different stages accordingly. Figure 2.2 shows an idealized variation of temperature with time, along with the growth stages, for the case where there is no attempt to control the fire. These stages are listed as follows [4]:

- ignition
- growth
- flashover
- fully developed fire
- decay

Figure 2.2 Simplified description of the temperature variation with time in an enclosure fire [1].

Ignition: Ignition can be considered as a process that produces an exothermic reaction characterized by an increase in temperature greatly above the ambient. It can occur either by piloted ignition (by flaming match, spark, or other pilot source) or by spontaneous ignition (through accumulation of heat in the fuel). The accompanying combustion process can be either flaming combustion or smoldering combustion.

Growth: Following ignition, the fire may grow at a slow or a fast rate, depending on the type of combustion, the type of fuel, interaction with the surroundings, and access to oxygen. The fire can be described in terms of the rate of energy released and the production of combustion gases. A smoldering fire can produce hazardous amounts of toxic gases while the energy release rate may be relatively low. The growth period of such a fire may be very long, and it may die out before subsequent stages are reached. The growth stage can also occur very rapidly, especially with flaming combustion, where the fuel is flammable enough to allow rapid flame spread over its surface, where heat flux from the first burning fuel package is sufficient to ignite adjacent fuel packages, and where sufficient oxygen and fuel are available for rapid fire growth. Fires with sufficient oxygen available for combustion are said to be fuel-controlled.

Flashover: Flashover is the transition from the growth period to the fully developed stage in fire development. The formal definition from the International Standards Organization [5] is given as “the rapid transition to a state of total surface involvement in a fire of combustible material within an enclosure.” In fire safety engineering, the word is used as the demarcation point between two stages of a compartment fire, i.e., pre-flashover and post-flashover. The given criteria usually demand that the temperature in the compartment has reached 500÷600°C, or that the radiation to the floor of the compartment is 15 to 20 kW/m^2, or that flames appear from the enclosure openings [1]. These occurrences may all be due to different mechanisms resulting from the fuel

properties, fuel orientation, fuel position, enclosure geometry, and conditions in the upper layer. Flashover cannot be said to be a mechanism, but rather a phenomenon associated with a thermal instability.

Fully developed fire: At this stage the energy released in the enclosure is at its greatest value and is very often limited by the availability of oxygen. This is called ventilation-controlled burning (as opposed to fuel-controlled burning), since the oxygen needed for the combustion is assumed to enter through the openings. In ventilation-controlled fires, unburnt gases can collect at the ceiling level, and as these gases leave through the openings they burn, causing flames to stick out through the openings. The average gas temperature in the enclosure during this stage is often very high, in the range of 700 to 1200°C.

Decay: As the fuel becomes consumed, the energy release rate diminishes. Therefore, the average gas temperature in the compartment declines. The fire may go from ventilation-controlled to fuel-controlled in this period.

2.1.3 Temperature curves

Building fire regulations commonly require that two main objectives be met: life safety of the occupants and structural stability of the building. Two distinctly different design procedures are applied in each case but both require a simplification in the description of fire phenomenon.

In the case of structural stability, the objective is to protect property and ensure that firefighters can gain entry to the building without the risk of a structural collapse. Here, the time frame is relatively long (often 30 to 180 minutes), the fire is assumed to have caused flashover, and the design fire is usually given as a temperature–time curve.

A standard curve used when testing the temperature exposure is the “cellulose curve” defined in several standards, e.g. ISO 834 [6]. This curve applies to materials found in typical buildings. This has been used for many years, also for tunnels, but it is clear that this curve does not represent all materials, e.g. petrol, chemicals, etc…, and therefore a special curve, the hydrocarbon curve (the HC curve, [7]), which was developed in the 1970s for use in the petrochemical and off-shore industries, has been applied to tunnels. The main difference between these two curves is that the HC curve exhibits a much faster fire development and consequently is associated with a faster temperature increase than the standard ISO 834 fire curve and has traditionally been seen to be more relevant for a petroleum fire.

Specific temperature curves have been developed in some countries to simulate hydrocarbon fires in tunnels. Examples of such curves are the RABT/ZTV Tunnel Curve in Germany [8] and the Rijkswaterstaat Tunnel Curve (RWS curve, [9,10]) in the Netherlands (based on laboratory scale tunnel tests performed by TNO in 1979). In France, a modified version of the hydrocarbon curve is used (HC_{mod}), which is the traditional HC curve increased by a factor 1300/1100. Figure 2.3 shows the five above-mentioned fire temperature curves

limited to the first two hours. It is worth noting that t = 0 s corresponds to the flashover.

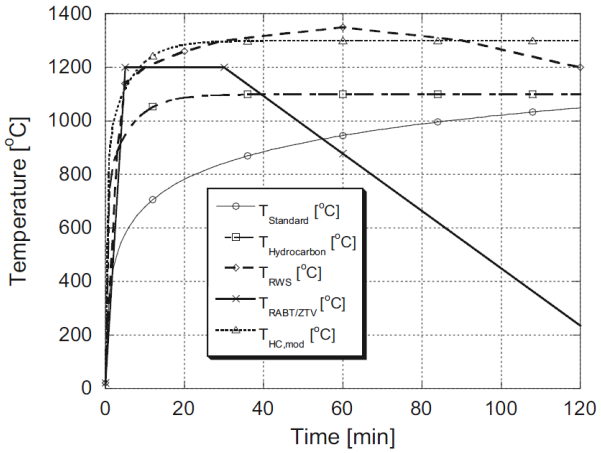

Figure 2.3 Fire temperature curves used for testing reaction of structures to heat exposure.

PIARC recommends the use of ISO 834 (60 min) for cars and vans and the RWS curve or the HC_{mod} curve (120 min) for trucks and tankers [11,12]. The recommendations are particularly for tunnels that are immersed, under/inside superstructures, or in instable ground. According to NFPA 502, the following maximum temperatures are assumed for different types of vehicle fires: Passenger car: 400 °C, Bus: 700°C, HGV: 1000°C, Tanker: 1200°C – 1400°C.

2.2 Ignition process of solids

When a solid material, initially at ambient temperature, is subject to an external source of energy, the temperature of the exposed surface starts to increase. This moment will be defined as the onset of the process leading to ignition (t=0 s). A series of physical and chemical processes are initiated as the energy reaches the surface of the material. Without loss of generality and for simplicity, the ignition process is described in a one-dimensional form with coordinate x. Moreover, this configuration is directly applicable to the pavement surface exposed to a vehicle fire.

Only one surface of the material is heated and the origin, x=0, is located at the exposed surface of the material. This frame of reference moves with a velocity v_r as the fuel is consumed and the surface regresses or expands.

V_r takes a positive value for regression and a negative one for expansion. For some materials, regression rates are very small and can be neglected, but this is not assumed at this stage. A schematic of a generic solid material undergoing heating is presented in Figure 2.4.

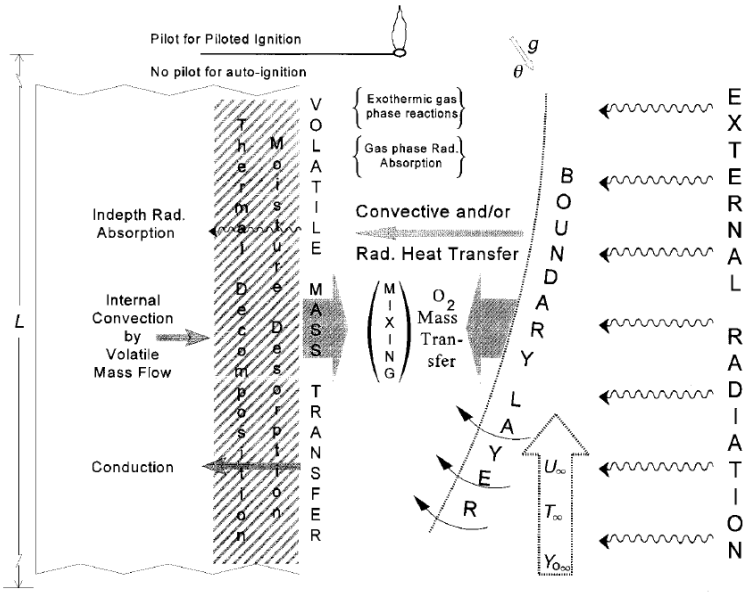

Figure 2.4 Schematic of the different chemical and physical processes occurring during ignition [10].

For simplicity, all processes involved are divided in two groups, those associated with the solid phase and those with the gas phase. The solid phase treatment will lead to a description of the production of gas phase fuel ($\dot{m}''$) and the gas phase analysis focuses on how the ensemble of gaseous fuel and oxidizer lead to a flame. The solid phase is described first, and then the boundary conditions between both phases are established. Finally, a description of the gas phase is given.

2.2.1 Solid phase

The temperature of the solid, initially at ambient (T_0), increases as the heat is transferred to the surface of the material. The highest temperatures are achieved close to the surface, but the in-depth energy transfer results in an increase in temperature of a significant part of the solid. Therefore, the temperature varies with depth and time. Thus, temperature needs to be represented as a function of both variables, T(x,t) [3].

The evolution of the temperature is defined by an energy balance in the control volumes between both surfaces of the solid (x=0 and x=L). The surfaces will define the heat transfer in/out of the solid fuel or mathematically, the boundary conditions. It is important to note, that if other dimensions were to be considered, similar boundary conditions would have to be established at each surface of the material.

2.2.1.1 Pyrolysis process

The process by which the solid transforms into gas phase fuel is called pyrolysis. This is the chemical degradation of a substance invoked by a heating process. Typical mechanisms of thermal decomposition of polymers, for example, are: random-chain scission, end-chain scission, chain-stripping and cross-linking [14]. Pyrolysis tends to be an endothermic process generally controlled by many chemical reactions (sometimes hundreds) which are highly dependent on temperature.

Often pyrolysis reaction rates are described by an Arrhenius type function. Svante August Arrhenius suggested in the late 1800s that the rates of many reactions vary with temperature in such a way that

$$k = A \cdot e^{-\frac{E}{RT}} \tag{2.1}$$

where k is the rate constant [3]. The Arrhenius equation is based on collision theory, which assumes that molecules must collide with both the correct orientation and with sufficient kinetic energy if the reactants are to be converted into products. The rate of a reaction is expressed in terms of a rate constant multiplied by a function of concentrations of reactants. The rate constant contains information related to the collision frequency, which determines the rate of a reaction.

When the rate constant is given by the Arrhenius equation (**2.1**) "E" is the activation energy [kJ/mol]. This is defined as the energy that must be overcome for a chemical reaction to occur. For molecules that undergo collision, the exponential is related to the number of molecular collisions that have the required energy to induce reaction. The pre-exponential factor "A" is the frequency factor or pre-exponential factor also given in inverse seconds [1/s], which is related to the frequency of collisions. "R" is the ideal gas constant with a value of 8.314 [J/mol·K] and "T" the temperature in Kelvin. The constants "E" and "A" are characteristic of each individual chemical reaction. If the natural logarithm of both sides of Equation (**2.1**) is taken, "$-\frac{E}{R}$" represents the slope and "ln A" the intercept of a linear relationship.

The process of pyrolysis can be extremely complex and, depending on the fuel and heating characteristics, can follow distinctively different paths. These paths can be a combination of numerous reactions that can be sequential or compete against each other. Furthermore, the chemical pathways can be strongly influenced by the presence (or absence) of oxygen, this is accounted for in equation (**2.2**).

$$\dot{\omega} = AY_0^m Y_s^n \cdot e^{-\frac{E}{RT}} \tag{2.2}$$

In this equation, $\dot{\omega}$ is the reaction rate which is generally defined in units of inverse seconds [1/s]. When this is multiplied by the fuel density, it gives a gasification rate per unit volume ($\dot{\omega}'''$ [kg/s·m^3]). In equation (**2.2**) Y_o and Y_S are generic representations of the oxygen and solid fuel mass fractions participating in the solid degradation and "m" and "n" are constants, otherwise it has the same

form as equation (**2.1**). It is important to note, that while degradation of some fuels will show dependency on the oxygen concentration, many others will not [14]. In those cases, "m" is assumed to be zero.

The chemical pathways leading to the pyrolysis of most solid fuels of interest in fire science are fundamentally incomplete as much as the constants associated to the equations that will serve to quantify the rate of each reaction step. Many studies have produced reduced chemical mechanisms for the pyrolysis of different solids [15,16]. Thermo-Gravimetric Analysis (TGA) has been used to establish reduced chemical reaction mechanisms, as well as the associated constants [17]. It is important to note that during the ignition process the presence of oxygen close to the surface will result in surface oxidation reactions. Once the flame is established, the region above the fuel is deprived of oxygen by the combustion reaction and all oxidative steps will cease to participate. Despite the generalized use of TGA data, there is increasing recognition that pyrolysis reaction pathways are sensitive to the heating rate. The basic nature of TGA studies requires heating rates of the order of 1 to 20 [ºC/min] which is generally an order of magnitude slower than the heating rates typical of fires. Therefore, the constants have to be validated for all the heating rates available, or preferably, obtained using multiple heating rates in that range to account for heating rate errors.

2.2.1.2 Gaseous fuel production

Before flaming ignition can occur, fuel needs to be produced in the gas phase. Solid materials that are not susceptible to spontaneous ignition will show very little evidence of chemical reactions at ambient temperatures, thus can be deemed as inert. The reaction rates associated with the pyrolysis can be considered negligible and therefore, the material will not undergo any transformation. As the temperature increases, the reaction rates increase and the solid fuel starts changing. Given the temperature distribution within the material, the rates of decomposition are function of "x," with larger production of pyrolysates close to the surface and lower production in-depth.

Local production of fuel is not the only important variable. The gas phase fuel produced might be the result of a combination of pyrolysis and oxidation reactions, thus its composition might include large quantities of fully oxidized compounds such as carbon dioxide (CO_2), partially oxidized gases such as carbon monoxide (CO) and other molecules that can have all levels of partial oxidation. Therefore, together with the reaction rates, the mass fraction of inert gases needs to be subtracted leaving the remaining reactive gases.

The mass fraction of flammable gases present in the local products of degradation can be described by means of a single variable, $Y_{F,S}(x,t)$, which represents a global contribution of all compounds that can be oxidized further. The fuel mass fraction can be obtained using TGA data in conjunction with an infrared spectrophotometer or mass spectrometer. Its results can be combined into a single parameter (mass fraction of flammable gases) that includes all compounds that are susceptible to further oxidation.

Oxygen and fuel concentrations in the solid will be controlled by the local permeability and by production/consumption rates thus, indirectly, by the temperature distribution (T(x,t)). To summarize, the production of fuel is controlled by the following parameters: temperature, local fuel concentration, local oxygen concentration, residual fuel fraction, oxygen penetration depth, parameters characterizing the Arrhenius equation (A and E).

2.2.1.3 Charring

For the purpose of ignition of a solid fuel, the process of charring has an impact on both heat and mass transport, and therefore needs to be briefly addressed. A general summary of the chemical processes leading to charring can be obtained from Cullis and Hirschler [18] for polymers, and in the case of wood, from Drysdale [3], thus will not be described here. Instead, an explanation is given concerning the influence of charring on ignition and burning rate.

For charring materials, pyrolysis leads to the production of gaseous fuel (pyrolysat) and a residual solid phase char. The char is commonly a carbonaceous solid that can be further decomposed. This secondary decomposition can also be complete, leading to an inert ash or to a secondary char that can be further decomposed in single or multiple steps. Non-charring materials decompose leaving no residue behind. It will be assumed that the char will not oxidize further, allowing for the definition of an empirical char thickness [16].

From the perspective of ignition, the exposed surface represents the boundary between the gas and the solid. This boundary moves as the material is completely removed. The rate at which the surface moves is the regression rate (v_R). For charring and non-charring materials, this is the boundary where complete consumption of the fuel is achieved. Furthermore, if during the charring process the material intumesces (swells), v_R takes a negative value. Although regression rates can be very different between charring and non-charring materials, at the surface the main difference between the two material types is the temperatures that can be achieved. Carbonaceous chars can reach much higher temperatures, leading in many cases to vigorous oxidation (surface glowing) that can be the catalyst for gas phase ignition. This is part of the gas phase discussion. Regarding the production of fuel, the differences appear mostly in-depth where heat transfer through the char controls temperature and fuel production is affected by an overall permeability function. The effects of temperature on fuel production are discussed in the context of the calculation of the temperature distributions.

2.2.1.4 Characteristic thermal conduction length

When a heat flux is applied to the solid surface, heat travels into the solid fuel, being conduction the governing mechanism of heat transfer in solid. Since fires are transient phenomena, the equation of non-steady state heat transfer must be used to interpret the details of fire behavior. The basic equations for non-steady state conduction can be easily found in literature [3,19] by considering the flow of heat through a small volume. The final equation is simplified as follows:

$$\frac{\partial^2 T}{\partial x^2} = \frac{1}{\alpha}\frac{\partial T}{\partial t} - \frac{\dot{Q}'''}{k} \tag{2.3}$$

where $\dot{Q}'''$ is the rate of heat release per unit volume, k is the thermal conductivity and α = k/ρc represents the thermal diffusivity of the material. In most problems, $\dot{Q}''' = 0$, thus equation (**2.3**) gives for one dimension:

$$\frac{\partial^2 T}{\partial x^2} = \frac{1}{\alpha}\frac{\partial T}{\partial t} \tag{2.4}$$

Many problems can be reduced to a single dimension. Thus, equation (**2.4**) can be directly applied to conduction through materials which may be treated as "infinite slabs" or "semi-infinite solids". Indeed, a relevant problem to ignition and flame spread is that of a slab heated on one side only, with heat losses potentially at both faces. The limiting case is that of the semi-infinite solid subjected to a uniform heat flux. "Thick" slabs will approximate to this model during the early stages of heating, before heat losses from the rear face have become significant. The relationship between heating time and thickness, which defines the limiting thickness to which this model may be applied, can be derived by considering a semi-infinite slab, initially at a temperature T_0, whose surface is suddenly increased to T_∞. Solving equation (**2.4**) (being $\theta = T - T_0$) with the boundary conditions:

- $\theta = 0$ at $t = 0$ $\forall x$
- $\theta = \theta_\infty$ at $x = 0$ for $t = 0$
- $\theta = 0$ as $x \to \infty$ $\forall t$

gives:

$$\frac{\theta}{\theta_\infty} = 1 - \mathrm{erf}\frac{x}{2\sqrt{\alpha t}} \tag{2.5}$$

where the error function is defined as:

$$\mathrm{erf}\,\xi = \frac{2}{\sqrt{\pi}}\int_0^{\xi} e^{-\eta^2} d\eta \tag{2.6}$$

While this cannot be evaluated analytically, it is given numerically in handbooks of mathematical functions, as well as in most heat transfer texts [11, 19].

Equation (**2.5**) can be used to define the temperature profiles below the surface of a slab of thickness L, heated instantaneously on one face, until the rear face becomes heated to a temperature significantly above ambient (T_0). If this is set arbitrarily as 0.5% of (T_S - T_0), then substituting in equation (**2.5**):

$$1 - \mathrm{erf}\left(\frac{L}{2\sqrt{\alpha t}}\right) = 5 \times 10^{-3} \tag{2.7}$$

which gives:

$$\frac{L}{2\sqrt{\alpha t}} \approx 2 \tag{2.8}$$

This indicates that at time t a wall, or slab, of thickness L can be treated as a semi-infinite solid with little error, provided that L > $4\sqrt{\alpha t}$. In many fire safety engineering problems involving transient surface heating, it is adequate to assume "semi-infinite" behavior if L > $2\sqrt{\alpha t}$ [20]. The quantity $\sqrt{\alpha t}$ is the characteristics thermal conduction length and will be used to estimate the thickness of the heated layer.

By including convective heat transfer from a stream of fluid at temperature T_∞ to the surface of the semi-infinite solid (initially at temperature T_0), the variation of the surface temperature (T_S) with time under a given imposed heat flux can be obtained (at x = 0):

$$\frac{\theta_S}{\theta_\infty} = 1 - \exp\left(\frac{\alpha t}{(k/h)^2}\right) \cdot \operatorname{erfc}\left(\frac{\sqrt{\alpha t}}{(k/h)}\right) \tag{2.9}$$

It is evident that the rate of change of the surface temperature depends strongly on the value of the ratio $k^2/\alpha = k\rho c$, a quantity known as "thermal inertia". The lower the thermal inertia, the higher the growth rate of the surface temperature: this will be of great relevance to the ignition and flame spread characteristics of combustible solids.

2.2.2 Gas phase

This section provides a brief description of the events leading to the ignition of a gas phase flame. After the onset of pyrolysis, gas begins to emerge from the fuel surface, initially in very small quantities, but as temperature T(x,t) increases, the fuel mass flux will also increases. The emerging fuel will encounter the ambient oxidizer and will eventually produce a flammable mixture. Given that fuel is migrating into the oxidizer flow, the definition of a flammable mixture is not a simple one. In standard test methods, the ambient flow is fairly well defined, while in real fires, flow fields are defined by the flames themselves and by the geometry of the environment (obstacles, fuel geometry, etc.) with the possibility of complex flow patterns. Nevertheless, what is required to achieve ignition is the production of a flammable condition in at least one location in the gas phase.

A flammable mixture occurs when the fuel concentration in a gas mixture is between the Lower (or Lean) Flammability Limit (LFL) and the Upper (or Rich) Flammability Limit (UFL). Limits of ignitability which vary with the strength of the ignition source can be distinguished from limits of flammability (Figure 2.5 a). The latter must be determined using an ignition source which is sufficiently large to ignite near-limit mixtures. However, as the limits vary significantly with temperature (Figure 2.5 b), flame may propagate in a mixture which is technically 'non-flammable' under ambient conditions if the ignition source is large enough to cause a local rise in temperature.

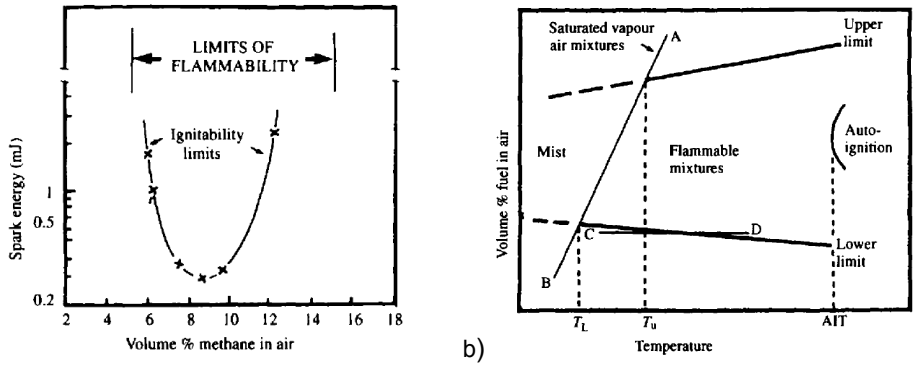

Figure 2.5 a) Ignitability curve and flammability limits for CH_4/air mixture at atmospheric pressure and 26°C;
b) Effect of temperature on flammability limits [3].

2.2.3 Pilot ignition of solids

Ignition may be defined as that process by which a rapid, exothermic reaction is initiated, which then propagates and causes the material involved to undergo change, producing temperatures greatly in excess of ambient. It is convenient to distinguish two types of ignition, namely piloted – in which flaming is initiated in a flammable vapour/air mixture by a 'pilot', such as an electrical spark or an independent flame – and spontaneous – in which flaming develops spontaneously within the mixture. To achieve flaming combustion of liquids and solids, external heating is required, except in case of some kind of flammable liquids. Keeping in mind the aim of the thesis, only pilot ignition of solid materials will be further discussed.

By assuming that sustained, piloted ignition can only occur if a critical mass flux of fuel vapours is exceeded, the process of piloted ignition can be described as Figure 2.6 shows. In this description "sufficient flow of volatiles" implies a mass flux greater than the critical value while "suitable conditions" corresponds to environmental conditions favourable for the flame to become established. Such particular condition can be identified as the firepoint of the solid material. In the following description it will be assumed that the pilot and the source of energy are distinct, thus excluding direct flame impingement where the flame acts both as the source of energy and the ignition source of the flammable vapours. Moreover, the specific boundary condition of continuous heat flux applied to the exposed surface will be assumed. This will become relevant in the following analysis of experimental data.

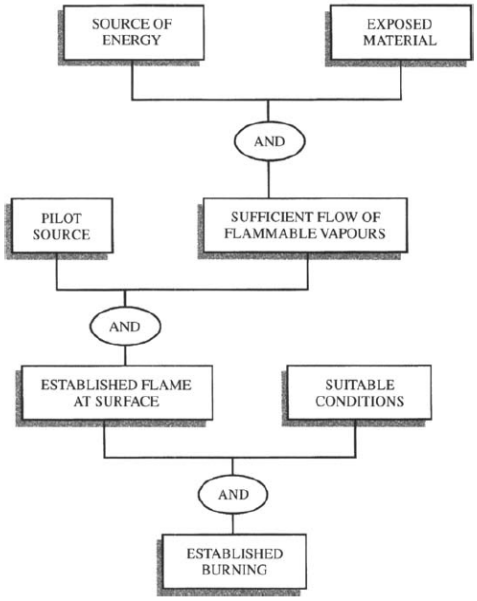

Figure 2.6 Scheme for piloted ignition [3].

2.2.3.1 Ignition during continuous heat flux

Assuming a continuous heat flux applied to the exposed surface of material, the firepoint condition, or the ignition, can be identified by the minimum surface temperature T_S at which the flow of volatiles is sufficient to allow flame to persist at the surface. A number of factors contribute to the attainment of the firepoint but generally the "inert solid" assumption is made in order to simplify the energy equation and reduce the problem to a simple heat transfer to a surface. This was originally introduced by Kanury [21] who considered different solution to equation (**2.3**) in which the boundary conditions were chosen to represent a number of configurations, including both the 'infinite slab' and the 'semi-infinite solid' discussed in Section 2.2.1.4.

Anyway, the solid is assumed to be opaque and inert, with uniform thermal properties which are independent of temperature. Obviously this is questionable but it can be initially relegated to second order status in order to underline the basic principles of ignition in solids. Moreover, most theoretical and experimental investigations concentrated on ignition brought about by radiative heat transfer although ignition by convection should not be neglected.

In modelling the ignition of solid fuels, it is generally adopted a closed solution of equation (**2.4**) that can be derived by considering the transient pyrolysis of a semi-infinite charring solid subject to a constant radiant heat flux [3]. This approach, known as semi-infinite solid assumption, holds for the early transient regime and it is well known that it can accurately approximate the real

behaviour of a plane wall of thickness 2δ provided the Fourier Number Fo= $\alpha t/\delta^2$ < 0.2 [19].

This assumption entails that during the pre-heating period up to ignition, the heat perturbation penetrates into the material by affecting a heated layer smaller than the actual thickness of the specimen. Furthermore, the initial and boundary conditions were that the initial temperature at t = 0 s was T_0 uniform inside the sample; the top surface was exposed to a constant heat flux $\dot{q}''_{ext}$, while the heat losses from the top surface were assumed to be negligible. Under such conditions, the time to ignition can then be calculated by equation (**2.10**), which is described and extensively detailed in [22,23]:

$$t_{ig} = \frac{\pi}{4} k\rho c \frac{\left(T_{ig} - T_0\right)^2}{\dot{q}''^{\,2}_{ext}} \tag{2.10}$$

where $k\rho c$ is the thermal inertia, T_{ig} and T_0 are the ignition temperature and the initial temperature respectively.

By plotting $t_{ig}^{-1/2}$ as a function of the external radiant heat flux, a linear trend can be identified (see Figure 2.7), whose slope allows the computation of the theoretical critical heat flux (CHF) [24].

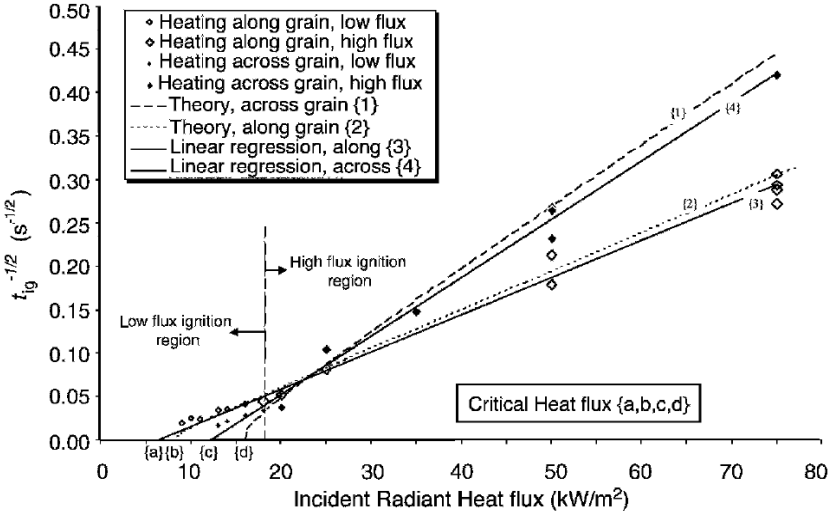

Figure 2.7 $t_{ig}^{-1/2}$ as a function of incident radiant flux. Experimental data for Douglas Fir [25].

Indeed, the CHF is defined as the minimum value of the imposed heat flux at which ignition is theoretically possible, i.e. $t_{ig} = \infty$ [3].

The boundary condition of the thermal problem at the exposed surface at the ignition can be specified as follows:

$$\dot{q}''_{ext} = \frac{1}{\varepsilon} \cdot \left[h_c\left(T_{ig} - T_0\right) + \varepsilon\sigma\left(T_{ig}^4 - T_0^4\right)\right] = CHF \tag{2.11}$$

where ε represents the emissivity, σ the Stefan–Boltzmann constant and h_c the convective heat transfer coefficient. Once the CHF has been determined, equation (**2.11**) can be iteratively solved in order to find the ignition temperature T_{ig}.

2.3 Overview of flame retardancy in polymer technology

As previously described, polymer combustion is driven by the thermally induced decomposition (pyrolysis) of solid polymer into smaller fragments, which then volatilize, mix with oxygen, and combust. This combustion releases more heat, which reradiates onto the unburned polymer, thus continuing to drive pyrolysis and combustion until a lack of heat/fuel/oxygen causes the fire to extinguish.

Depending on the burning polymer, physical and chemical processes may be extremely different. Basically, the chemical structure of material and its behavior upon exposure to heat determine the heat, smoke, and gas release during combustion.

In order to minimize polymers flammability, several techniques have been developed in the past decades [26]. The most widespread solution is the use of flame retardant additives (FRs), being a proven approach, very cost-effective and easy to incorporate in polymeric materials.

All types of flame retardant chemistries fall into one (or more) of three mechanisms of flame retardant action. These three mechanisms can be summed up as follows:

- Gas phase FRs: these materials reduce the heat released in the gas phase from combustion by scavenging reactive free radicals.
- Endothermic FRs: these materials operate in the gas phase and condensed (solid) phase by releasing non-flammable gases (H_2O, CO_2), which dilute the fuel and cool the polymer through endothermic decomposition of the flame retardant additive. The lower substrate temperature slows the pyrolysis rate. These materials also leave behind a ceramic-like residue, which protects the underlying polymer.
- Char-forming FRs: these materials operate in the condensed phase by preventing fuel release through binding up fuel as non-pyrolyzable carbon (char) and providing thermal insulation for underlying polymer through the formation of char protection layers.

It is worth noting that FRs are molecules designed for a particular application, tailored to be compatible with the polymer in a specific fire scenario. Thus, a detailed preliminary study must be carried out in order to achieve the aim of effectively reducing fire hazard.

2.3.1 Halogenated flame retardants

Halogenated FRs are molecules that incorporate elements from group VII of the periodic table – F, Cl, Br, and I. They can vary widely in chemical structure, from aliphatic to aromatic carbon substrates but it is the organo-halogen compounds that find the most effectiveness as flame retardant additives for polymers [27].

Organobromine and organochlorine are by far the most used, as the C-Br bond is stable enough for environmental exposure and yet unstable enough that heat can easily break the bond, releasing the bromine under fire conditions to inhibit combustion free radical reactions. Examples of the chemistry that bromine can undertake in the vapor phase to inhibit combustion are shown in Figure 2.8.

- $H\cdot + O_2 \rightarrow HO\cdot + O\cdot$ $HO\cdot + H\cdot \rightarrow H_2O$ $HO\cdot + CO \rightarrow CO_2 + H\cdot$
- $R\text{-}Br \rightarrow R\cdot + Br\cdot$ $Br\cdot + R\text{-}H \rightarrow HBr + R\cdot$ $H\cdot + Br\cdot \rightarrow HBr$
- $HO\cdot + HBr \rightarrow H_2O + Br\cdot$ $H\cdot + HBr \rightarrow H_2 + Br\cdot$
- $SbBr_3 + 3H\cdot \rightarrow Sb + 3HBr$
- $Sb + HO\cdot \rightarrow SbOH$
- $SbOH + HO\cdot \rightarrow SbO + H_2O$

Figure 2.8 Free radical combustion reactions with bromine [27].

These unique bond strengths make halogen-based flame retardants strictly vapor phase flame retardants, as the halogens work in the vapor phase to inhibit combustion. Halogenated FRs are sometimes used with synergists such as antimony oxide, zinc borate, or other phosphorus chemistry, as these other elements help make the halogens more efficient in the vapor phase [28].

This technology has been used since the 1930s, thus revealing a proven cost-effective solution for a wide range of polymers. Nevertheless, some relevant drawbacks raised, such as increase in smoke release under fire conditions, a release of corrosive gases during burning, and environmental scrutiny. The increase in smoke and release of corrosive gases (namely HBr) during burning is an effect of its flame retardant chemistry. Because it inhibits combustion through the formation of HBr, naturally it will cause the formation of partially combusted polymer decomposition products as well as CO. Additionally, once the bromine is consumed by the fire, any remaining polymer will burn if exposed to additional heat, and so halogenated FRs do not always perform well under very high heat flux conditions unless a lot of halogen is present in the polymer. The last drawback mentioned, environmental scrutiny, is related to how it has been used to date, as a normal additive. Because the additive is just put into the polymer and is not chemically bound to the polymer, it can leave the polymer over time and get into the environment, thus leading to toxicology problems.

First studies on asphalt binder modification concerned the use of such halogenated FRs [29-31] which showed to have good flame-retarding effects but also the well-known important drawbacks, like, i.e. the formation of very smoky, highly toxic and corrosive fire effluents rich in products of incomplete combustion.

Moreover, they can be expensive and the technology used to mix flame retardants may be quite complex and inappropriate for the production of an asphalt binder. Thus, despite of their effectiveness in improving fire reaction of asphalt, halogenated FRs are nowadays abandoned because of the risks associated to their chemical composition.

2.3.2 Phosphorous-based flame retardants

Phosphorus-based flame retardants incorporate phosphorus into their structure, and the structure can vary greatly from inorganic to organic forms, and between oxidation states (0, +3, +5). Inorganic forms of phosphorus flame retardants also tend to be phosphates, but one material, red phosphorus, has its own unique structure and is the only phosphorus (0) flame retardant in use.

Phosphorus compounds are unique in that they can be both vapor phase and condensed phase flame retardants, depending upon their chemical structure and their interaction with the polymer under fire condition. When they are combined with other materials, it is typically to enhance char formation or oxidative durability of the chars formed by the phosphorus flame retardant. Some examples of the vapor phase phosphorus chemistry are shown in Figure 2.9.

- $P_4 + 2O_2 \rightarrow 4PO\cdot$
- $H_3PO_4 \rightarrow HPO_2 + HPO + PO\cdot$
- $H\cdot + PO\cdot \rightarrow HPO$
- $H\cdot + HPO \rightarrow H_2 + PO\cdot$
- $2OH\cdot + PO\cdot \rightarrow HPO + H_2O$
- $OH\cdot + H_2 + PO\cdot \rightarrow HPO + H_2O$

Figure 2.9 Vapour phase flame retardant reactions for phosphorous [27].

Phosphorous-based FRs became more commonly used, as halogenated FRs were deselected for their drawbacks previously defined. They can be effective in both vapor and condensed phases, meaning that they can be useful in low loading levels when combined with polymers that inherently char on their own. Further, phosphorus flame retardants tend to do well in high heat flux fire conditions, and through char formation, can provide superior fire protection in combination with other flame retardants. Nevertheless, also phosphorous-based FRs generate more smoke and CO during fire conditions because they foster the inhibition of polymer combustion. Moreover, they are also starting to be under regulatory scrutiny for environmental impact.

2.3.3 Flame retardant mineral fillers

FR mineral fillers fall into the endothermic cooling mechanism of flame retardancy, and have a unique vapor/condensed phase activity. Specifically, under fire conditions, the mineral filler endothermically decomposes upon

exposure to heat. This cools the condensed phase, thus slowing thermal decomposition of the polymer. Further, the decomposition products of the mineral filler are non-flammable, and so the residue left behind from thermal decomposition (usually a metal oxide) dilutes the total amount of polymer fuel available (condensed phase), while the release of non-flammable gas from the mineral filler helps dilute the fuel available in the vapor phase for ignition.

The most commonly used mineral fillers in use today as flame retardants are metal hydroxides and metal carbonates. It is worth noting that the hydroxide or carbonate needs to be able to release its water or carbon dioxide at elevated temperatures, but not too high of a temperature that the polymer decomposes before the mineral filler activates. So, hydroxides and carbonates, which decompose between 180 and 400 °C tend to be the only materials in use today as flame retardant additives. More specifically, aluminum ($Al(OH)_3$) and magnesium ($Mg(OH)_2$) hydroxides are widely used. Aluminum hydroxide is often called “alumina trihydrate” (ATH: $Al_2O_3 \cdot 3H_2O$) because the water is hydrated on the aluminum oxide surface rather than predominated by Al-OH bonds, but the net stoichometry is the same and so the structures are used interchangeably. For the carbonates, magnesium carbonate is sometimes used, although calcium carbonate is also used in combination with other fillers (silicone) and activating materials to be active as a flame retardant for wire and cable compounds.

Mineral fillers do not typically get used with synergists, but in some cases are combined with other flame retardants to reduce smoke release. Some general schemes on these main classes of mineral fillers are shown in Figure 2.10.

- Aluminum hydroxide (or ATH)
  - $2Al(OH)_3$ + Heat (180 - 200 °C) $\rightarrow Al_2O_3 + 3H_2O$ (g)↑
- Magnesium hydroxide
  - $Mg(OH)_2$ + Heat (300 - 320 °C) $\rightarrow MgO + H_2O$ (g)↑

Figure 2.10 FR mineral fillers mechanisms [27].

FR mineral fillers are a proven low-cost technology (references from the 1920s), environmentally friendly. Furthermore, under fire conditions, they tend to greatly lower smoke and reduce overall toxic gas emissions because the mineral filler is replacing flammable polymer fuel with non-flammable inorganic mass. However, two main drawbacks affect the flame retardant performance. The first is that they have a limited fire performance window. Specifically, once enough heat has consumed all the mineral filler and all the water/CO_2 has been released, the metal oxide left behind provides no additional protection to the polymer. So, the mineral filler can delay ignition and slow initial flame growth, but it cannot stop it completely if enough constant external heat is applied. The other one is that, for mineral fillers to be effective, high loadings of mineral fillers are needed to flame retard the plastic, often at the expense of the polymer mechanical properties.

This last aspect could not be actually a drawback for the purpose of this thesis, being mineral filler an essential component of all the asphalt mixtures [32-35].

2.3.4 Intumescent flame retardants

Intumescent flame retardants create a protective carbon foam under fire conditions; they rise up in response to heat (intumesce). This class of flame retardants is strictly condensed phase in its activity, and either provides its own carbon char or uses the polymer as a carbon char source. Intumescents are typically composed of three components that make the carbon char form. The first is an acid catalyst, which causes the carbon source (the second component) to crosslink and form a thermally stable form of carbon. The last component is the spumific or gas former, which causes the carbon source to become a carbon foam. It is worth reminding that only the combination of these three components actually works providing a real protection. Figure 2.11 provides a schematic description of the intumescent action.

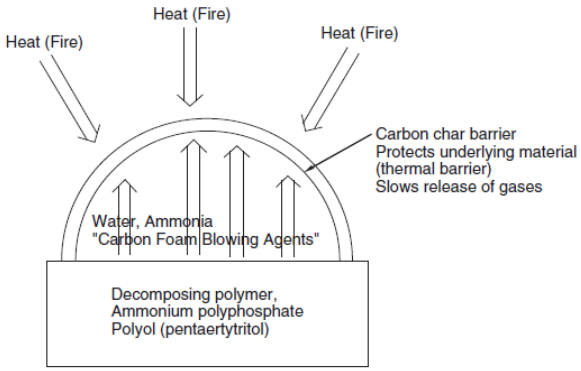

Figure 2.11 Intumescent FRs mechanisms [26].

Intumescent FRs are widely used as protective coating for fire barriers, steel, firewall holes due to high versatility and capability of providing robust fire safety. Nevertheless, water absorption issues and low thermal stability represent the most important drawbacks. Indeed, intumescent systems work effectively by activating before the polymer obtains a chance to thermally decompose, and so most intumescent materials activate around 180–200 °C. This fact could represent a limit in asphalt mixture applications, at least in the Hot Mix Asphalt (HMA) technology, due to the high temperatures achieved in the mixing process.

2.3.5 Inorganic frame retardants

This category covers a wide range of chemical structures that can act both in vapour and condensed phases. They help other FRs to work better, address a

particular effect of flame retardancy (reduce smoke formation) or have a specific FR effect in a limited number of materials. These FRs have no carbon in their structure being mainly composed of metal oxides and composites. Actually, the only commercial inorganic flame retardants are borates, stannates, and silicates. Borates used include zinc borates ($2ZnO{\cdot}3B_2O_3{\cdot}3{,}5H_2O$), which are used as synergists for halogenated flame retardants, mineral fillers, and phosphorus to help the systems work better. They also address afterglow conditions in highly mineral-filled systems where even after the fire is out, the remaining material can be quite hot and could reignite other objects.

The main advantage of using these FRs is that they address some flaw/weakness of another FR additive and because of their inorganic structure, are mostly perceived to have minimal environmental impact. However, because they are niche materials, they are used only sparingly and because of the low use levels, can be rather expensive.

2.3.6 Polymer nanocomposites

The polymer nanocomposite approach to flame retardancy represents the newest technology now in use. Polymer nanocomposites are filled with nanoparticles (basically clay nanoparticles – organically treated layered silicates- and carbon nanotubes/nanofibers) which interact with polymer molecules at the nanoscale. Among these, organically modified layered silicates represent the most used nano-additive [36,37,38]. The most recent methods to prepare polymer–clay nanocomposites have been developed by several groups. Two terms, intercalated and delaminated, are used to describe the two general classes of nano-morphology that can be prepared. Intercalated structures are well ordered multi-layered structures where the extended polymer chains are inserted into the gallery space between the individual silicate layers. Conversely, the delaminated (or exfoliated) structure results when the individual silicate layers are no longer close enough to interact with the adjacent layers' gallery cations [37]. In the delaminated cases the interlayer spacing can be on the order of the radius of gyration of the polymer; therefore, the silicate layers may be considered well dispersed in the organic polymer. The silicate layers in a delaminated structure may not be as well ordered as in an intercalated structure. Figure 2.12 a) shows a schematic representation of the two possible structures in nanocomposites.

For flame retardancy purposes, polymer nanocomposites are condensed FRs that mainly slow down (but do not stop) the mass loss rate of the polymer during heat exposure by means of the formation of a nanoparticle-rich fire protection barrier [36] (see Figure 2.12 b). More specifically, the intercalated or exfoliated architecture is generally achieved thanks to a quaternary ammonium compound which works as an organic intermediate between the hydrophobic polymer and the hydrophilic montmorillonite. The quaternary ammonium compounds remain stable up to approximately 250 °C and thereafter decompose, thus leading to the collapse of the nanostructure. The decomposition of these surfactants can lead to alternate effects since in some

cases it can anticipate the ignition phase [36]. Nevertheless, due to this process the OMMT (organic-modified montmorillonite) platelets are no longer linked to the polymer and become free to migrate, driven by different mechanisms such as: (i) temperature and viscosity gradients which create convective motion in the melt from the bulk towards the surface of the sample [36]; (ii) lower surface free energy compared with carbon-based polymers [37], and (iii) rising bubbles formed by the decomposing polymer and the clay surfactants [38]. All these mechanisms contribute to the formation of a thermal insulating and low permeability superficial clay-rich char which significantly reduces the peak of heat release rate for almost all types of nanocomposites, irrespective of the nature of the polymer matrix and the initial nanostructure (intercalated or exfoliated). However, the overall fire contrasting effect is strictly dependent on the chemical composition of the organomodified clay and on its consequent interaction with the base material.

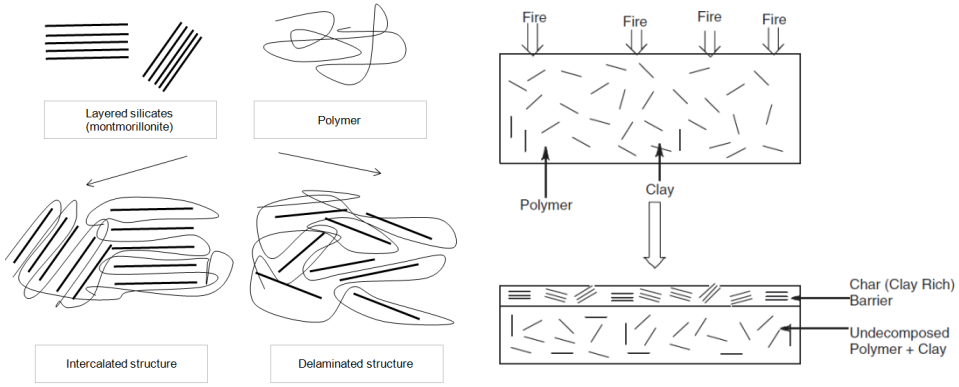

a) b)

Figure 2.12 a) Intercalated and delaminated structures in polymer nanocomposites b) FR mechanism in polymer nanocomposites [26].

Having in mind a similar effect with bitumen, special attention should be therefore paid to the interaction between clay and bitumen. This has been recently investigated by considering physical, mechanical and rheological properties of different asphalt binders modified with layered silicates [39,40]. Asphalt/clay binary blends can be obtained by physical mix of the two components and are characterized by a predominant intercalated structure with a partial degree of exfoliation, as highlighted by a significant increase in the interlayer spacing which is independent of the clay concentration .Focusing on the rheological properties, clay does not significantly change the overall mechanical response of the base bitumen, even if some important differences have been outlined. In fact, at high temperatures a filler-like effect was highlighted by a significant increase in the loss and storage moduli without affecting the onset of the Newtonian plateau [39,40]. At lower temperatures, asphalt/clay binary blends reached lower crossover frequency (ω_{cr}) than base asphalt, thus indicating a more complex interaction between the two components

and not only a filler-like modification. More specifically, asphalt/clay binary blends achieved the glass transition before the base asphalt, thus indicating a selective interaction between clay and aromatics. Even more complex outcomes were found when radial SBS block copolymer is added to generate an asphalt/SBS/clay ternary blend. In this case, the internal structure cannot be easily predicted and described, being particularly complex and primarily dependent on the mixing sequence [39].

Further investigation should address the impact of such new additives in the fire behaviour of bitumens.

References

[1] Karlsson B., Quintiere JG. “Enclosures Fire Dynamics” CRC Press LLC, Boca Raton, Florida, 2000.

[2] Quintiere JG, “Compartment Fire Modeling”, SFPE Handbook of Fire Protection Engineering, 2nd ed., National Fire Protection Association, Quincy, MA, 1995.

[3] Drysdale D, “An introduction to fire dynamics”; 2nd ed.; J. Wiley, Chichester, 1999.

[4] Walton WD and Thomas, PH, “Estimating Temperatures in Compartment Fires,” in The SFPE Handbook of Fire Protection Engineering, 2nd ed., National Fire Protection Association, Quincy, MA, 1995.

[5] ISO/CD 13943, “Glossary of Fire Terms and Definitions,”, International Standards Organization, Geneva, 1996.

[6] ISO 834-1, “Fire resistance test – Elements of building construction – Part 1: General requirements”, 1st ed. 1999-09-15, International Organization for Standardization, 1999.

[7] EN 1363-2, “Fire resistance test – Part 2: Alternative and additional procedures”, First ed. 1999-09-24, European Committee for Standardization, 1999.

[8] “Richtlinien fur Ausstattung und Betrieb von Tunnels (RABT)”, Ausgabe 1985 ed., Forschungsgesellschaft fur Straßen – und Verkehrswesen, 1985.

[9] “Beproeving van het gedrag bij verhitting van tween isolatiematerialen ter bescherming van tunnel bij brand“, Institut TNO voor Bouwmaterialen en Bouwconstructies, Rapport B-79-391, Delft, The Netherlands, 1979.

[10] “Rapport betreffende de beproeving van het gedrag van tween isolatiematerialen ter bescherming van tunnels tegen brand”, Institut TNO voor Bouwmaterialen en Bouwconstructies, Rapport B-80-33, Delft, The Netherlands, 1980.

[11] PIARC, 2006. Systems and Equipment for Fire and Smoke Control in Road Tunnels. PIARC Technical Committee C5 Road Tunnel.

[12] Lacroix D., Haack A., "PIARC Design Criteria for Resistance to Fire for Road Tunnel Structures", in Joint Issue ITA/PIARC of Route-Roads on Fire Safety in Tunnels, 2004.

[13] Atreya, A.; Ignition of Fires, Philosophical Transactions of the Royal Society A: Mathematical, Physical, and Engineering Sciences 1998, (356), 2787-2813.

[14] Di Blasi C., Physico-chemical processes occurring inside a degrading two-dimensional anisotropic porous medium, International Journal of Heat and Mass Transfer 41 (1998) 4139-4150.

[15] Rein, G; Lautenberger, C; Fernandez-Pello, AC; Torero JL.; Urban DL; Application of genetic algorithms and thermogravimetry to determine the kinetics of polyurethane foam in smoldering combustion, Combustion and Flame, 2006 146:1-2 95-108.

[16] Di Blasi, C; Modeling and Simulation of Combustion Processes of Charring and Non-Charring Solid Fuels, Progress in Energy and Combustion Science, 1993 (19) 71-104.

[17] Matala A., Hostikka S., Mangs J. Estimation of Pyrolysis Model Parameters for Solid Materials using Thermogravimetric Data, Fire Safety Science–Proceedings Of The Ninth International Symposium, 2008, pp. 1213-1224.

[18] Cullis, CF.; Hirschler, MM; The combustion of organic polymers; Clarendon Press: Oxford University Press, Oxford, 1981.

[19] Bergman T, Lavine A, Incoprera F, Dewitt D, "Fundamentals of heat and mass transfer"; 7th ed.; J. Wiley, Chichester, 2011.

[20] McCafFrey, B.J., Quintiere, J.G., and Harkleroad, M.F. (1981). 'Estimating room temperatures and the likelihood of flashover using fire test data correlations'. Fire Technology, 17, 98-119; 18, 122.

[21] Kanury, AM (1972). 'Ignition of cellulosic materials: a review'. Fire Research Abstracts and Reviews, 14, 24-52.

[22] Delichatsios MA, Panagiotou Th, Kiley F. The use of time to ignition data for characterizing the thermal inertia and the minimum (critical) heat flux for ignition or pyrolysis. Combustion and Flame 1991; 84:323-32.

[23] Hopkins JrD, Quintiere JG. Material fire properties and predictions for thermoplastics. Fire Safety J 1996; 26:241–68.

[24] Quintiere JG. "Fundamental of Fire Phenomena" J. Wiley, Chichester, 2006.

[25] Spearpoint, M.J., Predicting the ignition and burning rate of wood in the cone calorimeter using an integral model, MS Thesis, Department of Fire Protection Engineering, University of Maryland, College Park, Maryland 1999.

[26] Morgan AB, Gilman JW., An overview of flame retardancy of polymeric materials: application, technology, and future directions. Fire and Materials, 2013; 37:259-279.

[27] Fire retardancy of polymeric materials, 2nd ed. In: Wilkie CA, Morgan AB, editors. CRC Press; 2010.

[28] Lyon RE, Takemori MT, Safronava N, Stoliarov SI, Walters RN. A molecular basis for polymer flammability. Polymer 2009; 50:2608–2617.

[29] Cong P, Yu J, Wu S, Luo X. Laboratory investigation of the properties of asphalt and its mixtures modified with flame retardant. Constr Build Mater 2008;22(6):1037–42.

[30] Wu S, Cong PL, Yu J, Luo X, Mo L. Experimental investigation of related properties of asphalt binders containing various flame retardants. Fuel 2006;85(9):1298–304.

[31] Wu S, Mo L, Cong PL, Yu J, Luo X. Flammability and rheological behavior of mixed flame retardant modified asphalt binders. Fuel 2008;87(1):120–4.

[32] Hu SG, Zhang H, Wang J. Research on alkaline filler fire-retarded asphalt pavement. J Wuhan Univ Technol 2006;21:146–8.

[33] Yu J, Cong P, Wu S. Investigation of the properties of asphalt and its mixtures containing flame retardant modifier. Constr Build Mater 2009;23:2277–82.

[34] Xu T, Huang X, Zhao Y. Investigation into the properties of asphalt mixtures containing magnesium hydroxide flame retardant. Fire Safety J 2011;46:330–4.

[35] Xu T, Huang X. A TG-FTIR investigation into smoke suppression mechanism of magnesium hydroxide in asphalt combustion process. J Anal Appl Pyrolysis 2010;87:217–23.

[36] Kiliaris P, Papaspyrides CD, Polymer/layered silicate (clay) nanocomposites: an overview of flame retardancy. Progress in Polymer Science 35 (2010) 902–958.

[37] Gilman JW, Flammability and thermal stability studies of polymer/layered silicate (clay) nanocomposites. Applied Clay Science 15 (1999) 31–49.

[38] Lewin M., Flame retarding polymer nanocoposites: synergism, cooperation, antagonism. Polymer Degradation and Stability 96 (2011) 256-269.

[39] Polacco G., Kriz P., Filippi S., Stastna J., Biondi D., Zanzotto L., “Rheological properties of asphalt/SBS/clay blends”, European Polymer Journal, 44 (2008) 3512-3521.

[40] Golestani B, Nejad FM, Galooyac SS, Perfomance evaluation of linear and nonlinear nanocomposite modified asphalts. Constr Build Mater 35 (2012);197-203.

3 Materials and Methods

The analysis of the fire behaviour of asphalt develops through the investigation of three stages: asphalt binders, asphalt mastics and asphalt mixtures.

This work of thesis starts from investigating the flammability and thermal stability of asphalt binders and mastics. Different kinds of neat asphalt binders were investigated in order to outline possible correlations with the S.A.R.A. fractions. The influence of both conventional and flame retardant fillers is then addressed, by considering different percentages and mixes of fillers.

Finally, the role played by the aggregate gradation, bitumen contents and the physical properties of aggregates is evaluated by means of cone calorimeter test.

3.1 Materials

3.1.1 Asphalt binders

Three different neat asphalt binders were investigated and subsequently referred to as B50, B70, B170, where the number identifies the penetration grade. Basic characterization of the three asphalt binders is reported in Table 3.1.

Table 3.1 Main conventional and basic rheological properties of neat asphalt binders.

Asphalt Binder	Penetration	Softening Point	Penetration Index	Complex Modulus (10rad/s @ 20°C)	Phase angle (10 rad/s @ 20°C)
	[dmm]	[°C]	[-]	MPa	[deg]
B50	44	52.0	- 1.0	6.45	60.8
B70	68	50.7	- 0.3	4.19	65.3
B170	150	44.5	+0.5	1.42	71.3

The ring and ball softening point was measured according to ASTM D36-95 and the penetration was assessed according to ASTM D5 - 06e1. Penetration Index is a measure of temperature susceptibility and was evaluated according to the equation developed by Pfeiffer and Van Doormaal [1] considering the penetration corresponding to the Softening Point equal to a conventional value of 800 dmm. Basic rheological properties were determined through a Dynamic Shear Rheometer (DSR Physica MCR 101) with a parallel-plate testing system consisting of 8 mm diameter plates with 2 mm gap. The general testing procedure was referred to the standard ASTM D7175 – 08.

Conventional and rheological properties of unmodified asphalt binders are integrated by a preliminary analysis of Saturates, Aromatics, Resins and Asphaltenes (S.A.R.A.) fractions carried out through the Thin Layer Chromatography – Flame Ionization Detection (TLC-FID) technique by using a IATROSCAN MK-5. This information is extremely relevant because asphalt binders contain chemical components significantly different in terms of molecular weight and structure which may have different influence on the fire reaction, as already observed by Jimenez et al [2].The obtained results are reported in Table 3.2, where I_C is the Gaestel Index [1] and represents a measure of the dispersing capability of maltenes to asphaltenes. When the I_C increases, colloidal stability decreases, thus highlighting a limited solubilizing power of the resins, probably due to the high degree of aromaticity in the molecules.

Table 3.2 SARA fractions of neat asphalt binders.

Asphalt Binder	Saturates	Aromatics	Resins	Asphaltenes	I_C
	[%]	[%]	[%]	[%]	[-]
B50	3.1	70.1	16.9	9.9	0.149
B70	3.0	68.6	17.6	10.8	0.160
B170	4.7	71.0	14.9	9.4	0.164

In order to outline the possible influence of polymeric modification of asphalt binders on ignitability and thermal stability, styrene-butadiene-styrene (SBS) block copolymer modified asphalt, subsequently referred to as B50-SBS, was prepared by adding 5%wt of SBS to B50. The SBS was EUROPRENE® SOL T 161B, a radial block copolymer with 30%w of styrene, kindly provided by Versalis S.p.A.

With the aim of investigating the consequences on fire behaviour of nanomodified binders, bitumen B50 was then selected as a base for the subsequent modification with clay. The chosen layered silicate was Cloisite 20A, an organo-modified clay subsequently referred to as 20A, provided by Southern Clay Products Inc. 20A was prepared from a sodium montmorillonite characterized by a cation exchange capacity of 0.926 meq/g of $Me_2(HT)_2NCl$

(dimethyldihydrogenated-tallow ammonium chloride). Hydrogenated tallow is a blend of saturated n-alkyls groups approximately composed of C_{18} at 65%, C_{16} at 30% and C_{14} at 5%. The organic content of 20A was 38.0%, as previously determined through TGA. 20A maximum particle size was 13.0 µm.

Three B50/20A blends were prepared with contents of clay equal to 3.33%, 6.00%, and 8.00% by weight. The obtained nanoclay-modified asphalt binders are referred to as 3.33BC, 6.00BC, and 8.00BC respectively. The asphalt binder modification process followed this procedure: aluminium cans of approximately 500 ml were filled with 200-250 g of base asphalt binder and put in a thermoelectric heater. When the asphalt temperature reached 160°C, a high shear mixer Silverson L4R wad dipped into the can and set to about 4000 rpm. The 20A was added gradually, while keeping the temperature within the range of 160 ± 5°C during the addition and the subsequent 30 minutes of mixing.

3.1.2 Fillers

Asphalt binder B50 was subsequently used to prepare several asphalt mastics obtained using three classes of fillers:

- Aluminum hydroxide (ATH)
- Magnesium hydroxide (MH)
- Conventional limestone filler (C)

ATH is by far the largest-selling inorganic hydroxide used as a fire retardant for polymeric materials and it is produced through two main processes which lead to different particle size gradations and flame-retardant effectiveness. In order to evaluate the influence of particle size, three different commercial ATH, subsequently referred to as ATH-1, ATH-2 and ATH-3, were tested. All these ATH are characterized by minimum $Al(OH)_3$ content equal to 99.0%. The same purity degree characterizes the MH and the conventional limestone filler, referred in the text to as C. The main physical and chemical properties of the fillers are summarized in Table 3.3.

Table 3.3 Main physical and chemical properties of the fillers.

Mineral Filler	Main chemical component	Specific gravity	Bulk Density	pH	Specific surface area (BET)	Rigden Voids
	[>99%wt]	[g/cm^3]	[kg/m^3]	[-]	[m^2/g]	[%]
C	$CaCO_3$	2.71	600	9	N.A.	39
MH	$Mg(OH)_2$	2.36	300	10	10.0	58
ATH-1	$Al(OH)_3$	2.42	1100	9	3.4	41
ATH-2	$Al(OH)_3$	2.42	350	9	7.0	50
ATH-3	$Al(OH)_3$	2.42	200	9	11.0	62

The “Rigden Voids” test outlines the main factor defining the consistency of filled systems. Currently, this test is adopted by the international standards and it is suggested by National Asphalt Pavement Association [3] as a part of asphalt mixture design and quality control. In this investigation, Rigden voids test is performed according to EN 1097-4:2008 using the apparatus shown in Figure 3.1.

Figure 3.1 Rigden voids apparatus.

Particle size analyses were performed using the laser diffraction method, as this aspect showed great relevance in the flame retardant performance of fillers [4]. Laser diffractometry size analysis is based on the principle that particles of a given size diffract light with a given angle depending on particle size. The bigger is the angle the lower is particle size. A narrow beam of monochromatic light (λ=750nm) is passed through a sample cell containing a moving suspension. The diffracted light is focused onto specific detectors. Two different theories permit to calculate grain-size distribution starting from light intensity reaching the array of detectors: Fraunhofer’s Approximation and Mie’s Theory.

The Mie’s theory allows to obtain a rigorous solution in particle size analysis and is based on Maxwell’s electromagnetic fields equations. This method permits to consider particle refraction that is of particular importance for particles which present diameter smaller than 50 micron and for those transparent.

The Fraunhofer theory is based on the principle whereby there is only diffraction and no refraction, even if this is not completely correct for organic materials due to light absorption. Variations in results deriving from different models are negligible for sand-sized particles and only became important for samples containing a significant amount of material finer than 10 μm.

If particles are large compared to the wavelength of the light, the interaction can be interpreted in terms of diffraction. This means that measurements for particles with size equivalent to wavelength may be problematic. The continuous pumping around of particles during size distribution measurement ensures random orientation of most particles relative to the laser beam, so that the equivalent spherical cross sectional diameter is measured.

The grain-size analysis of all mineral fillers was carried out with a Coulter LS laser grain-sizer. The results are given in different grain-size classes between 0,040 and 2000 μm. Samples were subjected to ultrasound during measurements. This implies that all macro-aggregates were destroyed before measurements.

The results are expressed as an average value of at least two independent replications. Test results are reported in Table 3.4; the whole particle size distribution is synthesized by three main characteristic diameters: d_{10}, d_{50} and d_{90} where the number specifies the volume percentage of particles smaller than the specified value.

Table 3.4 Characteristic diameters of mineral fillers.

Mineral Filler	**d_{10}**	**d_{50}**	**d_{90}**
	[μm]	[μm]	[μm]
C	0.76	5.00	34.40
MH	0.56	0.93	1.39
ATH-1	1.16	9.31	29.29
ATH-2	0.74	1.83	3.88
ATH-3	0.45	0.99	1.53

3.1.3 Asphalt mastics

Asphalt mastics were prepared and analysed in the second phase of the research program, using only asphalt binder B50 as base bitumen. This choice will be supported by results reported in the following chapter concerning asphalt binder flammability, and thermal stability.

Asphalt mastics were prepared with a high shear mixer Silverson L4R using the typical mixing procedure described as follows: aluminium cans of approximately 500 ml were filled with 250 – 260 g of B50 asphalt binder and put in a thermoelectric heater. When the asphalt temperature reached 170 ± 5 °C, the high shear mixer was dipped into the can and set to about 4,000 rpm. Mineral filler was then added gradually (5 g/min), while keeping the temperature within the range of 170 ± 5 °C during addition and the subsequent 30 minutes mixing.

Binary blends (bitumen B50 and one kind of filler) were initially considered. Five asphalt mastics were then prepared: 100C, 100MH, 100ATH-1, 100ATH-2 and 100ATH-3, where 100 indicates that all mastics were prepared at 1/1 asphalt/filler ratio by weight. This composition was selected according to the most common specifications for the mix design of typical asphalt mastics and traditional Hot Mix Asphalt.

Ternary blends were then obtained by adding one of the FR-fillers (ATH-1 or MH) coupled with C to the base asphalt binder B50. In this case, the overall filler content (intended here as the sum of FR-filler and limestone) was always equal to 100% by weight of the base bitumen. These ternary blends are consequently defined as CAx or CMx where x is the weight fraction relative to the FR-filler (e.g.

in CA20 total filler is composed by 80% of limestone and 20% of ATH-3). Table 3.5 synthetically describes the asphalt mastics analysed in this second step.

Table 3.5 Binary and ternary blends: weight fractions.

Asphalt Mastic	C	MH	ATH-1	ATH-2	ATH-3
100C	1.0				
100MH		1.0			
100ATH-1			1.0		
100ATH-2				1.0	
100ATH-3					1.0
CA20	0.8		0.2		
CA40	0.6		0.4		
CA60	0.4		0.6		
CA80	0.2		0.8		
CM20	0.8	0.2			
CM40	0.6	0.4			
CM60	0.4	0.6			
CM80	0.2	0.8			

3.1.4 Asphalt mixtures

Asphalt mixture is composed of asphalt binder, mineral filler and mineral aggregates. Moreover, the composition can be dramatically different depending on the content of bitumen and the selected aggregate gradation. Therefore, a large number of variables which significantly affect the overall fire behaviour of the mixture can be identified.

With the aim of exploring all these aspects, the following series were prepared.

Two distinct aggregate gradations were considered: open and dense graded mixtures. Furthermore, keeping constant the aggregate gradation, the influence of the physical properties of aggregates was investigated.

Particle size distributions were defined according with ANAS requirements (2010) [5] for dense and porous wearing courses. Moreover, the selected curve for dense graded mixture satisfied also the SHRP/Superpave requirements [6] for a dense wearing course with nominal maximum aggregate size of 12.5 mm. The aggregate particle size distributions are displayed in Figure 3.2.

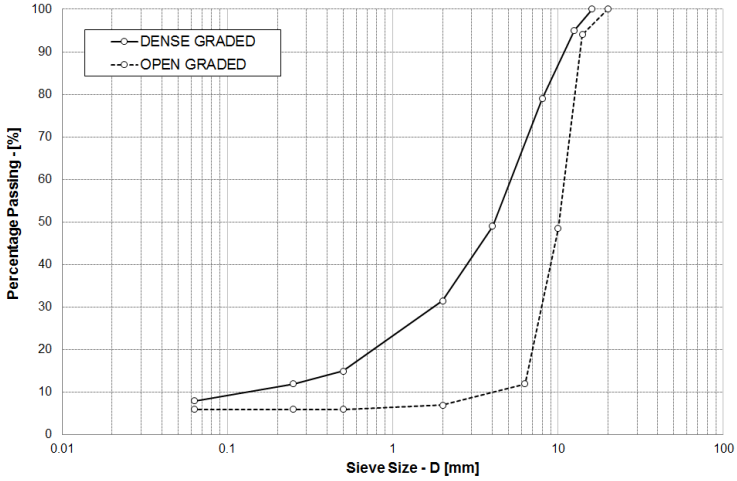

Figure 3.2 Particle size distributions for open and dense graded mixtures.

Initially, three different dense graded mixtures were produced with the aim to highlight the influence of aggregates on the fire behaviour of asphalt mixtures. Limestone 0÷4 mm fraction was combined with the 4÷16 mm fraction composed of porphyry, EAF steel slag, and LECA (light expanded clay aggregates). The specific gravity of porphyry, EAF, and LECA were respectively equal to 2.58, 3.92, and 1.13 gcm^{-3}. The thermal conductivity of LECA aggregates provided by the supplier was equal to 0.13 $Wm^{-1}K^{-1}$. No technical data were available for the EAF aggregates while for porphyry aggregates an average thermal conductivity value of 2.80 $Wm^{-1}K^{-1}$ could be derived from literature [7].

Open graded mixture was produced with the following fractions: 0÷4 mm limestone and 4÷20 mm crushed porphyry; in this case, only natural aggregates were used in order to focus the attention on the aggregate gradation. The asphalt binder was kept constant for all the asphalt mixtures produced and equal to 5.5 wt% referred to the weight of mineral aggregates. This strategy allowed to investigate the effect of the structure of the mixtures, being independent of the content of the combustible portion. Only one kind of asphalt binder was used in order to limit the number of variables. Based on the results of flammability and thermal stability analyses, bitumen B50 was then selected.

The mineral filler content was chosen in order to obtain asphalt mastics characterized by bitumen/filler ratio equal to 1/1 (wt/wt) whose flammability and thermal stability were studied in the first step of the thesis. Table 3.6 summarizes the asphalt mixtures prepared in this first phase.

After having investigated the role of physical properties of aggregates, the influence of nanomodified asphalt binder was taken into account. Thus, for both the aggregate gradations considered two further series were prepared by using the asphalt binder modified with 3.33wt% of organomodified-montmorillonite previously studied. This nanomodified binder is subsequently referred to as 3.33BC.

Table 3.6 Asphalt mixtures identification and composition.

Asphalt Mixture ID	Aggregate Grading	Coarse Fraction (> 4 mm)	Theoretical Maximum Specific Gravity G_{mm}	Air Voids content	Bulk Specific Gravity G_{mb}
	[-]	[-]	[gcm^{-3}]	[%]	[gcm^{-3}]
D-BC	Dense	Porphyry	2.444	6.91	2.275
D-EAF	Dense	EAF Steel Slag	2.997	6.95	2.789
D-LECA	Dense	LECA	1.686	6.81	1.571
O-BC	Open	Porphyry	2.430	22.3	1.888

Figure 3.3 shows the internal structure of the asphalt mixtures analysed in the first step of the analysis. It is worth noting that only the “black” face of the sample was exposed to the radiant heating in cone calorimeter test.

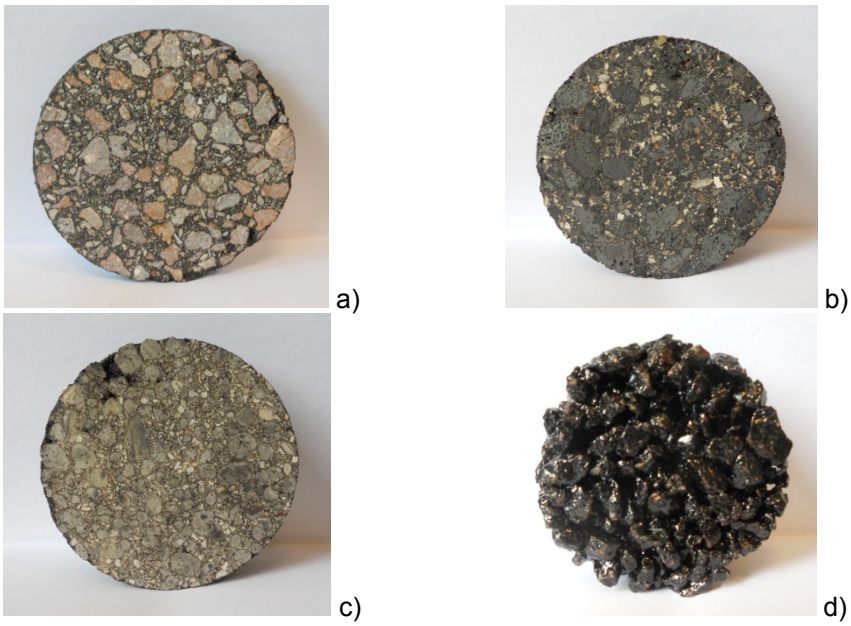

Figure 3.3 First phase: a) D-POR; b) D-EAF; c) D-LECA; d) O-POR.

Finally, the influence of mineral filler was addressed. Magnesium hydroxide named MH and aluminium hydroxide named ATH -3 were used to prepare open and dense graded mixtures with both neat and nanomodified asphalt binders. Table 3.7 provides an overall description of the FR-asphalt mixtures prepared in this second section.

Table 3.7 FR-Asphalt mixtures identification and composition.

Asphalt Mixture ID	Asphalt Binder	Asphalt Binder Content	Mineral Filler	Mineral Filler Content
	[-]	[%wt]	[-]	[%wt]
O-BC	B50	5.5	C	5.5
O-BA	B50	5.5	ATH-3	5.5
O-BM	B50	5.5	MH	5.5
O-NBC	3.33BC	5.5	C	5.5
O-NBA	3.33BC	5.5	ATH-3	5.5
O-NBM	3.33BC	5.5	MH	5.5
D-BC	B50	5.5	C	5.5
D-NBC	3.33BC	5.5	C	5.5
D-NBA	3.33BC	5.5	ATH-3	5.5
D-NBM	3.33BC	5.5	MH	5.5

For each asphalt mixture, three 100 mm diameter cylindrical samples were prepared by using a Superpave gyratory shear compaction technique, with a vertical pressure of 600 kPa and setting the compaction level to 100 gyrations, which is the recommended N_{des} for traffic within the range 10÷30 MESALs. During compaction, the temperature was kept constant at 130 °C. In order to comply with ISO 5660-1:2002 requirements for cone calorimeter test samples, the specimens were cut to obtain 100 mm diameter and 50 mm height cylindrical samples.

3.2 Methods

In this section the testing methods used are briefly described. The testing methods for the evaluation of fire retardancy are not univocally defined in technical specifications for asphalt pavements and materials. The first approach was therefore to observe the techniques used for polymers for which many national and international bodies establish testing methods to be adopted.

3.2.1 Thermal gravimetric analysis (TGA)

TGA is an analytical method in which the mass change of a sample is measured as a function of the temperature and time, where the mass change of a solid probe is observed during a known heating or cooling process. The most common application of this is the heating process with a constant heating rate. Changes in the mass can have the following causes:

- physical processes such as phase transformation;

- chemical decomposition (breakup of a chemical compounds into elements or smaller compounds);
- chemical reaction mass loss and increase.

From the changes in the mass, the reduced chemical reaction mechanisms can be derived or the composition of the test specimen can be determined. More information about TGA can be obtained from literature [8].

TGA was performed using a Q500 thermogravimetric analyser produced by TA Instruments under air atmosphere on 5.0 ± 0.5 mg samples with the following procedure: specimens were heated at 50°C, then a ramp of 10.00°C/min was applied until 900 °C under air flow.

3.2.2 Limiting oxygen index (LOI) test

Ignitability was assessed by the Limiting Oxygen Index (LOI) test which determines the minimal oxygen concentration in an oxygen/nitrogen mixture which allows the sample to burn in a stable way. The higher is LOI the higher is the oxygen concentration required to burn. Since oxygen volumetric content in atmosphere is approximately 21%, materials characterised by LOI bigger than 21 will burn with difficulties or will not even ignite, being their oxygen request bigger than the natural supply. An effective FR should significantly increase the LOI of the base materials. Since no technical specifications are available for LOI of asphaltic materials, the experimental procedure was initially based on the ASTM D-2863-10 ‘‘Standard Test Method for Measuring the Minimum Oxygen Concentration to Support Candle-Like Combustion of Plastics (Oxygen Index)’’.

LOI test was performed by Limiting Oxygen Index Analyser LOI-Smoke-230, from Dynisco & Alpha Technologies, USA equipped with a smoke detector. The basic test procedure was the same as for polymeric materials, being the most important modification related to sample preparation and geometry. In the case of polymeric materials, LOI test is performed on self-supporting samples, flexible films or sheets.

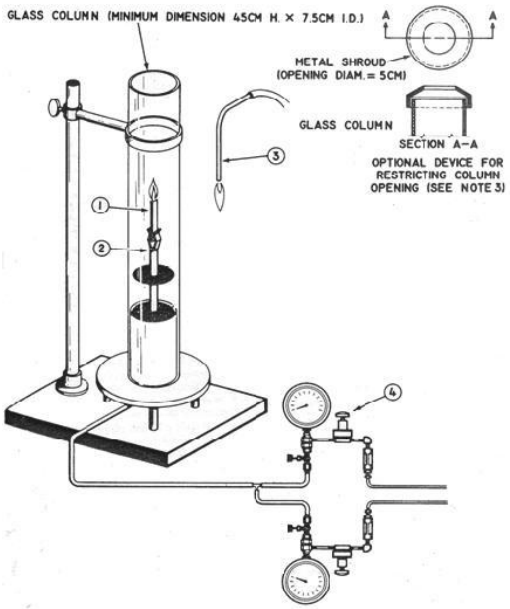

Figure 3.4 Description of LOI apparatus.

A first problem to be solved while transferring the methodology to asphaltic samples was a proper selection of the specimen type, since they are subjected to consistent melting and dripping while burning. A possible solution is the loading of binder with high quantities of mineral aggregates as in the case of asphalt mixtures. However, in the latters, the largest stones may have dimensions higher than the sample thickness and the largest aggregate grains drop as the sample is ignited [9]. Thus, a first attempt was carried out by preparing samples where only mineral powder was employed to simulate the presence of aggregates. A first set of samples was prepared by pouring B50/C (1/1 w/w) blends into moulds, previously coated with a thin silicon rubber film in order to facilitate the subsequent sample extraction. Specimens' dimensions were 60 x 10 x 10 mm. Before performing LOI test, samples were cleaned from silicon residue. Unfortunately, the samples revealed to be inappropriate since as the gas flame was drawn up to the top of the sample they started melting without igniting even at high oxygen concentration. A second set of samples with asphalt binder/mineral powder equal to 1/3 w/w was prepared and tested, but with similar results. Therefore, a completely different kind of samples was prepared by using synthetic pumice stone as a porous and inert support.

Two different geometries were obtained by cutting the pumice stone through a band saw: type A had dimensions chosen in accordance to ASTM D2863-10 requirements for self-supporting polymeric materials: 100 mm length, 19 mm width and 4 mm thickness. Type B, not indicated in ASTM requirements, was a squared cross section specimen with dimensions: 100 mm length, 9 mm width and 9 mm thickness. The selection of the best geometry and the calibration of

the test method were obtained by using asphalt binder B50. The asphalt binder was heated at 170 ± 5 °C, then the porous supports were dipped into the liquefied asphalt in order to cover a length of 50 mm with a thin asphaltic film. The time of immersion was the same for all samples and equal to 30 s during which asphalt could fill the most superficial voids. Samples were then cooled to room temperature before performing LOI test. The glass chimney of LOI analyser was saturated with an oxygen/nitrogen mixture with controlled oxygen content and flow rate of 40 ± 2 mm/s. The gas flame was then drawn up to the top surface of the upper end of the sample, paying attention not to maintain the flame against the vertical faces or edges of the specimen.

According to ASTM D2863-10 Procedure A, the flame was applied for up to 30 s, removing it every 5 s to observe whether or not the entire top surface of the specimen was burning on its own. Both specimen geometries allowed successfully test execution. The oxygen/ nitrogen mixture was characterised by a specific Oxygen Index, which is defined as the following equation (3.1) where C_{O2} and C_{N2} are, respectively, the oxygen and nitrogen volume percentages.

$$OI\ (\%) = \frac{C_{O2}}{C_{O2} + C_{N2}} 100 \tag{3.1}$$

Limiting Oxygen Index was then defined as the minimum Oxygen Index (OI) that met the criteria specified in the ASTM D-2863-10 for self-supporting moulding materials: (1) OI correspondent to a period of burning after ignition equal to 180 s, or (2) OI correspondent to the extent of burning below the top of the specimen equal to 50 mm. When 180 s or 50 mm were reached, test was forcedly stopped by turning off oxygen flow.

Test procedure was as follow: a first oxygen concentration was chosen and if none of the criteria (180 s or 50 mm) was met, the corresponding OI was marked as C_X and the test repeated increasing the OI until the specified criteria were met. The corresponding OI was named C_O, which is the minimum OI that allows a sustainable burning. Once the minimum C_O and the maximum C_X are identified, the LOI test procedure is repeated for at least five times both at C_O and C_X concentrations to validate the results and LOI is assumed equal to C_X.

Once the most proper sample geometry was identified, twenty samples were prepared for each asphalt binder and mastic to be tested. For all the samples the asphalt quantity was equal to 1.2 ± 0.2 g. Since the surface of the sample covered by asphalt and the porosity of the support are fixed, it is reasonable to assume that all the specimens were characterised by a similar thickness of the asphaltic film exposed to the flame.

3.2.3 Cone calorimeter test

Cone calorimeter was performed at Fire Laboratories of the CNR-IVALSA Institute, in San Michele all'Adige (TN) by means of a FTT (Fire Testing Technology) cone calorimeter apparatus.

Cone calorimeter has been widely used to analyse fire properties of several materials and it is extensively described by Babrauskas [10,11]. This test

consists in subjecting samples exposed in horizontal orientation to a specified external heat flux within the range 0-100 kW/m^2. ISO 5660-1:2002 (Reaction to fire tests - Heat release, smoke production and mass loss rate. Cone calorimeter method) requires squared samples with sides measuring 100 mm while the maximum allowed thickness is equal to 50 mm.

The external irradiance is provided by a cone-shaped radiant electric heater; the specified heat flux is kept at the defined level through three thermocouples symmetrically positioned and in contact with the heater element. Figure 3.5 provides a description of the cone calorimeter apparatus.

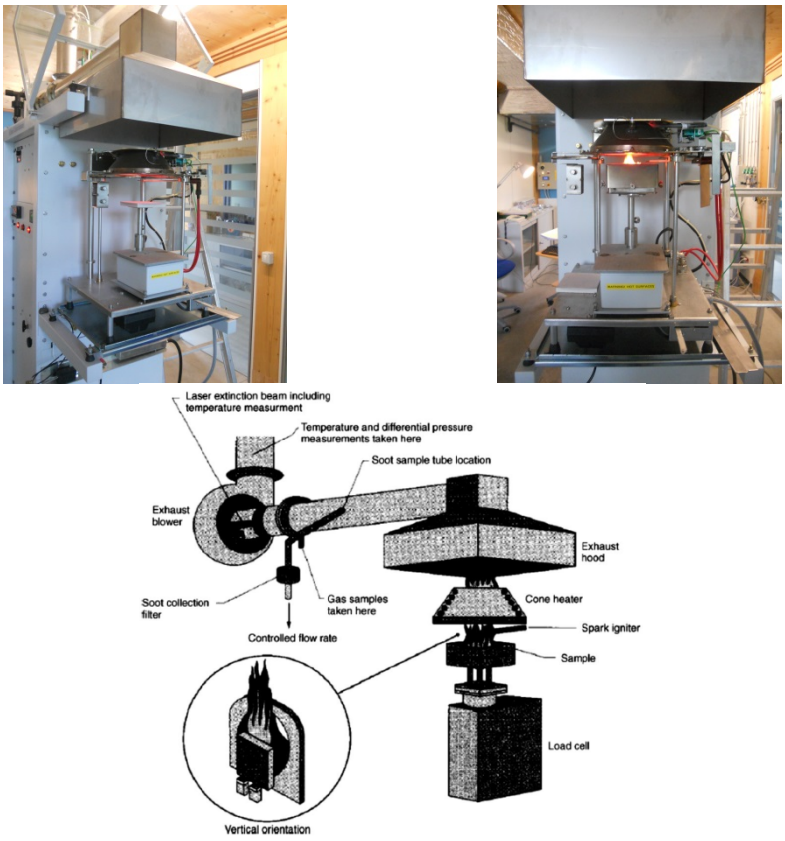

Figure 3.5 Schematic of cone calorimeter apparatus [10].

Schartel [12] highlights the key-role of the specimen thickness in influencing all the important fire properties which can be defined through this test. Moreover, the thickness to be tested should be defined by the end-use conditions, preferring thicker samples to study material properties. So, keeping in mind that the main objective of the present research is the assessment of asphalt pavements fire properties, the maximum allowed thickness equal to 50 mm was

chosen. This choice is also supported by previous literature (Babrauskas [11] and Drysdale [13]).

Cone calorimeter test covers the ignition phase, followed by flaming combustion. During the test, a number of important fire properties can be defined, thus allowing a comparison between different materials in terms of fire performance. The most important parameters are the Heat Release Rate (HRR), the Total Heat Release (THR), the mass loss, the time to ignition (t_{ig}), the Total Smoke Release (TSR), and the CO and CO_2 emissions. Among these, HRR is broadly considered the most significant factor in the assessment of materials' fire hazard [11].

HRR is evaluated through the oxygen consumption method, introduced by Thornton [14] and Huggett [15], by measuring the flow rate of the exhaust gases through the duct system and the oxygen depletion in this flow.

The whole HRR curve represents the evolution of the Heat Release Rate with respect to time and provides the best representation of the fire behaviour controlled by specific properties of the tested materials. However, for practical reasons, it is often condensed by few characteristic values, such as its maximum (Peak of Heat Release Rate, PHRR) and the average evaluated referring to the first 180 seconds after ignition (HRR-180). The latter is considered more reliable than the former to predict the peak real-scale HRR in actual fire scenarios [11].

Another important parameter defined through the Cone Calorimeter test is the THR which is formally the integral of the HRR curve with respect to time, thus determining the heat output up to an assigned point. THR is strictly related to the mass loss which is measured through a weighing device during all the duration of the test. Of course, mass loss is mainly governed by the pyrolysis, which is in turn controlled by the net heat flux applied to the surface, the decomposition temperatures, heat transfer and kinetics. Here the total mass loss is reported, calculated as the difference between the weights of the specimen at the beginning and at the end of the test.

From cone calorimeter test, the main parameter which gives information about ignition is the time to ignition (t_{ig}) which can be defined as the time necessary for the mass loss rate to reach its critical value or, in other words, it is the time necessary for the top surface to reach its ignition temperature.

Finally, the products of combustion, such as smoke, CO and CO_2 production can highlight further more important information about the fire risks in confined environments like highway tunnels, even if correlations between data obtained from this bench-scale test and large-scale tests are complex and not yet fully understood [12]. The smoke production is evaluated on the basis of the theory of the attenuation of a beam of light by suspended aerosol particulates, thus it is expressed in m^2. The amount of smoke is measured during all the duration of the test and the Total Smoke Production (TSP) is referred to the entire testing period. The TSR is then calculated as the ratio of the TSP to the exposed surface area; this is the reason why TSR is expressed in terms of $m^2 \cdot m^{-2}$. Finally, CO and CO_2 yields are measured through gas analyser and are evaluated per unit of mass loss ($kg \cdot kg^{-1}$).

A preliminary phase was planned in order to verify the effective applicability of the cone calorimeter test to asphaltic materials. First, the influence of the specimen shape was analysed by considering two possible geometries: circular shape (100 mm diameter) or square shape (98 mm side), see Figure 3.6. The latter is specifically required by the ISO 5660-1 but the former is doubtless the most common for road engineering, both for laboratory samples and for in-situ core drilling. However, the circular shape specimens have side protected only by the aluminium foil and not by the retainer frame, so possible influence of lateral flame spreading deserves careful analysis. The analysis was performed on D-POR mixture.

Figure 3.6 Square and circular samples for the cone calorimeter test.

Circular specimens generally showed a greater standard deviation than the square ones. Moreover, square specimens lead to slightly higher values for each considered parameter. However, the fire response parameters defined using square samples remain always inside the variability range identified by circular specimens. Moreover, the main geometrical parameter that influences the cone calorimeter test is the total exposed sample surface [16] and in this case, the two exposed areas are negligibly different (88.4 cm^2 vs 75.3 cm^2). Of course, the main weak point of the circular geometry remains the poor protection of the specimen side, provided only by the aluminium foil. Furthermore, samples obtained by cutting into two parts a single lab compacted asphalt mixture could be characterized by different bitumen contents, thus negatively affecting the reliability of the assessed fire performance. However, the obtained results didn't show significant differences depending on the position of the sample in the original specimen, thus this aspect can be assumed negligible for this particular case.

Before testing, samples were conditioned at 23 ± 2°C, and relative humidity equal to 50 ± 5% in accordance with ISO 554. Then, conditioned samples were wrapped in a single layer of aluminium foil to cover the bottom and sides of the specimen, thus avoiding mass-transfer along all boundaries except for the burning face of the specimen. Finally, the wrapped specimen was adjusted in a specimen holder and covered by a stainless steel retainer frame. The distance between the bottom surface of the electric heater and the top of the specimen was set to 25 ± 1 mm.

A fundamental parameter to be set is the external heat flux applied to the samples. In previous experiences [17,18], it was observed that asphalt mixture samples did not ignite if exposed to radiant fluxes smaller than 30 kW/m^2. It is also worth noting that cone calorimeter setup aims at reproducing a forced-flaming combustion scenario which is typical of developing fires or of well-developed fires in a post-flashover scenario (heat fluxes higher than 50 kW/m^2). Moreover, the external irradiance should be defined considering what happens during a vehicle fire in tunnel where gas temperature over 1000°C can be reached. Thus, if ignition in post-flashover fires is the condition to be simulated, external heat fluxes over 70 kW/m^2 should be considered, and preferably closer to 100 kW/m^2 which is the maximum attainable flux by the standard cone calorimeter.

3.2.4 Rheological characterization of asphalt mastics

With the aim to investigate the influence of different mineral fillers on the physical and mechanical properties of asphalt mastics, rheological analysis was performed with a dynamic shear rheometer (DSR). A parallel plates testing system was used. The geometry (25 or 8 mm diameter plates with 1.00 or 2.00 mm testing gap) was selected according to the expected stiffness [19].

The samples preparation was referred to EN 12594. Special attention was then paid to the thermal history and the storage conditions because of their influence on rutting indicator measurements [20,21,22].

The specimens were squeezed out between the two plates, trimmed off using a hot spatula, and then the gap was set as required in order to guarantee the correct geometry of each sample. The temperature was controlled by a Peltier conditioning system with a maximum admitted deviation of ±0.01°C.

Linear viscoelastic conditions were previously established using amplitude sweep tests. Stress-controlled frequency sweeps were then carried out using angular frequencies from 1 to 100 rad/s and temperatures ranging from 0 to 80°C with 10 °C steps. Complex (|G*|), storage (G_0), and loss (G_{00}) moduli and phase angle (δ) were measured and used to generate rheological master curves according to the TTSP [23], at reference temperature equal to 20°C.

Furthermore, creep-recovery test, multiple stress creep recovery test (MSCR test), and viscosity tests were performed. Creep-recovery test was performed at 40°C and repeated for each sample at three different shear stresses: 100, 1000 and 10000Pa. The test is performed by applying the defined stress for 10 s and then 30 s of recovery where the torque is set to zero and only the strain is recorded. Data were recorded with 0.5 s frequency.

MSCR test was performed according to the following sequence of 1 s creep loading followed by 9 s recovery. Each phase of loading-recovery was repeated for 10 cycles for 11 different stress levels, varying in the range 25÷25600 Pa [24]. Each sample was tested starting from the lower stress level with no time lag between cycles. The stress level doubles after every 10 cycles. The loss compliance, J_{NR}, was then defined for each stress as the ratio between the

average non-recovered strain at the end of 10 cycles and the stress applied in those cycles.

The test results are largely influenced by the shear stress and the temperature at which samples are tested. In order to evaluate the influence of temperature, the test was then repeated for each specimen at 3 characteristic temperatures: 50, 60 and 70°C.

Finally, to investigate the behaviour of asphalt mastics in the whole range of the operative temperatures, the experimental program focused on the flow properties at the mixing and compaction temperatures. Viscosity was then measured using rotational rheological tests to evaluate the blend flow curve at different temperatures, from 80°C to 160°C. For each temperature, the measure was extended for 4 minutes in order to evaluate the influence of the transient thixotropic effects. In the entire temperature range investigated, the measurements were performed in strain-controlled mode using shear rates from 10^{-2} to 10^{-3} s^{-1} [25,26].

References

[1] The shell bitumen handbook. 5th ed. London: Thomas TELFORD Publishing; 2003. p. 29–41.

[2] Jimenez-Mateos JM, Quintero LC, Rial C. Characterization of petroleum bitumens and their fractions by thermogravimetric analysis and differential scanning calorimetry. Fuel 1996; 75:1691–700.

[3] Kandhal P. Evaluation of baghouse fines for hot mix asphalt. NAPA IS 127; 1999.

[4] Fire retardancy of polymeric materials, 2nd ed. In: Wilkie CA, Morgan AB, editors. CRC Press; 2010.

[5] Capitolato Speciale ANAS 2010 – A.N.A.S. S.p.A.

[6] American Association of State and Highway Transporation Officials. Standard specification for SuPerPave volumetric mix design. AASHTO M323-04 2004.

[7] Vosteen HD, Schellschmidt R. Influence of temperature on thermal conductivity, thermal capacity and thrrmal diffusivity for different types of rocks. Physics and Chemistry of the Earth 2003; 28:499-509.

[8] Gabbott, P.; Applications of thermal analysis; 1st ed.; Blackwell Pub., Ames, Iowa, 2007.

[9] Cong P, Yu J, Wu S, Luo X. Laboratory investigation of the properties of asphalt and its mixtures modified with flame retardant. Constr Build Mater 2008;22(6):1037–42.

[10] Babrauskas V., Parker W.J. (1987). Ignitability measurements with the Cone Calorimeter. *Fire and Materials,* 11, pp. 31-43.

[11] Babrauskas V., Peacock R.D. (1992). Heat Release Rate: The Single Most Important Variable in Fire Hazard. *Fire Safety Journal,* 18, pp. 255-272.

[12] Schartel B., Hull T.R. (2007). Development of fire-retarded materials. Interpretation of cone calorimeter data. *Fire and Materials*, 31, pp. 327-354.

[13] Drysdale, D, "An introduction to fire dynamics"; 2nd ed.; J. Wiley, Chichester, 1999.

[14] Thornton W.M. (1917). The relation of oxygen to the heat of combustion of organic compounds. *Philosophical Magazine and Journal of Science,* 33, pp. 196-203.

[15] Huggett C. (1980). Estimation of rate of heat release by means of oxygen consumption measurements. *Fire and Materials,* 4, pp. 61-65.

[16] Lindholm J., Brink A, Hupa M. (2012). Influence of sample size on cone calorimeter results. *Fire and Materials,* 36(1), pp. 63-73.

[17] Colwell, S. et al: "Test Methodologies for Reaction to Fire of Pavement Materials". Document SAM-04-D20, SAMARIS (Sustainable and Advanced MAterials for Road InfraStructure) Research Project, 2005.

[18] Carvel, R.O. and Torero, J.L.: "The contribution of asphalt road surfaces to fire risk in tunnel fires: preliminary findings". Proceedings Int. Conf. Risk and Fire Engineering for Tunnels, Stations and Linked Underground Spaces, 19-20 April 2006, Hong Kong. Organized by Tunnel Management International, Tenbury Wells, Worcs., United Kingdom.

[19] Polacco G, Vacin OJ, Biondi D, Stastna J, Zanzotto L (2003) Dynamic master curves of polymer modified asphalt from different geometries. Appl Rheol 13:118–124.

[20] Anderson, DA, Marasteanu, MO, "Factors affecting the variability in the SHRP binder tests", 79th Annual Report, Transportation Research Board (TRB), Washington D.C., USA, 2000.

[21] Soenen, H., De Visscher, J., Vanelstraete, A., Redelius, P., "The influence of thermal history on binder rutting indicators", International Journal of Road Materials and Pavement Design, Vol.6, Issue 2, 2005.

[22] Soenen, H., De Visscher, J., Tanghe, T., Vanelstraete, A., Redelius, P., "Selection of binder performance indicators for asphalt rutting based on triaxial and wheel tracking test", Journal of the Association of Asphalt Paving Technologists, Vol. 75, USA. 2006.

[23] Ferry JD (1980) Viscoelastic properties of polymers. Wiley, New York.

[24] Wasage TLJ, Stastna J, Zanzotto L.(2011) Rheological analysis of multi-stress creep recovery (MSCR) test. International Journal of Pavement Engineering 12(6):561-568.

[25] Bahia HU, Hanson DI, Zeng M, Zhai H, Khatri MA, and Anderson RM (2001) Characterization of modified binders in Superpave Mix Design, NCHRP Project 9-10, Transportation Research Board – National Research Council, Washington DC, USA.

[26] Yildrim Y, Solaimanian M, Kennedy TW (2000), Mixing and compaction temperatures for Hot Mix Asphalt Concrete, Research Project 0-1250-5, South Central Superpave Center for Transportation Research, University of Texas at Austin, Texas, USA.

4 Asphalt binders and mastics

4.1 Neat and SBS-modified asphalt binders

The results of flammability and thermal stability analyses performed on asphalt binders are discussed in this section.

As shown in Chapter 3, three different neat asphalt binders and an SBS-modified binder were first considered.

Asphalt binders B50, B70, B170 and B50-SBS were initially analysed through TGA under air atmosphere (DTG: first derivative of sample mass over temperature curve, usually named “TG” curve - Figure 4.1 and Figure 4.2).

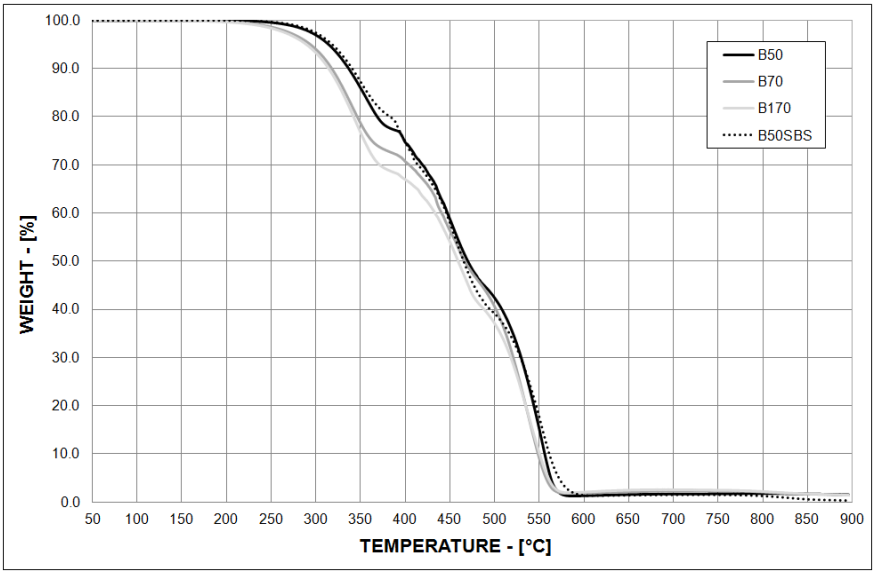

Figure 4.1 TG curves of asphalt binders.

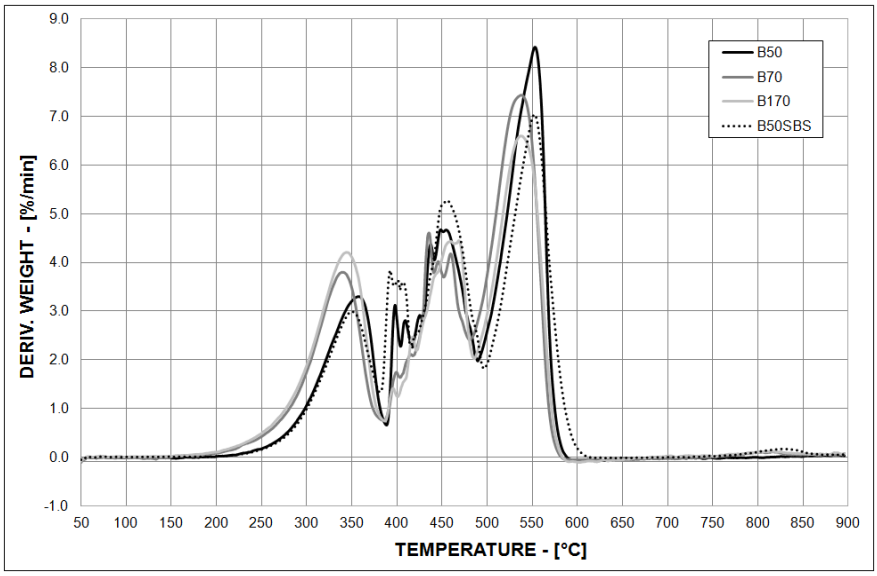

Figure 4.2 DTG curves of asphalt binders.

As already observed in previous works [1-4], the thermal decomposition of asphalt binder under air atmosphere is somehow multistage and occurs in three (or four) distinct phases. In agreement with the observations of Jimènez et al. [1], the first phase is characterized by a continue mass loss due to the volatilization of the lightest components, such as saturates and apolar aromatics, which ends when temperature reaches 380°C, irrespective of the asphalt binders.

The second phase covers the range 380–500°C and is characterized by the presence of several peaks in the DTG curve. In other cases, as showed in Xu et al. [3], only a single peak was observed during this second step where the decomposition of resins, together with aromatics and some asphaltenes, becomes more important.

Finally, there is a third phase, which basically ends at around 600°C and shows the highest value of mass loss rate, that can be mainly ascribed to the asphaltenes thermal decomposition, even if the contributions of resins and aromatics are still relevant.

It is important to underline that the mass loss is due to the contemporary contribution of a simple physical evaporation and to the development of light components due to thermal degradation and pyrolysis reactions. While moving from the lowest to the highest temperature, the relative weight of the two contributions obviously shifts in favour of the second one. The main characteristics of the TG and DTG curves are pointed out in Table 4.1 and Table 4.2: the temperature corresponding to 2% mass loss ($T_{2\%}$), the maximum mass loss rate (M_{PEAK}), the temperature corresponding to this maximum value (T_{PEAK}) and the final residue (M_F). Since different peaks are present, two couples of

M_{PEAK} and T_{PEAK} are identified: one is referred to the first phase (M^1_{PEAK} and T^1_{PEAK}) and the other (M^3_{PEAK} and T^3_{PEAK}) to the third phase.

Table 4.1 Main features in asphalt binder thermal decomposition.

Asphalt Binder	$T_{2\%}$	T^1_{PEAK}	M^1_{PEAK}	T^3_{PEAK}	M^3_{PEAK}	M_F
	[°C]	[°C]	[%/min]	[°C]	[%/min]	[%]
B50	288.9	358.2	3.3	552.8	8.4	1.56
B70	262.7	341.1	3.8	537.7	7.4	1.35
B170	257.3	343.9	4.2	537.4	6.6	1.48
B50SBS	293.7	350.5	3.0	552.5	7.0	0.29

No values are specified for the second phase because of its non-univocal definition. Mass losses corresponding to each phase are specified in Table 4.2.

Table 4.2 Mass loss values for each phase.

Asphalt Binder	I phase	II phase	III phase
	[%]	[%]	[%]
B50	22.72	32.45	43.28
B70	27.75	28.44	42.46
B170	31.61	28.69	38.23
B50SBS	19.78	40.58	39.35

The three unmodified asphalt binders show a few differences which can be related with their different composition and physical properties (Tables 3.1 and 3.2). In fact, pre-qualification results performed on the neat asphalt binders showed that the three base binders have a different Gaestel Index, with I_c(B170) > I_c(B70) > I_c(B50); also, the B170 is characterized by the highest content of saturates and aromatics (Table 3.2).

Basic rheological properties showed a similar trend (Table 3.1), with the complex modulus decreasing and the phase angle increasing as the Pen Grade and the Gaestel Index increase. So, during phase I, B50 shows the higher thermal stability compared to the other unmodified binders: the mass loss is low and the DTG peak is reached at the highest temperature. This trend is partially reversed during phase III, where the DTG peak of B50 is still the highest one.

These results are directly linked with the chemical composition and coherent with the low content of light fraction (phase I) and, conversely, with the high content of asphaltene (phase III). Analogously, when considering the other base asphalts, there is a behaviour which reflects the distribution of mass losses in the three fractions. However, it must be noticed that no direct correlation between the relative abundance of the single S.A.R.A. fractions and the quantification of the single mass losses can be easily outlined. In fact, irrespective of their compositions, all asphalt binders were completely degraded during the test and the final mass residue is similar for all the three binders.

The case of modification with SBS deserves specific attention. B50 and B50-SBS curves are qualitatively similar and suggest that SBS mainly degrades during phase II together with a part of the light components which degrades in phase I in the unmodified binder. This is not surprising if we consider that the light components are also the most compatible with the polymer. In fact, they swell the polymer and remain entrapped in the polymer-rich phase which characterises the morphology of polymer-modified asphalts. In other words, the polymer somehow captures and hides part of the asphalt molecules, thus reducing their volatility. Analogously, also part of the resins is driven to the polymer-rich phase, thus altering their bonding with asphaltenes and anticipating their decomposition from phase III to phase II. This mechanism of polymer swelling and asphalt components migration is deeply discussed in [5]. Thus, based on thermogravimetric data, B50 shows the highest thermal stability, thanks to its lower content of the lightest fractions, and its modification with SBS partly shifts the volatilization/degradation of phase I to higher temperatures.

LOI analyses introduce further elements of discussion. As described in Chapter 3, the calibration of the test method was done using B50 and changing the sample geometry in order to outline the most appropriate one. LOI tests with Type A and Type B geometries were carried out and a great influence of the specimen cross section on both final results and combustion process was observed. With Type A geometry, B50 is characterized by a LOI value equal to 24% while, in case of Type B samples, the LOI becomes 26%. Moreover, the ignition of Type A samples always starts from a single edge of the top surface; conversely, ignition in Type B samples instantly involved the whole top surface. This fact influenced the subsequent flame spread on the vertical faces of the specimen. Indeed, in Type A samples, the flame front was inclined with respect to a horizontal alignment and propagated down with trapezoidal shape, thus making non univocal the reaching of the 50 mm criterion. Conversely, Type B samples showed a homogeneous progress, keeping the flame front sub-horizontal and at the same height on the entire vertical faces. Since Type B specimens demonstrated a more regular combustion progress, they were selected and used in all subsequent tests to define ignitability. During LOI test, the duration and extent of burning were recorded for each sample; thus a flame spread rate was calculated and reported, together with LOI and smoke emission, in Table 4.3.

Table 4.3 LOI values of asphalt binders.

Asphalt Binder	LOI	Flame spread rate	Smoke emission
	[%]	[mm/s]	[arbitrary units %]
B50	26	0.35	100
B70	26	0.37	77
B170	25	0.37	41
B50SBS	25	0.37	68

Of course, the obtained LOI cannot be directly compared with those of polymers, obtained by using the ASTM procedure, being the geometry of the sample an important parameter affecting the numerical data. Nevertheless, they are useful in order to have a self-consistent parameter to discern among flammability of asphalt binders.

LOI and rate of burning are slightly influenced by binder type, which, on the contrary, shows to be important with respect to smoke emission. Coherently with TGA results, the asphalt binders with the higher content of low molecular weight components show the lower LOI, the higher flame spread rate and the lower smoke emission (being 100 the arbitrary value assigned to B50). Again, the higher volatility of the light components plays an important role and probably favours the ignition process.

Once combustion is started, the temperature of the sample most likely corresponds to those of phase III in TGA and its propagation along the sample proceeds in a similar manner for all the binders, being all fractions equally involved. Nevertheless, the light components may easily pass in the gas phase, where the combustion process takes place, thus probably giving a higher conversion to water and carbon dioxide and therefore a reduced smoke emission.

With regard to the effect of SBS, the polymeric modification worsens asphalt binder flammability since LOI is decreased by a unit percent and the flames propagate down the sample a little bit rapidly. This is not surprising if we consider the unsaturated nature of the polymer and therefore its intrinsically higher sensitivity to flammability, which is reflected in a reduction of smoke emission with respect to the unmodified binder. Since the LOI values for the three asphalt binders were found to be quite similar, B50 was used in all subsequent asphalt mastics and mixtures formulation.

4.2 Organoclay-modified asphalt binders

B50 neat asphalt binder was then selected as the base bitumen for the production of organoclay-modified binders. Three increasing contents of nanoclay were considered: 3.33, 6.00, and 8.00%wt; the obtained blends were tested by means of LOI test and TGA analysis.

LOI and TGA results are synthetically reported in Table 4.4. Moreover, in Figure 4.3 and Figure 4.4 the TG and DTG curves are plotted. The parameters reported in Table 4.4 are referred to the temperatures corresponding to the first and third peaks (T^1_P and T^3_P) of DTG, while no specific values are pointed out for the intermediate phase which has a multi-peak trend. $T_{10\%}$ and $T_{50\%}$ are the temperatures corresponding to mass losses respectively equal to 10% and 50%. Residue is the final mass at the end of the test at 900°C.

Table 4.4 TGA and LOI results of organoclay-modified asphalt binders.

	TGA					**LOI**	
Asphalt Binder	T^1_P	T^3_P	$T_{10\%}$	$T_{50\%}$	Residue	LOI	Flame Spread Rate
	[°C]	[°C]	[°C]	[°C]	[%]	[%]	[mm/s]
B50	358.2	552.8	336.9	470.2	1.56	26	0.35
3.33BC	350.6	555.1	338.1	469.0	3.11	23	0.24
6.00BC	357.6	576.7	351.0	470.1	4.51	21	0.19
8.00BC	353.6	575.2	344.4	472.4	5.16	21	0.17

Considering the effect of nanoclay-modification, it can be observed that both the onset decomposition temperatures and T^1_P seem not to be affected by clay addition. On the other hand, clay plays an important role in governing the peak values of the first and third phases, with the latter dramatically reduced and postponed to higher temperatures with increasing 20A content. A completely different outcome is found considering the second phase where the 20A seems to concentrate the mass loss in a more narrow range of temperatures and consequently leads to higher peak values.

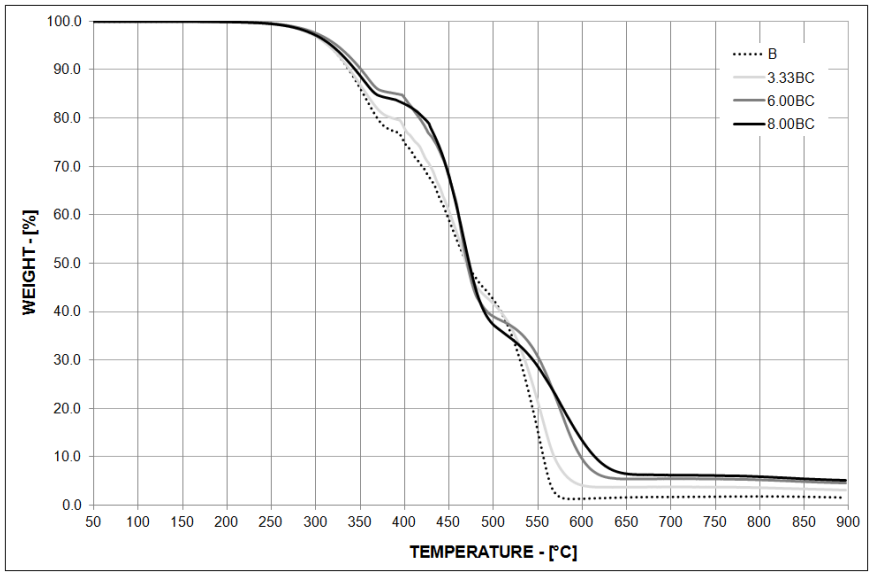

Figure 4.3 TG curves of organoclay-modified asphalt binders.

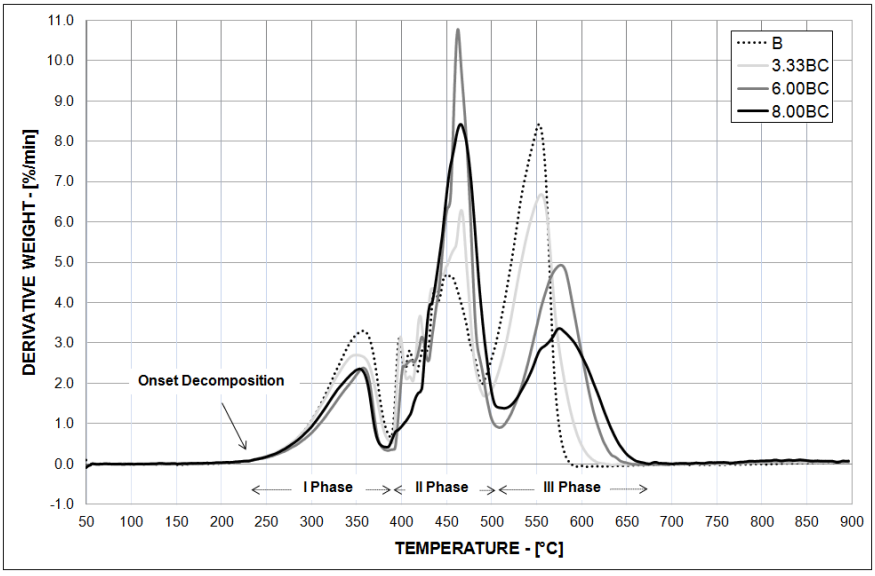

Figure 4.4 DTG curves of organoclay-modified asphalt binders.

These results could be interpreted keeping in mind what the organoclay modification involves. Indeed, thanks to the organic modification of the original sodium montmorillonite through specific surfactants (in this case: $Me_2(HT)_2NCl$),

the asphalt may be able to intercalate the organoclay and partially exfoliate its stacks [6,7]. In this way, the introduction of layered silicate intercalated and in some measure exfoliated into the bitumen matrix results in a sort of labyrinth effect [8] which limits the escape of flammable volatiles, thus significantly reducing the mass loss rate. The protective mechanism is also strengthened by the formation of a multi-layered carbonaceous-silicate structure on the surface of the asphalt binder nanocomposites, as well as for polymers nanocomposites [9].

The combination of these actions protects the substrate from heat and oxygen and slows down the escape of flammable volatiles generated during asphalt binder decomposition. A parallel mechanism of char forming was also introduced by Lewin [10] who suggested that the accumulation of montmorillonite layers on the pyrolysis material surface results also from the migration of silicates driven by their lower surface free energy. Moreover, this migration is further aided by temperature and viscosity gradients which foster a convective motion from the interior towards the external portion of the sample.

On the other hand, the significant increase of mass loss rate during the second phase worsens base asphalt binder thermal stability within the range 400÷500°C. This fact could be related to the thermal decomposition of the organic surfactants [11] or to a postponed decomposition of the lightest fractions which is shifted to higher temperatures. It is also worth noting that nanocomposite asphalt binders are characterized by higher $T_{10\%,}$ thus outlining an effective slowdown of the early thermo-oxidative decomposition. Nevertheless, $T_{50\%}$ is not quite affected by clay addition and is almost equal to 470°C, irrespective of the asphalt binder composition.

Finally, increasing 20A content leads to increased final residue thanks to the incombustible silicate, thus indicating that modified clay can partially act as an inert nano-filler.

During LOI test, time and extent of burning were also recorded, thus outlining a sort of flame spread rate referred to the LOI of each blend. The first important result is the significant decrease in LOI values with increasing content of organo-modified clay (Table 4.4). Thus, nanocomposite asphalt binders not only show no improvement in LOI, but even a significant worsening (Δ_{MAX} = -5%).

On the other hand, the combustion process is significantly slowed down, with a decrease in the flame spread rate almost equal to 50% in the case of 8.00BC binder. Moreover, during combustion the base asphalt specimen showed a consistent dripping, which was not observed in the presence of clay.

These results are consistent with LOI tests performed to assess flammability of polymer nanocomposites [12]. The reason of this outcome probably resides in the increased melt viscosity which reduced dripping propensity and slowed down the flame spread velocity. Anyway, this fact can also show negative consequences, as highlighted by the significant decrease in LOI values. Indeed, because of wicking more combustible material remained in the original location attacked by fire rather than flowing down to the sample. Thus, more material is subjected to pyrolysis resulting in a higher flammable volatile release. Asphalt flammability is therefore worsened, coherently with results found by Schartel et

al. [13] for a few polymeric materials. As well as for polymer nanocomposites [10], beneficial effects of barrier forming cannot be outlined in this test because of the too small external heat flux applied through the gas flame.

4.3 Asphalt mastics

4.3.1 Flammability and thermal stability

In this section the results of the analysis performed on asphalt mastics will be described starting from the thermal characterization of each mineral filler.

TG and DTG curves are reported in Figure 4.5 and Figure 4.6.

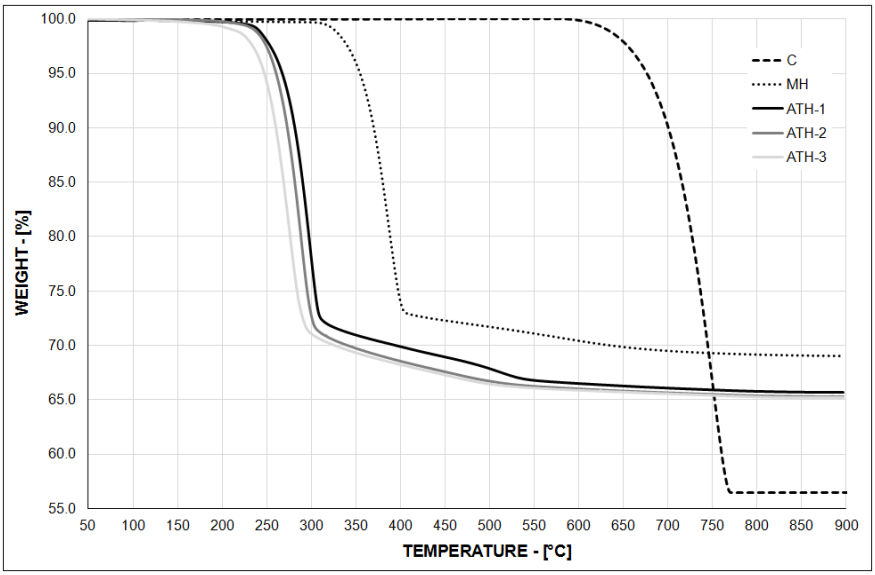

Figure 4.5 TG curves of mineral fillers.

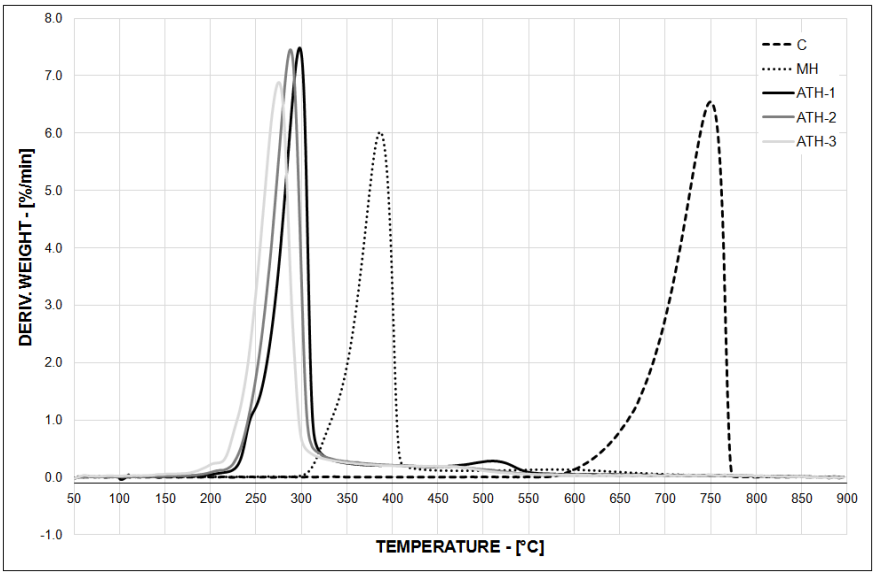

Figure 4.6 DTG curves of mineral fillers.

Conventional limestone filler C is mainly composed of calcium carbonate ($CaCO_3$) which starts decomposing approximately at 650°C producing calcium oxide and carbon dioxide. This is an endothermic decomposition characterized by an enthalpy of 12070 J/g and leading to a final solid residue theoretically equal to 56.0%, corresponding to the calcium oxide content.

Magnesium hydroxide decomposes at 300-320°C producing magnesium oxide and water vapour; the endothermic decomposition has an enthalpy equal to 1450 J/g and the final solid residue is 68.9%.

Finally, aluminium hydroxide decomposes at the lowest temperature, around 200 °C, and produces aluminium oxide and water vapour while absorbing 1300 J/g; it is characterized by a final solid residue equal to 65.4%.

It is well known that the kinetics of the decomposition process can be significantly influenced by the morphology and particle size of the material and in fact the three ATH showed slight differences in the TG curves: the smaller the particle size, the lower the onset decomposition temperature. Of course, no significant differences were observed in the final solid residue.

It is worth noting that all mineral fillers can be appropriate to be used in Hot Mix Asphalt since all their onset temperatures are higher than the typical mixing temperature of the asphalt mixtures.

Different asphalt mastics were then analysed in order to outline the influence of conventional and FR fillers on flammability and thermal stability. As for the asphalt binders, they were initially analysed through TGA under air atmosphere. All the mastics were prepared using B50 and filler at 1/1 ratio by weight. Initially, only binary blends were analysed (see § 3.1.3) The obtained results are reported

in Figure 4.7 and Figure 4.8, while the main characteristics of the TG and DTG curves are pointed out in Table 4.5.

Table 4.5 Main features in asphalt mastics thermal decomposition.

Asphalt Mastic	$T_{2\%}$	T^1_{PEAK}	M^1_{PEAK}	T^3_{PEAK}	M^3_{PEAK}	M_F
	[°C]	[°C]	[%/min]	[°C]	[%/min]	[%]
100C	310.7	349.8	1.6	533.4	4.5	29.35
100MH	321.0	358	1.1	500.8	4.4	35.46
100ATH-1	270.3	312.8	5.8	544.7	3.4	35.01
100ATH-2	281.3	311.4	6.9	565.8	3.1	33.51
100ATH-3	266.5	303.0	5.1	543.6	2.5	34.49

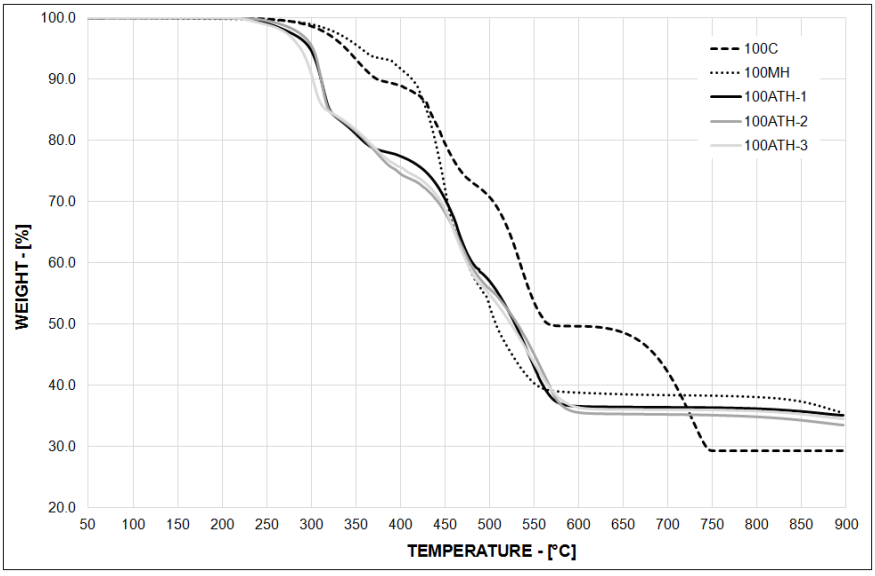

Figure 4.7 TG curves of asphalt mastics.

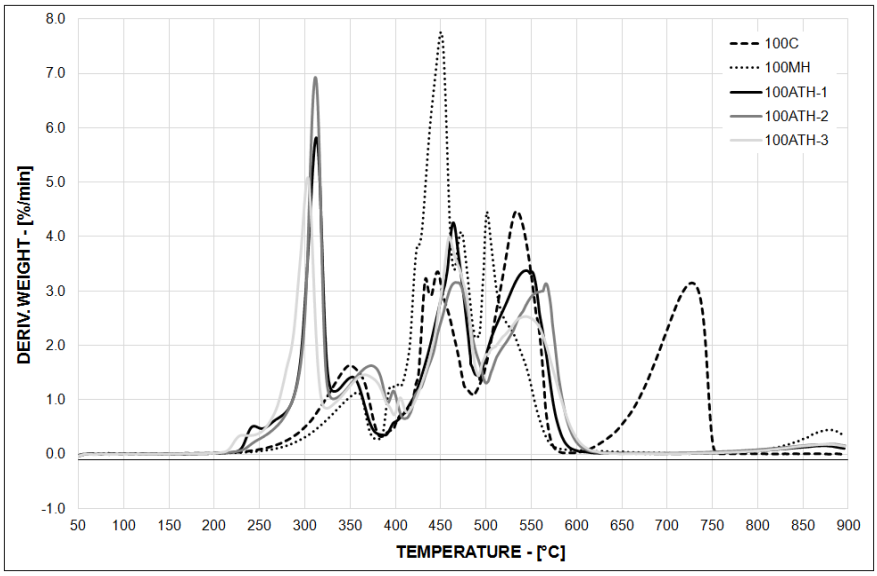

Figure 4.8 DTG curves of asphalt mastics.

As expected, asphalt mastics with ATH show $T_{2\%}$ lower than binder B50 due to the water released by the mineral filler, whose decomposition precedes the inception of asphalt binder decomposition.

Conversely, asphalt mastics 100C and 100MH reach 2% mass loss at higher temperatures than B50, thanks to the presence of a material which is inert until higher temperatures. The final solid residue can be verified through a simple calculation under the hypothesis that no chemical interactions occur between base asphalt binder and filler. Considering the asphalt mastic composition, the final solid residue of B50 and the final oxide/filler ratio specific for each filler, asphalt mastic final char yield is due to addition of the respective final products. So, theoretically asphalt mastic 100C should be 28.8%, mastic 100MH 35.2% and all ATH mastics 33.5%. The small differences between theoretical and observed values can be considered within the experimental error.

A first general observation is that all mastics have a behaviour which qualitatively can be obtained by a simple superposition of the thermal decomposition curves of the two ingredients (asphalt binder and filler). Therefore, in the mastics ATH decomposes during phase I while MH decomposes during phase II and calcium carbonate during phase III. As a consequence, 100-ATH and 100-MH curves are below those of B50 alone and mastic 100C, but of course this has not to be interpreted as an accelerating effect on thermal decomposition. On the contrary, the water released during FR decomposition is expected to disturb the combustion process.

In summary, the general information which derives from TGA is that asphalt binder and filler decompose independently and with the same mechanisms showed when not mixed. LOI results are shown in Table 4.6 and Figure 4.9.

Table 4.6 LOI values of asphalt mastics.

Asphalt Binder	LOI	Flame spread rate	Smoke emission
	[%]	[mm/s]	[arbitrary units %]
100C	27	0.35	113
100MH	31	0.29	53
100ATH-1	41	0.49	17
100ATH-2	44	0.54	47
100ATH-3	48[a]	0.56	26

a – performed at 3.2 cm/s gas flow rate

Keeping in mind that B50 showed LOI equal to 26%, a Flame Spread Rate of 0.35 mm/s and a smoke emission assumed to be 100 in arbitrary units, it can be stated that conventional limestone behaves like an inert material, while ATH and MH significantly improve asphalt binder flame resistance.

A positive effect was expected, considering that even inert filler may improve the flame resistance at least because its presence reduces the total amount of fuel and the rate of diffusion of oxygen and combustion products. In addition, the endothermic decomposition of the filler and the heat capacity of both the filler and its residue increase the amount of heat necessary to vaporize the fuel. Nevertheless, the magnitude of LOI increase of FR asphalt mastics is really high and promising. To interpret the data, it is useful to remind that in order to be effective, the filler decomposition must occur in a narrow range above the asphalt mixture processing temperature and at or below asphalt binder decomposition temperature. This is the reason why the most interesting results are obtained with ATH whose onset temperature is the closest to the asphalt binder one.

Despite of the carbon dioxide release and of the relative endothermic effects, conventional limestone filler does not produce the same outcome because its decomposition occurs at temperatures higher than 600°C, which are too high compared to asphalt binder decomposition onset, thus preventing all the beneficial effects which characterize the asphalt mastics with FR filler: 1) the heat absorbed by $Mg(OH)_2$ or $Al(OH)_3$ which cools the asphalt matrix and 2) the vapour released which dilutes the volatile products and consequently hinders the soot aggregation which is the most important responsible for smoke production.

Moreover, the water released makes free radicals concentration fall sufficiently so that it becomes insufficient for flaming reactions to self-sustain. Besides, the presence of water vapour tends to swell the flame, thus reducing its temperature and the amount of heat transferred back to the asphalt binder. The total amount of flammable volatile products is strictly reduced, thus limiting fuel availability and flame extinction occurs. Finally, the MgO and Al_2O_3 promote the formation of a thick charring layer acting as a barrier which not only hinder

oxygen and heat from spreading into the non-combusted asphalt matrix, but also prevent flammable volatiles from releasing out of the asphalt. This fact could be extremely relevant since it should make ignition time delay.

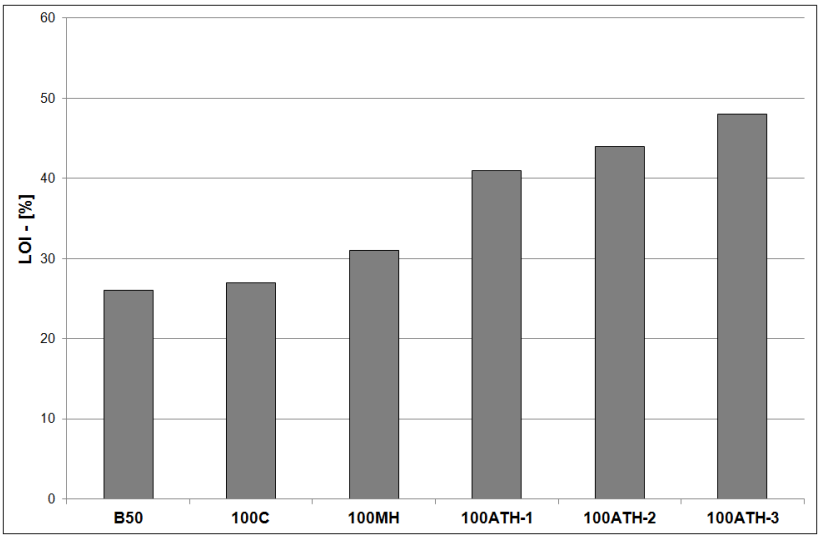

Figure 4.9 LOI values for binary blends.

Comparing to 100MH, ATH leads always to the higher LOI values, thus emphasizing its greater effectiveness. Once again, this fact can be justified by its lower decomposition temperature, close to asphalt binder onset temperature. Nevertheless, we must observe that different ATH fillers lead to different LOI: ATH-1 allows to obtain a 41% LOI while ATH-3 allows to reach 48% LOI. This cannot be related to the filler composition because all ATH fillers are characterized by the same $Al(OH)_3$ content, always greater than 99%, thus showing that chemical composition is not the only factor influencing the effectiveness of flame-retarding modification. ATH-1 is obtained by milling and it is characterized by a median particle size (d_{50}) of 9.8 μm. ATH-2 and ATH-3 are produced through precipitation from purified sodium aluminate which allows to obtain smaller median particle size: d_{50} of ATH-2 is 1.8 μm while that of ATH-3 is 1.1 μm. So, ATH-2 and ATH-3 are characterized by median particle almost ten times smaller than ATH-1; furthermore, they have greater Rigden voids and specific surface area, as specifically reported in Table 3.3.

Based on similar results found for polymeric materials [14], the combination of these differences in physical properties not only facilitate the dispersion in material matrix but also seems to favour the decomposition kinetic of the filler, thus explaining the differences in LOI values obtained for ATH asphalt mastics.

The addition of limestone to the asphalt mastics introduces further elements of discussion. CA-series and CM-series are ternary blends characterized by total filler ratio equal to 1/1 by weight, where the overall filler consists in a blend of limestone filler C and FR-filler. The results collected during LOI test on ternary blends are displayed in Figure 4.10.

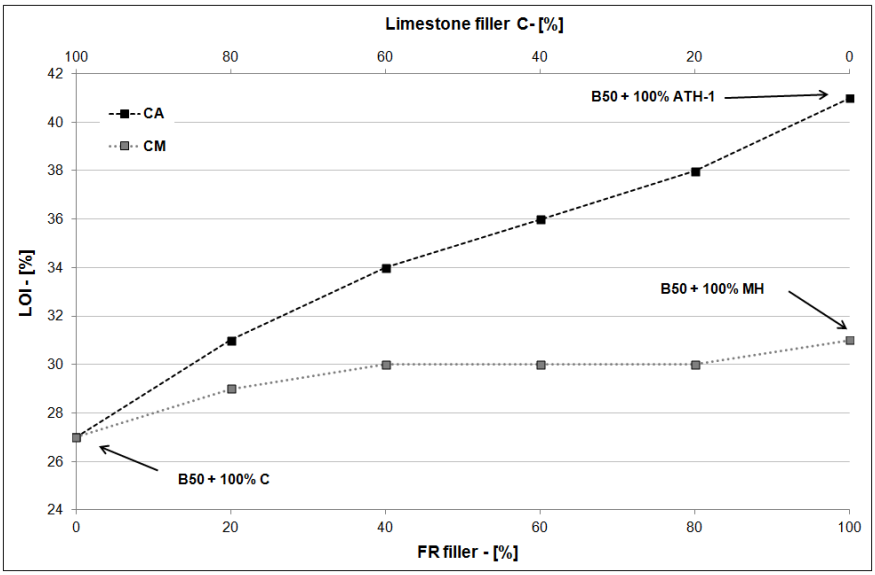

Figure 4.10 LOI values for ternary blends.

As previously found in the case of binary blends, limestone filler has a very limited influence on asphalt binder flammability due to the very high decomposition temperature of such material. The same scarce contribution of limestone filler is observed in all the CA and CM sample series. A more clear comparison between A-series and CA-series can be observed in Figure 4.11 where the effect of limestone in increasing LOI is displayed.

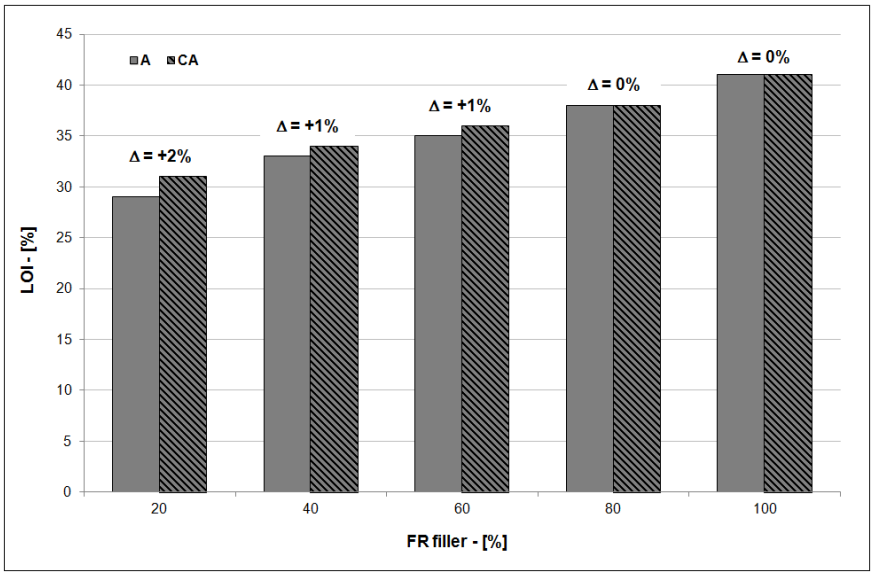

Figure 4.11 LOI values for ternary blends.

As can be observed, the difference in LOI is 2% when 20% of FR-filler is considered, then it goes to 1% and finally the effect of limestone completely vanishes at high FR-filler contents (≥ 80%).

This is probably due to the fact that the physical effect is strictly related to the inert material's volume fraction, so when this fraction decreases below a critical threshold, it becomes inappreciable.

Apart from the effect of limestone filler, remarkable differences between ternary blends of different composition can be outlined again. The most important one regards the general trends of CA-series and CM-series. Indeed, CM-series shows a slight rise in LOI from CM0 to CM40, then the results seem to flatten out producing a plateau (between 40% and 80%) which ends with a small final increase. On the contrary, CA-series is characterized by a gradual but uniform growth which leads to the highest LOI value equal to 41%.

4.3.2 Rheological analysis

With the aim to obtain results comparable with previous experience found in literature [15-18], asphalt mastics containing fillers described in Chapter 3 were prepared by setting the %vol of mineral filler referred to the mastic volume.

Three different composition were considered: 10%vol, 20%vol, and 30%vol which is almost equal to the 50%wt referred to the weight of mastic, as can be verified in Table 4.7. Thus, mastics defined by 30%vol are comparable with mastic 1/1 (wt/wt) filler/bitumen ratio used for the thermal stability and flammability analysis.

Table 4.7 Asphalt mastics identification for rheological analysis.

Asphalt Mastic	Mineral Filler	Filler Specific Gravity	Bitumen Specific Gravity	%vol. Filler	Filler/Bitumen Ratio	%wt. Filler
	[-]	[g/cm^3]	[g/cm^3]		[-]	
30C	C	2.71	1.02	30	1.14	0.53
30A1	ATH-1	2.42			1.02	0.50
30A2	ATH-2	2.42			1.02	0.50
30A3	ATH-3	2.42			1.02	0.50
30M	MH	2.36			0.99	0.50
20C	C	2.71		20	0.66	0.40
20A1	ATH-1	2.42			0.59	0.37
20A2	ATH-2	2.42			0.59	0.37
20A3	ATH-3	2.42			0.59	0.37
20M	MH	2.36			0.58	0.37
10A1	ATH-1	2.42		10	0.26	0.21
10A2	ATH-2	2.42			0.26	0.21
10A3	ATH-3	2.42			0.26	0.21

Rheological analyses were also performed on base bitumen B50 in order to outline the effects of different kinds and contents of mineral fillers. The selected amounts of mineral fillers were defined in order to reproduce asphalt mastics in the so-called “diluted region”, defined by Faheem and Bahia [17] and characterised by linearly increasing stiffness with filler volume fraction.

4.3.2.1Stress-controlled frequency sweep

Asphalt binder B50 and mastics were tested by means of stress-controlled frequency sweep in order to determine the fundamental rheological properties, such as the complex modulus G* and the phase angle δ. Tests were performed at nine different temperatures: 0, 10, 20, 30, 40, 50, 60, 70 and 80°C.

The load frequency was assumed log-variable in the range 1÷100 rad/s, keeping constant the range and ramp variation for all the temperatures considered. Linear viscoelastic (LVE) conditions were previously established using amplitude sweep tests.

Complex (|G*|), storage (G_0), and loss (G_{00}) moduli and phase angle (δ) were measured and used to generate rheological master curves according to the TTSP [19], at reference temperature 20°C. To this aim, data were first displayed in the Black diagram representing phase angle vs the magnitude (norm) of

complex modulus [20] thus verifying whether materials could be termed “thermo-rheologically simple” materials, i.e. materials whose rheological properties can be shifted by TTSP to produce smooth continuous master curves.

Indeed, a smooth curve in a black diagram is a useful indicator of time-temperature equivalency, while a disjointed curve indicates the breakdown of TTSP and the presence of either a high wax content bitumen, a highly asphaltene structured bitumen or a highly polymer-modified bitumen [21,22]. In addition, rheological measurements taken outside the LVE region or with inappropriate DSR spindle geometries also disrupt the smooth shape of a Black diagram curve.

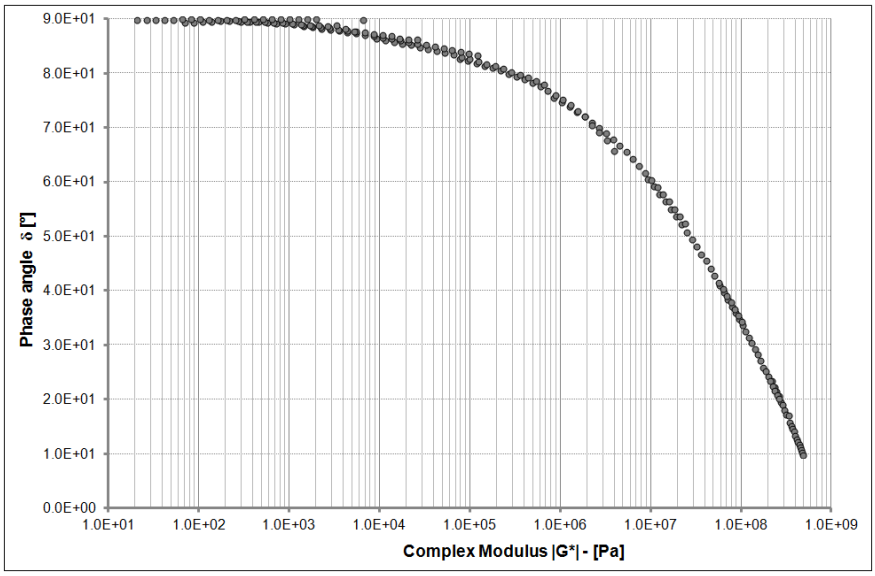

Figure 4.12 Black diagram for base bitumen B50.

Figure 4.12 displays the Black diagram referred to base bitumen B50. The collected data confirmed the “thermo-rheologically simple” hypothesis and were then used to identify the master curves by the application of the TTSP. Figure 4.13 shows the obtained master curves at reference temperature 20°C and the horizontal shift factors following the WLF equation.

a)

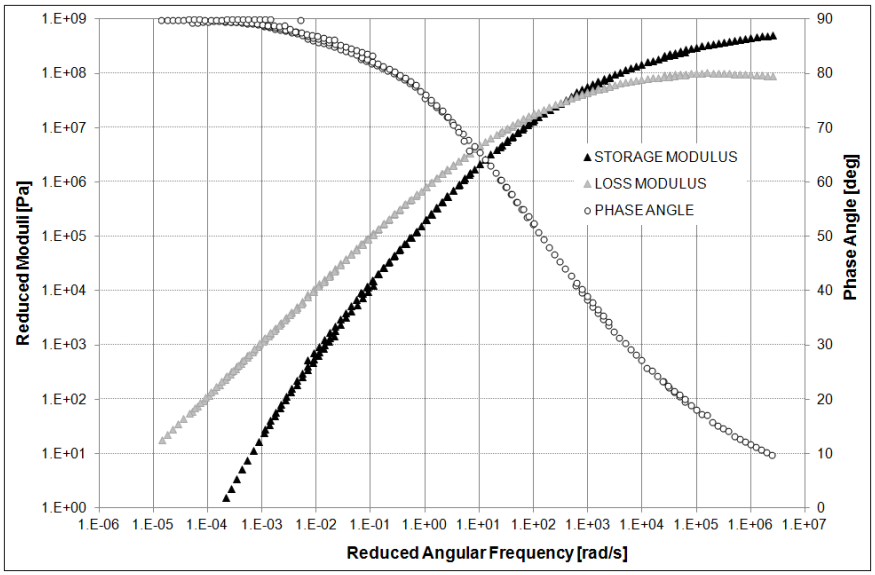

b)

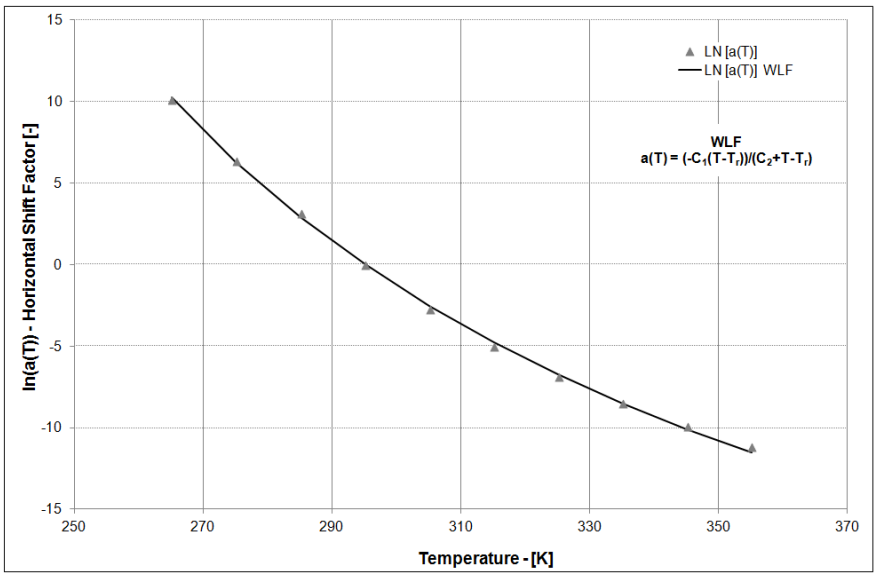

Figure 4.13 a) Master curves for base bitumen B50;
b) Shift factor according to WLF equation.

Figure 4.14 displays the master curves referred to the complex modulus and phase angle defined for mastic 30%vol.

a)

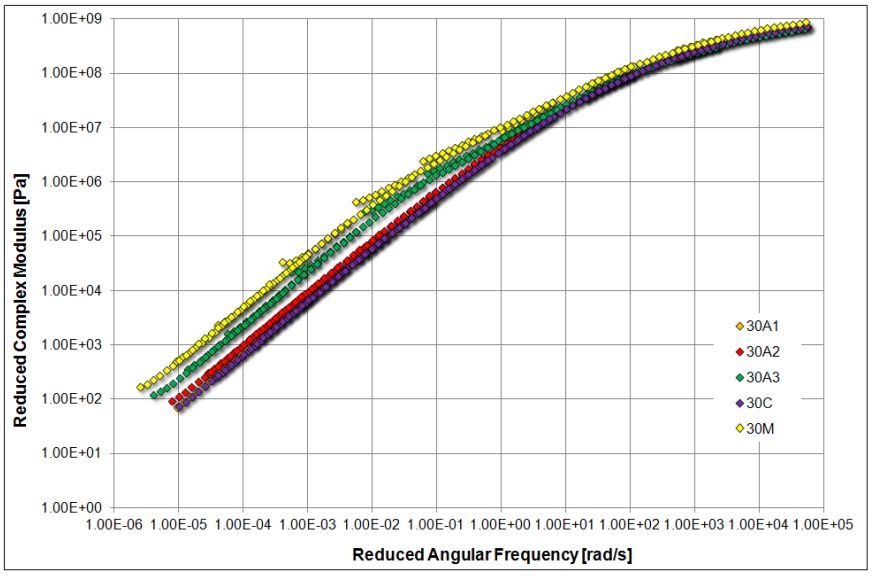

b)

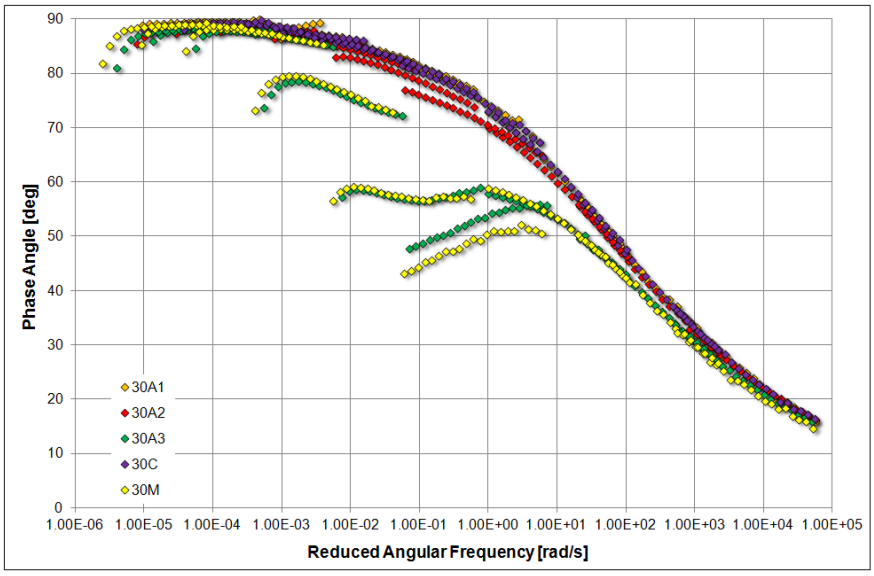

Figure 4.14 a) Complex modulus master curves for 30%vol series;
b) Phase angle master curves for 30%vol series.

a)

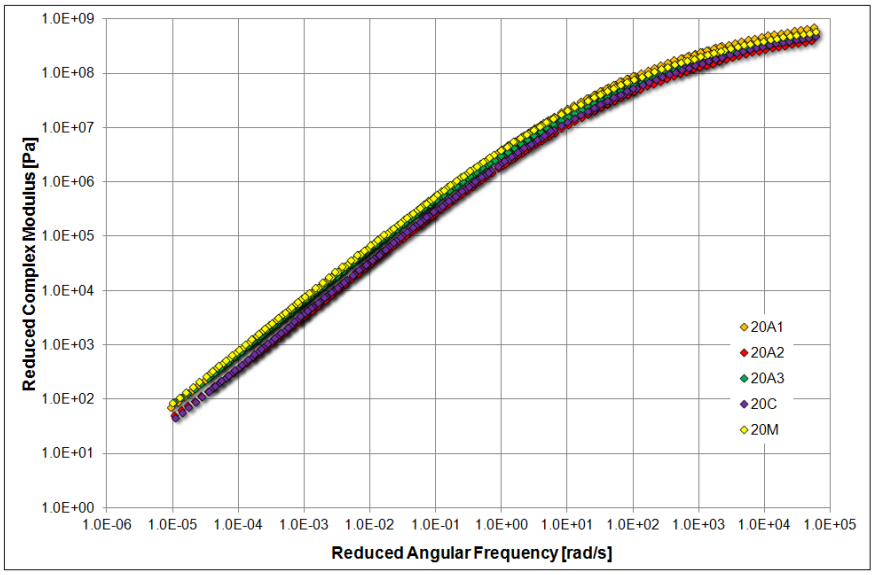

b)

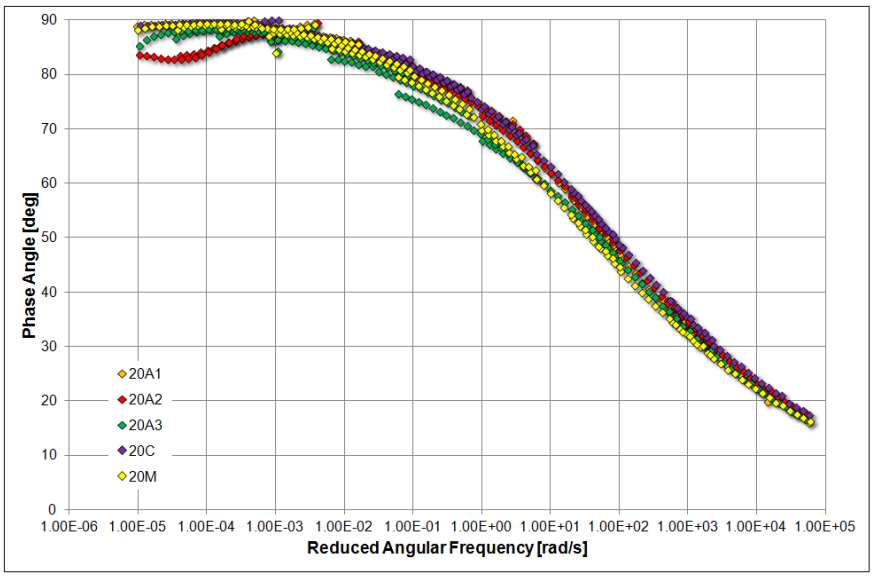

Figure 4.15 a) Complex modulus master curves for 20%vol series;
b) Phase angle master curves for 20%vol series.

Figure 4.15 and Figure 4.16 displays the master curves referred to the complex modulus and phase angle defined for mastic 20%vol and 10%vol respectively.

a)

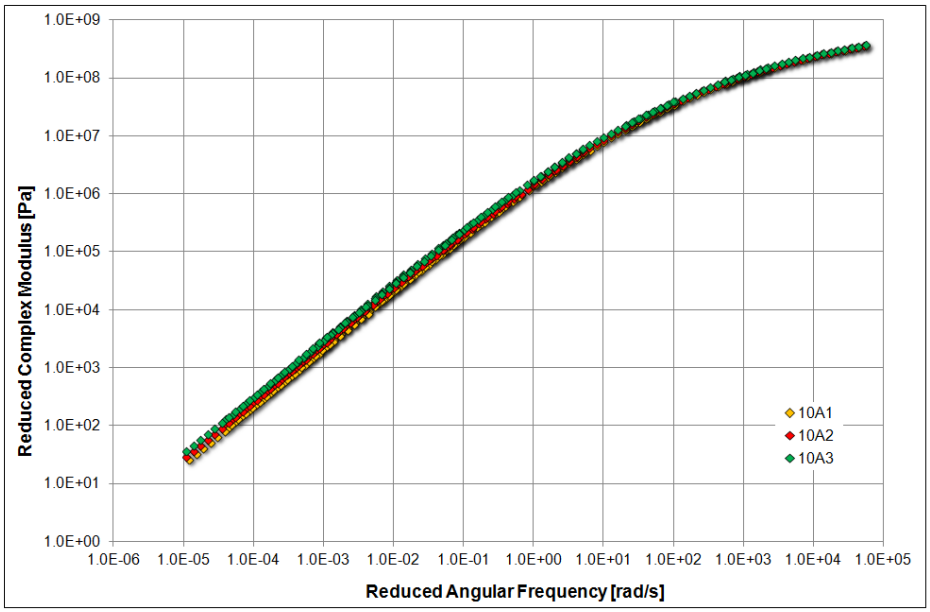

b)

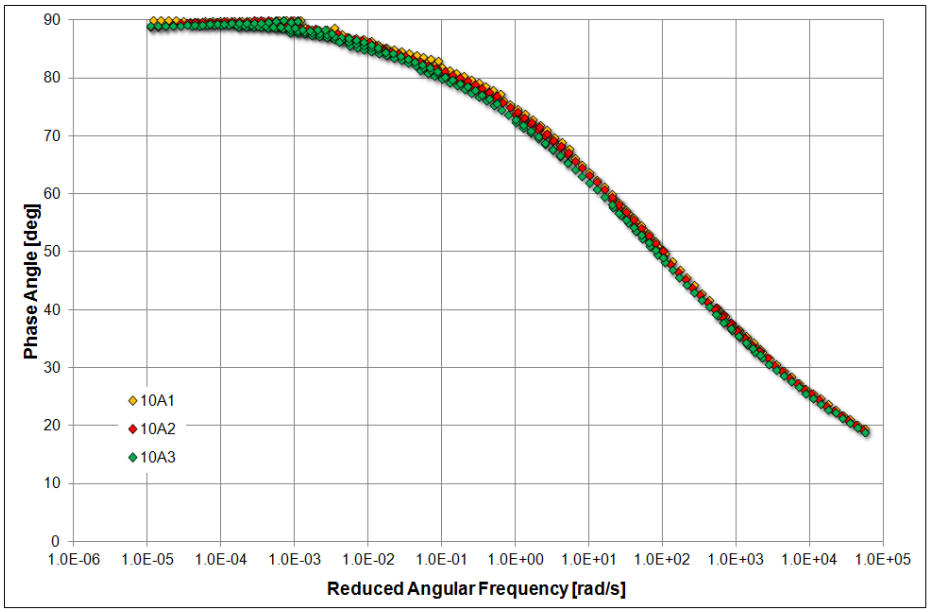

Figure 4.16 a) Complex modulus master curves for 10%vol series;
b) Phase angle master curves for 10%vol series.

Numerical data are also reported to best outline possible differences ascribable to the different fillers. The comparison is based on the complex modulus and the phase angle evaluated at T = 20°C and frequency equal to 10 rad/s. The effect on the asphalt binder mechanical response is highlighted by the parameters G^*_{RATIO} and δ_{RATIO}, defined as the ratio between the characteristic values of the mastics and those of the base bitumen B50.

Table 4.8 Rheological properties of asphalt mastics.

Asphalt Mastic	**Volume Fraction**	**|G*|**	**δ**	**G^*_{RATIO}**	**δ_{RATIO}**
	[%]	[Pa]	[°]	[-]	[-]
30C	30	2.28E+07	6.20E+01	4.28	0.95
30A1	30	2.26E+07	6.18E+01	4.25	0.94
30A2	30	2.41E+07	5.99E+01	4.53	0.91
30A3	30	2.78E+07	5.32E+01	5.23	0.81
30M	30	3.85E+07	5.34E+01	7.23	0.81
20C	20	1.29E+07	6.32E+01	2.43	0.96
20A1	20	1.22E+07	6.39E+01	2.29	0.97
20A2	20	1.15E+07	6.20E+01	2.16	0.95
20A3	20	1.61E+07	5.88E+01	3.02	0.90
20M	20	2.13E+07	5.82E+01	4.00	0.89
10A1	10	8.14E+06	6.38E+01	1.53	0.97
10A2	10	8.64E+06	6.34E+01	1.62	0.97
10A3	10	9.64E+06	6.20E+01	1.81	0.94

As can be clearly seen, asphalt mastics produced with mineral fillers characterized by the highest specific surface area shows a peculiar trend in the range of the medium-high service temperatures. Indeed, FR fillers MH and ATH-3 significantly influence the mechanical behavior of the base binder by increasing the complex modulus and the consequent stiffness of mastic. Conversely, ATH-2, ATH-1 and limestone fillers basically act in the same way, without outlining a possible contribution due to the chemical composition of mineral filler. These facts are more clearly defined in Figure 4.17. Thus, from these preliminary analyses, the specific surface area of mineral fillers emerged as the key-factor in governing the mechanical behavior of mastics while no considerable role is played by the chemical composition.

a)

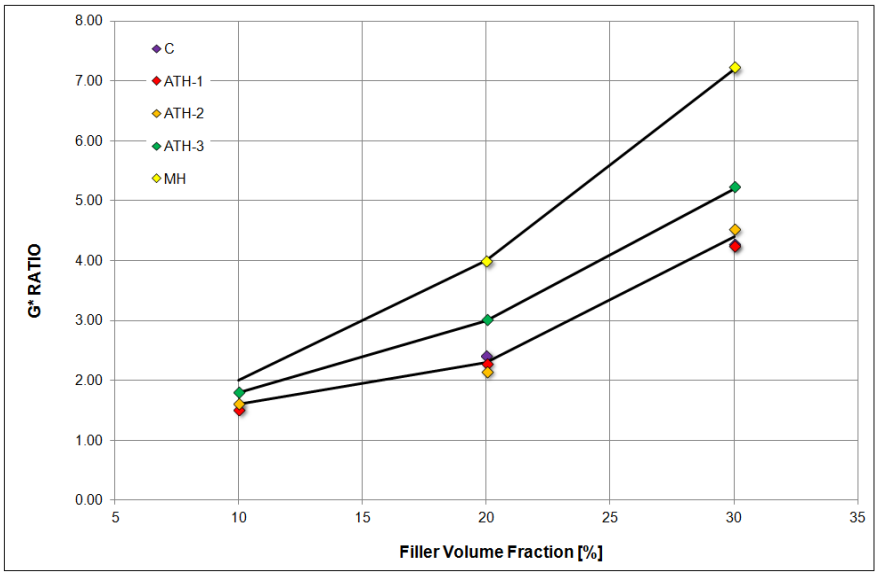

b)

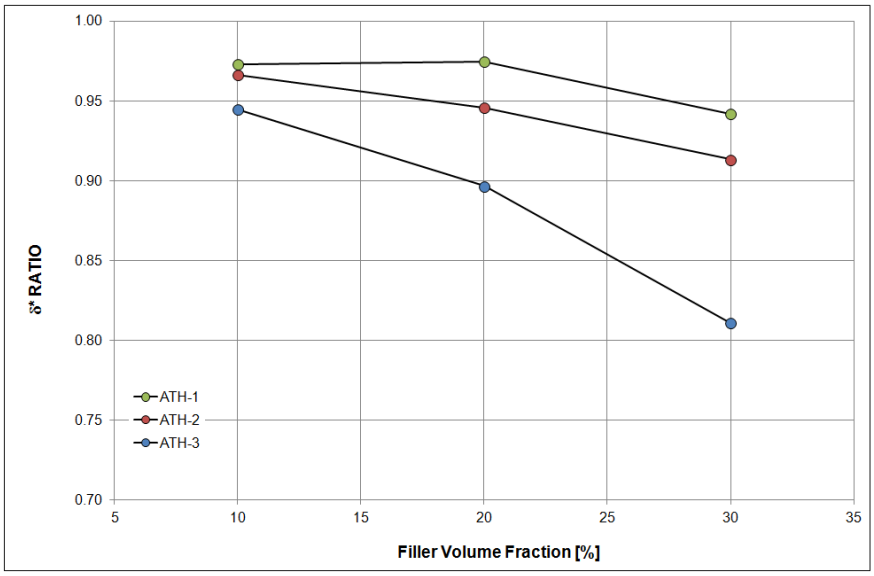

Figure 4.17 a) G*ratio influenced by the filler volume fraction;
b) δ ratio influenced by the filler volume fraction.

4.3.2.2 Viscosity test

Rheological measurements were carried out using a dynamic shear rheometer (DSR). The parallel plate testing system consisting of 25 mm diameter plates with 1 mm gap was used. Temperature during the DSR tests was controlled by means of a Peltier conditioning system with a maximum admitted deviation of ±0.01 °C. Due to the influence of temperatures on rheological measurements, specimens were subjected to 30 min thermal-conditioning period before each test with the aim of guaranteeing a constant temperature during the whole experiment. In order to avoid errors due to instrument's sensitivity, the torque applied was higher than the minimum suggested by the instrument producer (min. torque = 0.5 μNm).

Viscosity of binders was measured at different temperatures in strain-controlled mode using shear rates from $1 \cdot 10^{-2}$ to $1 \cdot 10^{-3}$ s^{-1}. Figure 4.18 shows the viscosity-temperature trends obtained for base bitumen and mastics.

a)

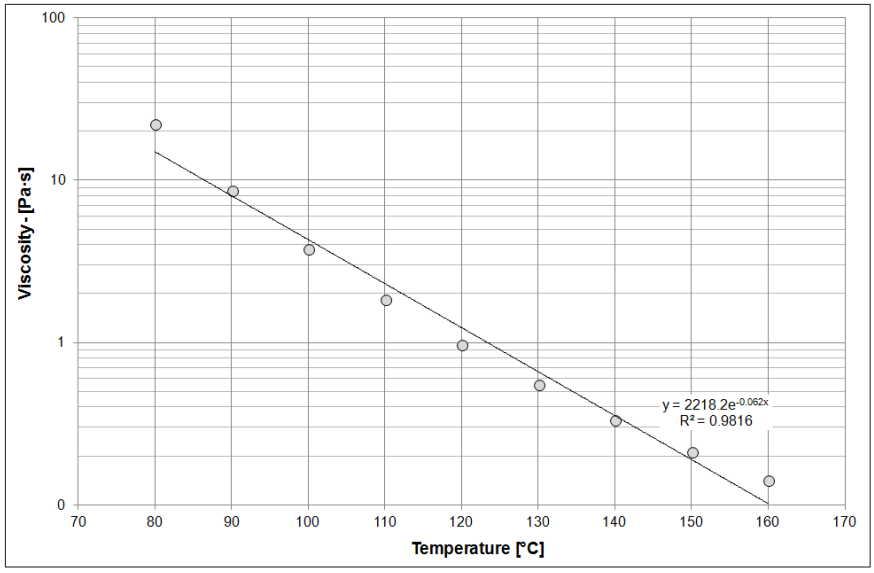

b)

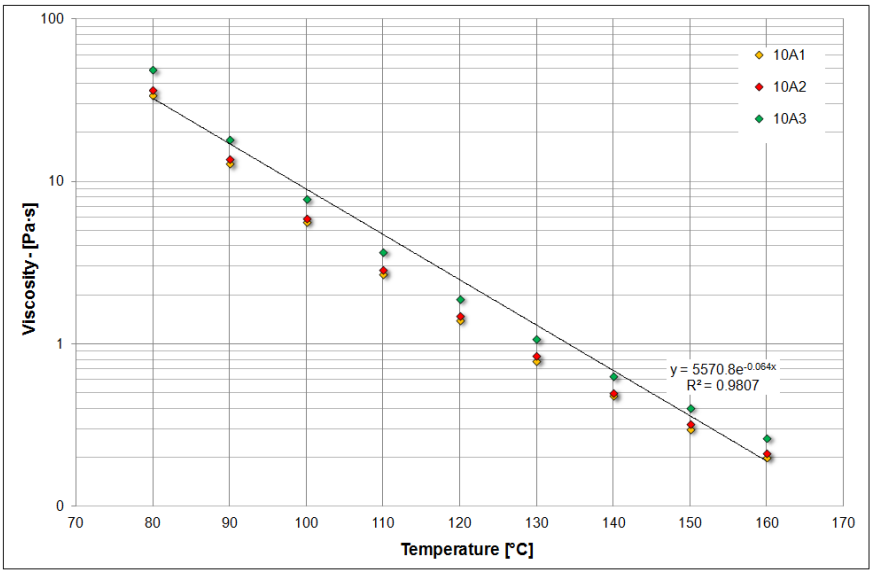
100
10
1
0
Viscosity - [Pa·s]
70
80
90
100
110
120
130
140
150
160
170
Temperature [°C]
10A1
10A2
10A3
y = 5570.8e-0.064x
R² = 0.9807

c)

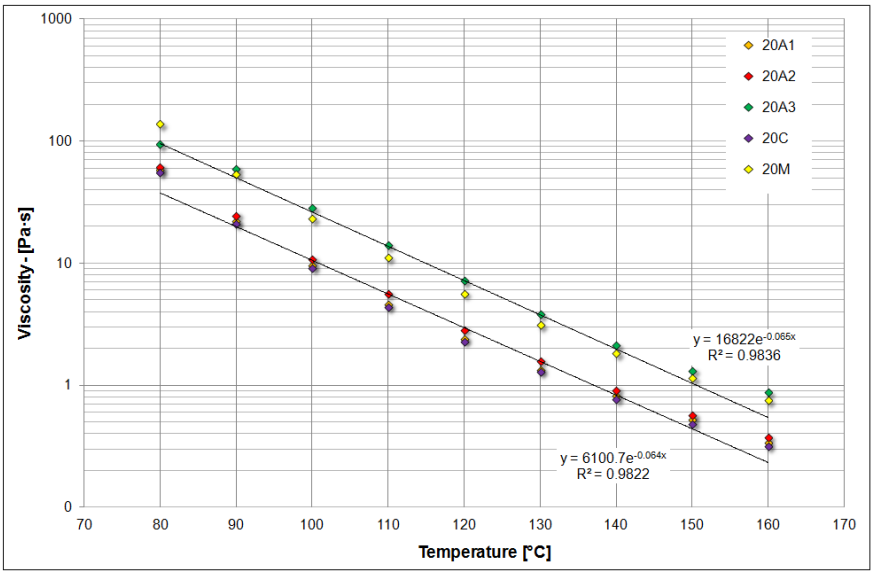
1000
100
10
1
0
Viscosity - [Pa·s]
70
80
90
100
110
120
130
140
150
160
170
Temperature [°C]
20A1
20A2
20A3
20C
20M
y = 16822e-0.065x
R² = 0.9836
y = 6100.7e-0.064x
R² = 0.9822

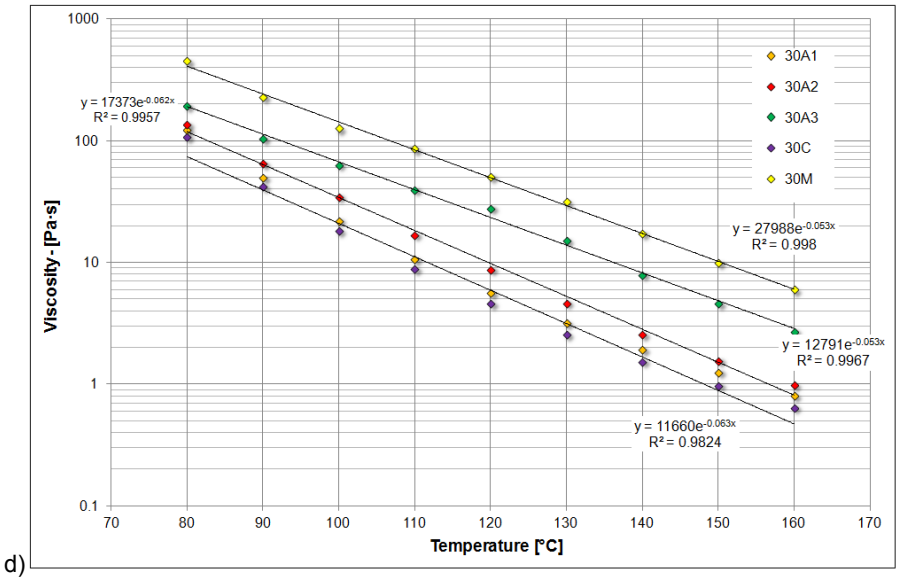

d)

Figure 4.18 Viscosity-temperature trends for a) base bitumen B50, B) mastics 10%vol, c) mastics 20%vol, d) mastics 30%vol.

In these cases, according to previous experiences [23,24], viscosity-temperature relationships were described by means of the classical Arrhenius equation (4.1), due to the Newtonian characteristics of the fluids considered:

$$\eta(T) = Ae^{\frac{E_f}{RT}} \tag{4.1}$$

where η is the viscosity, T is the temperature in Kelvin, E_f is the flow activation energy, R is the universal gas constant (8.3015 J/(molK) and A is a fitting parameter. As can be clearly observe in Figure 4.18, the fitting curves found for all the asphalt mastics are almost parallel, being the flow activation energy substantially constant with the composition of mastic. The most relevant increase in viscosity is achieved with MH and ATH - 3 fillers, characterized by the highest surface area. This fact has a relevant importance in the mixing process of asphalt mixture, since too high viscosity could result in bad mixing and in-situ scarce workability.

4.3.2.3 Creep and recovery test

Creep tests are performed in order to evaluate the resistance to non-reversible deformation and the existence of elastic recovery properties. The test methodologies are standardized in ASTM code regulation for the multiple loading cycles case [25]. Creep and recovery test involve the imposition of a step change in stress and the observation of the subsequent development in time of the strain; the stress level applied is constant and can be also increased for successive tests.

The increasing shear stress allows the evaluation of the binders mechanical behaviour and their comparison; the resistance to non–reversible deformation is identified as the binders ability to contrast the propagation of the viscous flow and their behaviour can be then described by separating the delayed elastic phenomena from the effective residual deformation.

The most relevant results that can be obtained consist in the creep compliance as a function of time and the strain versus time diagrams: the creep compliance function corresponds to the inverse of the creep stiffness function, as described by Eq. (4.2).

$$J(t) = \frac{\gamma(t)}{\tau(t)} \tag{4.2}$$

Constant stress is applied at t = t_0 and removed at t = t_1. Strain develops through three different regions: instantaneous ($0 \div \gamma_1$); retardation ($\gamma_1 \div \gamma_2$) and constant rate ($\gamma_2 \div \gamma_3$), as shown in Figure 4.19.

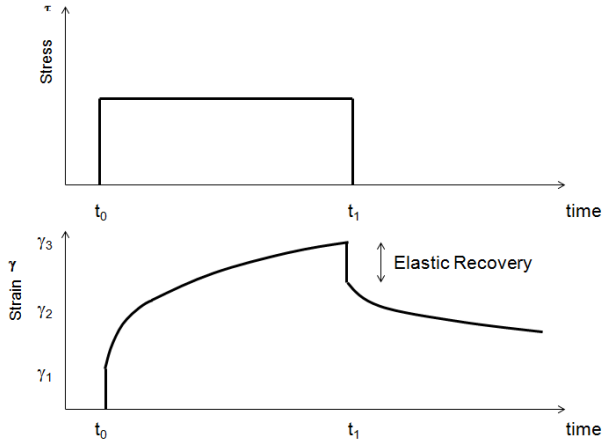

Figure 4.19 Creep-recovery test. Stress and strain versus time diagrams.

When the material shows a completely Newtonian behaviour, no elastic recovery exists while with the addition of modifiers, the elastic properties improve and the delayed elastic component becomes more relevant. This depends on the capacity of the blends to store and release energy when a load is applied and then removed, which determines the consequent binders ability to recover the strain developed during the creep phase.

On the basis of this concept, the discrimination between what is actually lost and what is storage and recoverable (in a deferred time) is a consequence of the accumulation of non-reversible deformation and of the distribution of the delayed elastic and essential viscous components in binders mechanical response.

The diagram of the recorded strain during the test as function of time allows the definition of the highest strain and of the elastic recovery, when it exists.

The elastic recovery can be evaluated with the following equation:

$$elastic\ recovery\ [\%] = {}^{\gamma_f}/_{\gamma_{peak}} \cdot 100 \tag{4.3}$$

where γ_f is the final strain value and γ_{peak} is the maximum strain value.

This ratio is always non-dimensional and assumes values between 0 and 1: for values close to 0 the materials show a significant elastic recovery, while for ratio values equal to 1 the material behaviour is essentially viscous and when the load is removed the strain keeps constant and equal to its maximum value.

In this research, creep and recovery test was initially performed by applying the shear stress for a time period of 10 s and then the shear stress is removed while the strain is monitored for the subsequent 30 s of recovery.

Tests are carried out by means of the DSR in the stress-controlled mode at temperature 40°C and considering three different stresses: 100, 1000, and 10000 Pa. Figure 4.20 show the results collected testing base bitumen B50. As can be clearly seen for all the stress levels considered, no elastic recovery could be highlighted due to the completely Newtonian behavior of neat binder.

a)

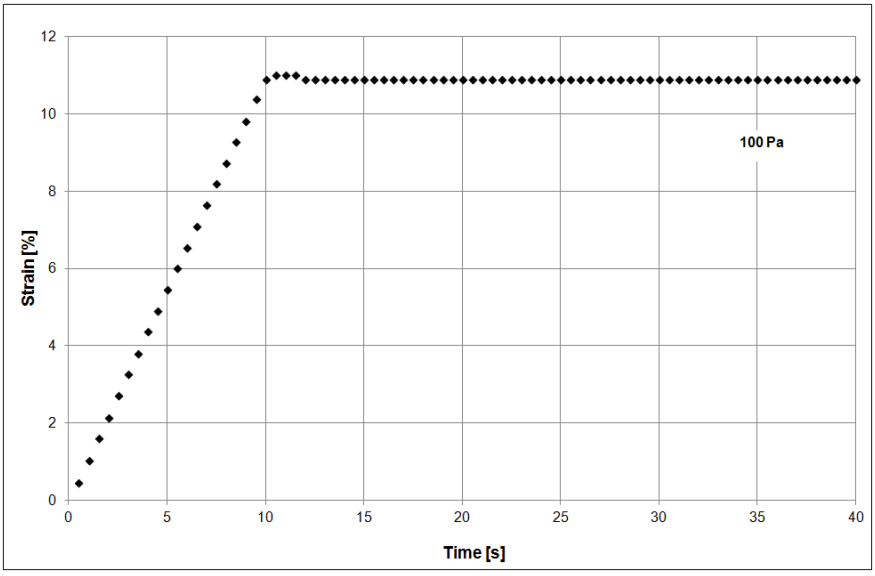

b)

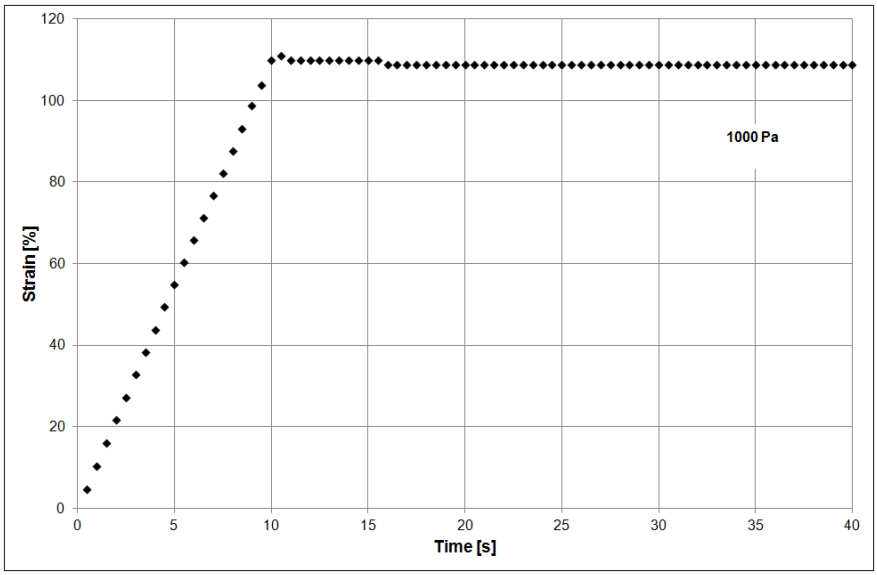

c)

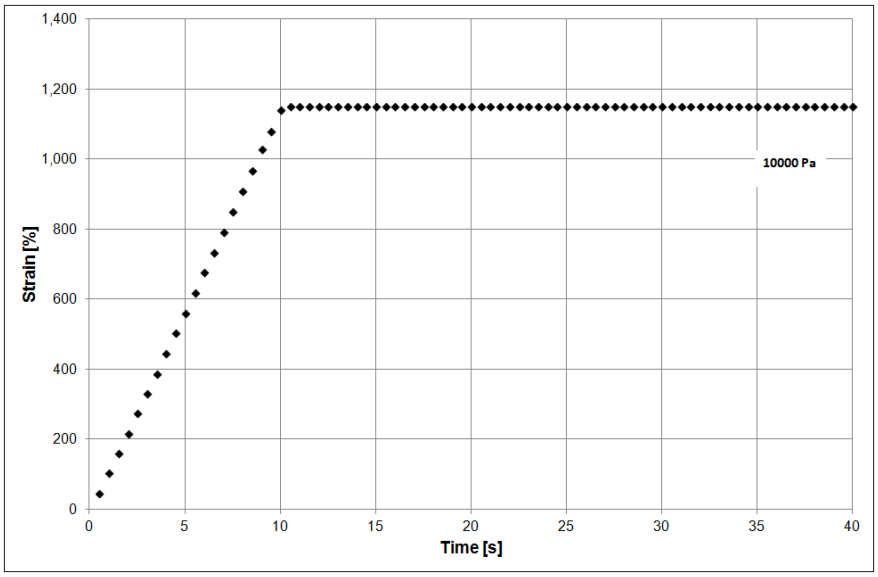

Figure 4.20 Creep-recovery test. Stress and strain versus time diagrams. a) 100 Pa; b) 1000 Pa; c) 10000 Pa - Base bitumen B50.

Figure 4.21, 4.23 and 4.24 describe the collected results for asphalt mastics with 10%vol, 20%vol, and 30%vol respectively.

a)

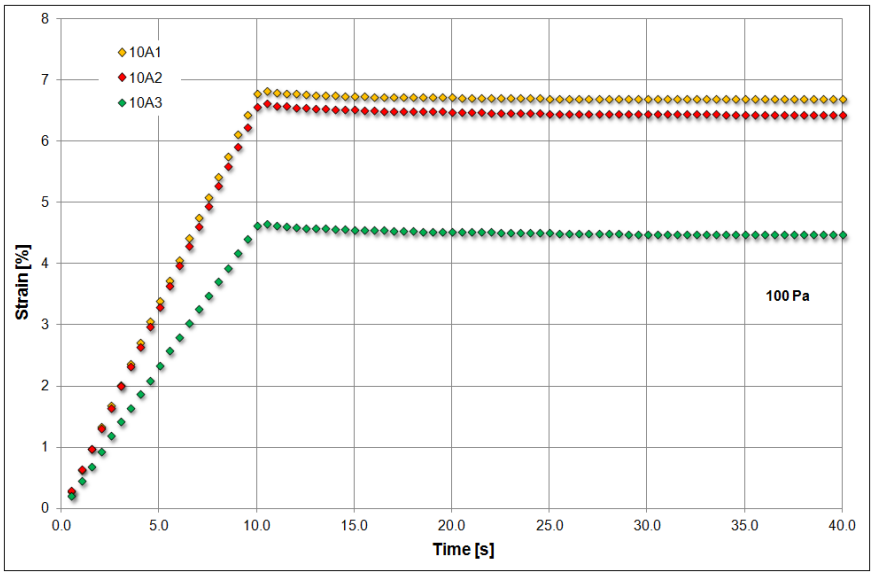
10A1
10A2
10A3
Strain [%]
Time [s]
100 Pa
0
1
2
3
4
5
6
7
8
0.0
5.0
10.0
15.0
20.0
25.0
30.0
35.0
40.0

b)

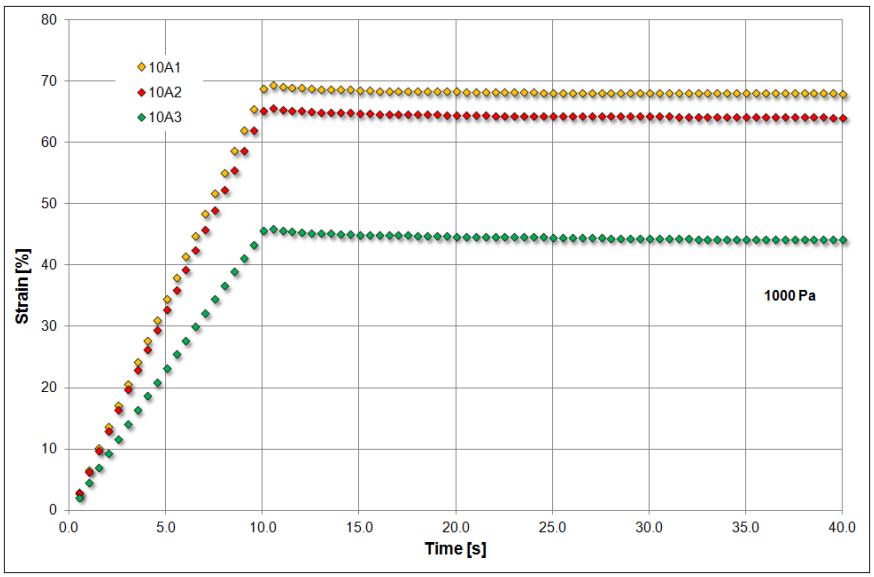
10A1
10A2
10A3
Strain [%]
Time [s]
1000 Pa
0
10
20
30
40
50
60
70
80
0.0
5.0
10.0
15.0
20.0
25.0
30.0
35.0
40.0

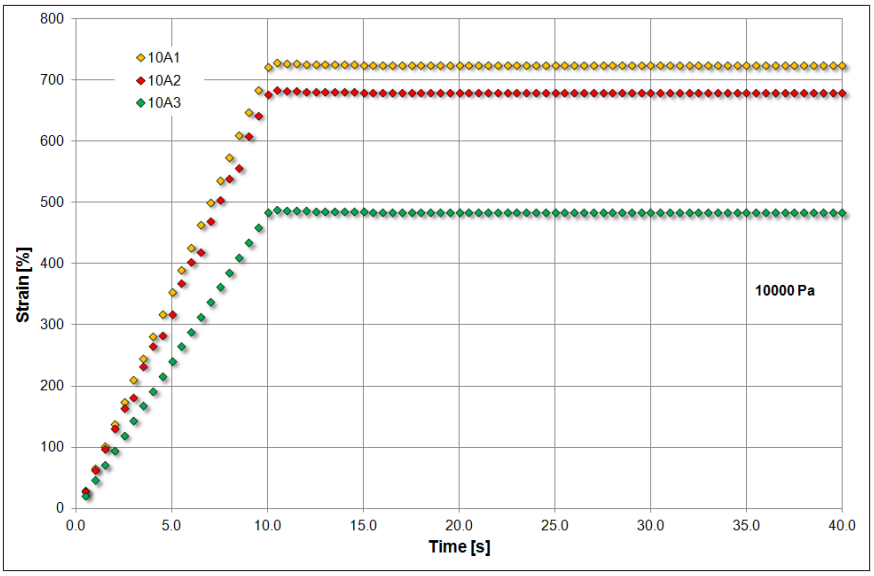

c)

Figure 4.21 Creep-recovery test. Stress and strain versus time diagrams. a) 100 Pa; b) 1000 Pa; c) 10000 Pa – Mastic 10%vol.

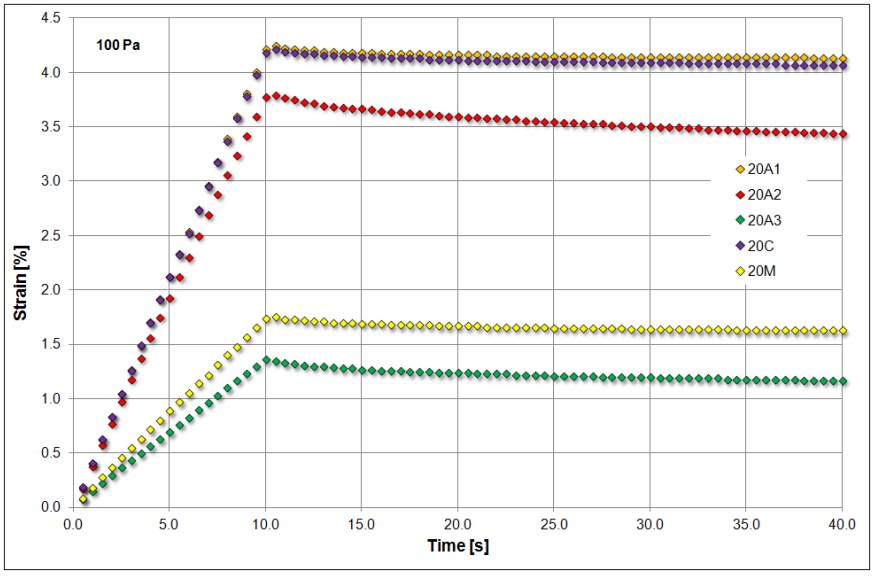

a)

b)

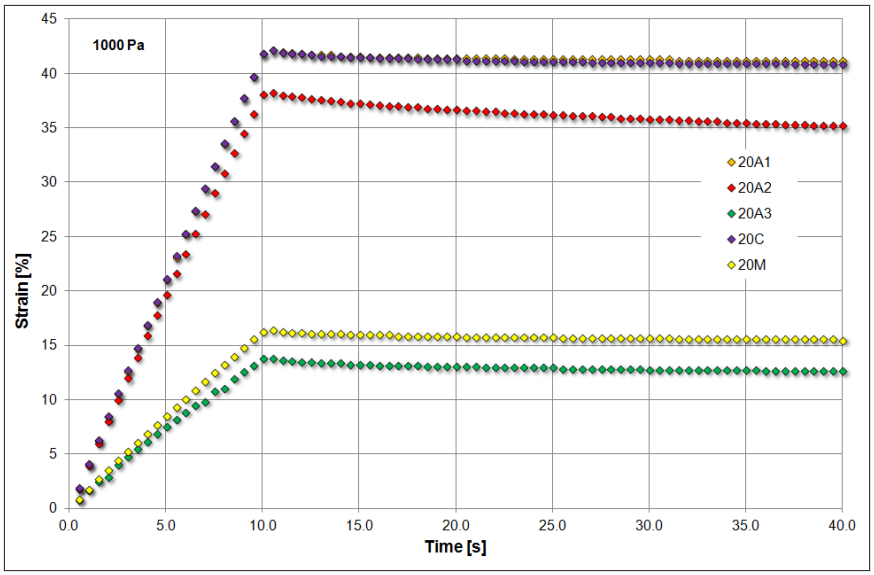

c)

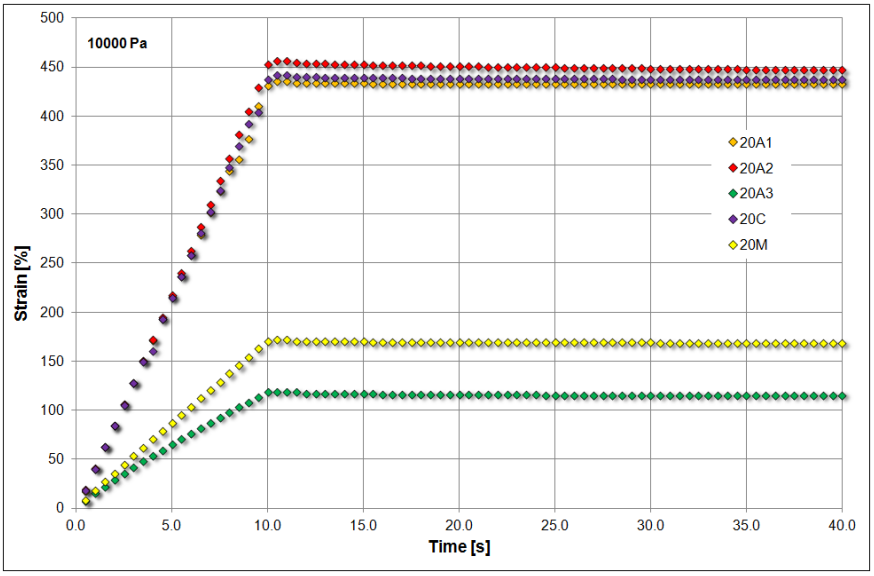

Figure 4.22 Creep-recovery test. Stress and strain versus time diagrams. a) 100 Pa; b) 1000 Pa; c) 10000 Pa – Mastic 20%vol.

a)

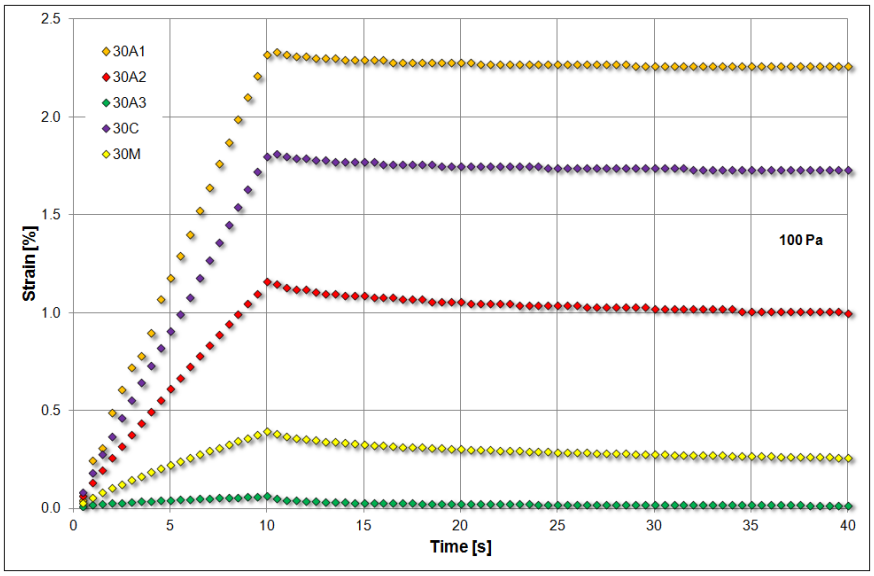
30A1
30A2
30A3
30C
30M
Strain [%]
Time [s]
100 Pa
0.0
0.5
1.0
1.5
2.0
2.5
0
5
10
15
20
25
30
35
40

b)

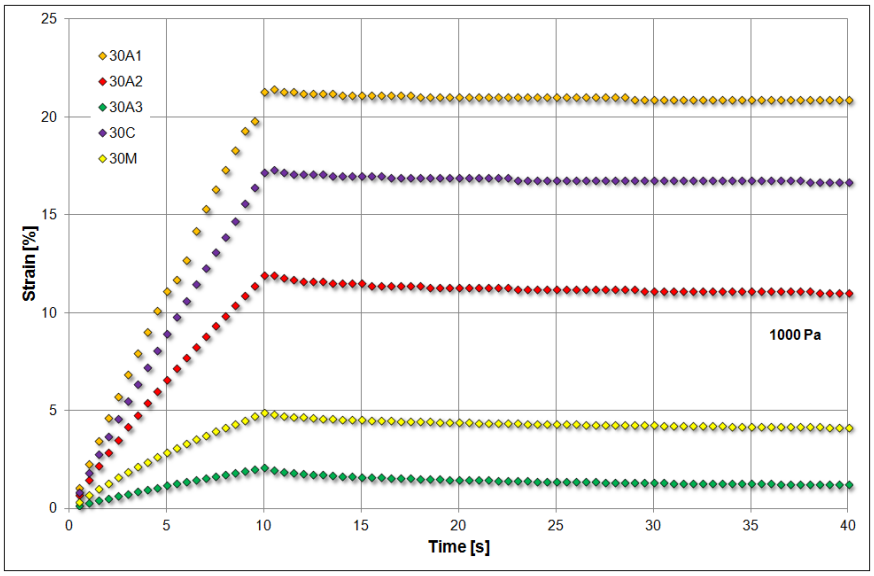
30A1
30A2
30A3
30C
30M
Strain [%]
Time [s]
1000 Pa
0
5
10
15
20
25
0
5
10
15
20
25
30
35
40

c)

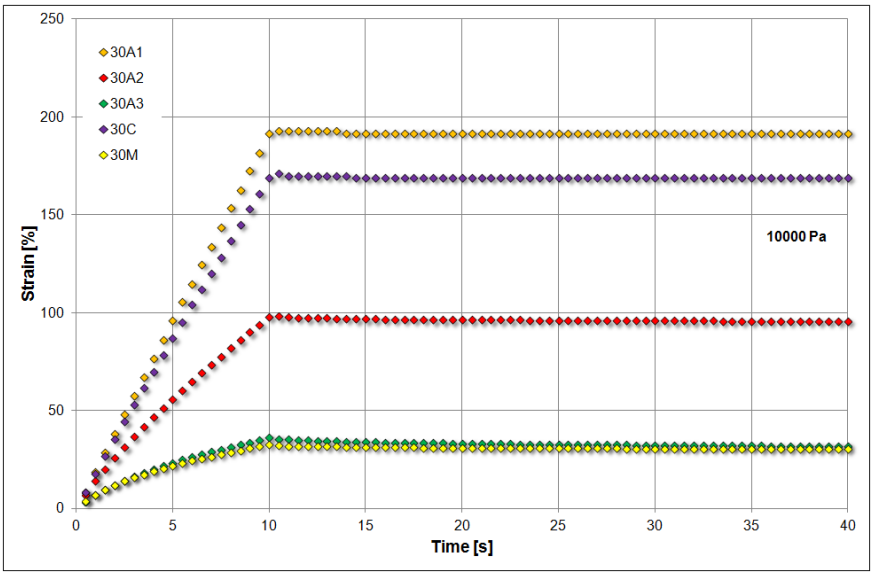

Figure 4.23 Creep-recovery test. Stress and strain versus time diagrams. a) 100 Pa; b) 1000 Pa; c) 10000 Pa – Mastic 30%vol.

With increasing filler volume fraction an improvement in the elastic property is achieved probably due to an overall increase in the total stiffness of mastic.

Focusing the attention on mastics of 30-series, the greatest effectiveness in increasing asphalt mastic stiffness and elastic recovery is achieved when using mineral fillers characterized by the smallest particle size. Conversely, mastic containing mineral filler C and ATH-1 are characterized by scarce stiffening contribution. More specifically, the major contribution in increasing the elastic recovery is achieved by mastics produced with mineral fillers characterized by the greatest specific surface area, which in turn involves the greatest Rigden Voids parameter. Figure 4.24 shows the influence of specific surface area on the elastic properties of mastics containing ATH fillers. As can be clearly seen, not only the filler volume fraction plays an important role in governing the mechanical behavior of mastics but also their particle size, giving rise to a more intense bitumen-filler interaction.

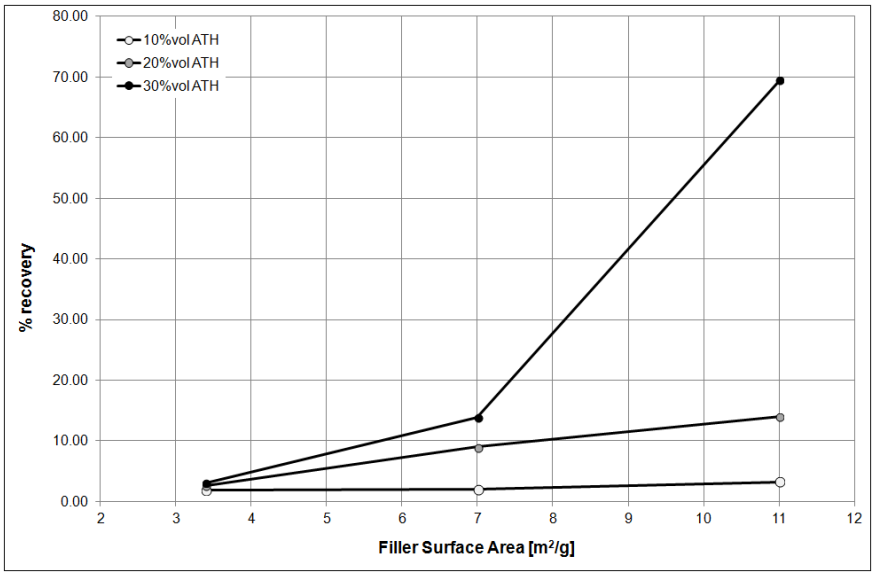

Figure 4.24 Influence of specific surface area on elastic recovery.

4.3.2.4 Multiple Stress Creep Recovery test (MSCRt)

The Multiple Stress Creep Recovery (MSCR) test defines a parameter of non-recoverable compliance, J_{NR}, which identifies the rutting potential of unmodified asphalt binder. The loss compliance J_{NR} describes the amount of energy dissipated by the binder when subjected to a cyclic deformation. This is the reason why a binder showing a great value of J_{NR} is more susceptible to rutting.

The MSCRT consists in a sequence of loading and recovery phases. In this work a sequence of 1s creep loading followed by 9s recovery was adopted. Each phase of creep-recovery was repeated for 10 cycles for 11 different stress levels, varying in the range 25÷25600 Pa. Each sample was tested starting from the lower stress level with no time lag between cycles. The stress level doubles after every 10 cycles. The loss compliance, J_{NR}, was then defined for each stress as the ratio between the average non-recovered strain at the end of 10 cycles and the stress applied in those cycles (see Eq. (4.4).

$$J_{NR} = \frac{\gamma(10n) - \gamma\{10(n-1)\}}{10 \cdot \tau_n} \tag{4.4}$$

where:

- n is the phase index (each phase corresponds to 10 cycles) varying from 1 to 11;
- τ_n is the characteristic shear stress of each sequence of cycles;
- γ is the non-recovered strain.

In order to evaluate the influence of temperature, the test was repeated for each specimen at 3 characteristic temperatures: 50, 60 and 70°C. The strain evolution is schematically shown in Figure 4.25.

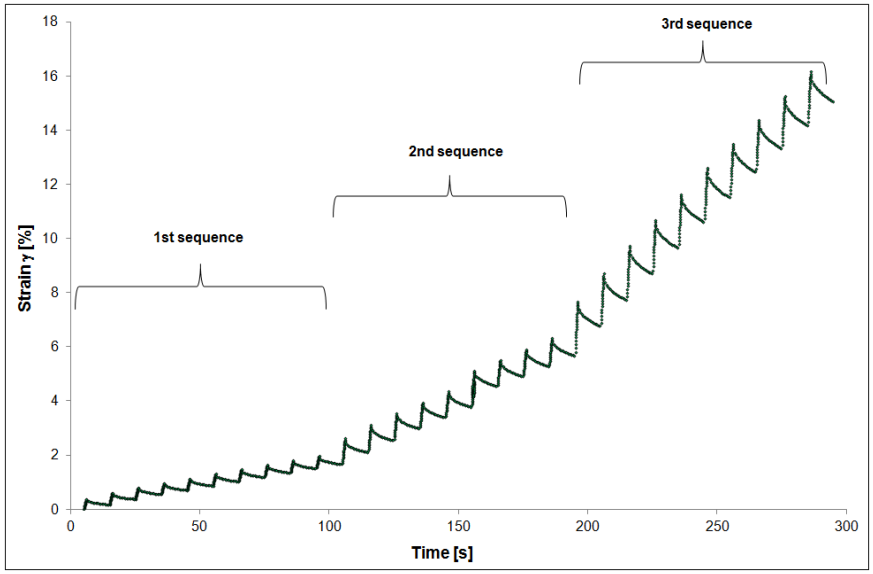

Figure 4.25 Schematic of strain development in MSCR test.

Figure 4.26 displays the results collected at different test temperatures for base bitumen B50. The most relevant outcome is that, in case of base bitumen, the non-recoverable compliance is almost load-independent, as clearly expected in case of Newtonian behavior.

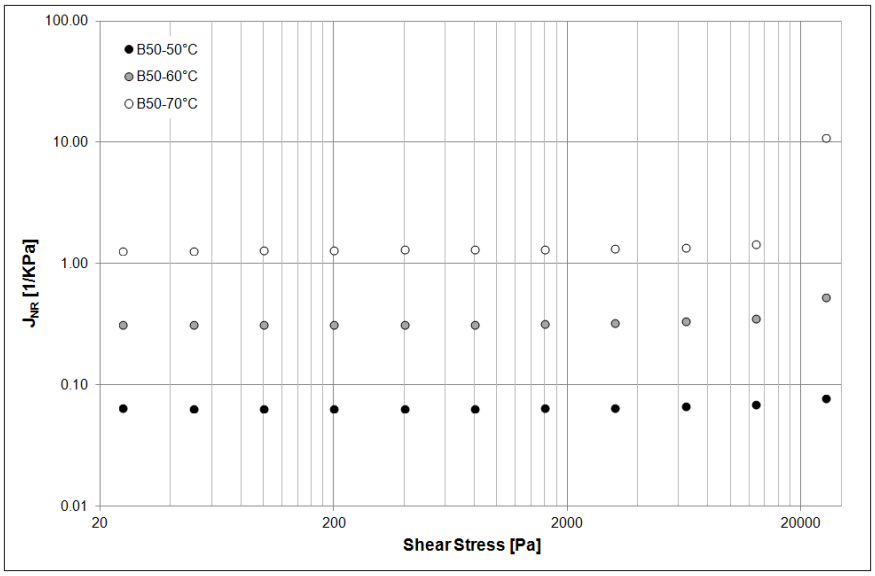

Figure 4.26 J_{NR} vs shear stress – B50.

Figure 4.27 outlines clear differences in mechanical behaviour according to the filler volume fraction. Indeed, strong load-dependence can be observed for ATH-2, ATH-3 and MH. In these cases, mastics generally present an initial decrease in J_{NR}, which subsequently tends to increase as the stress becomes higher. Furthermore, it must be observed a substantially equivalent behaviour of ATH-3 and MH, as already observed in previous rheological tests. This can be considered a further clue of the key-role played by the particle size of the mineral filler.

Similar trends were recorded in case of mastics containing 20%vol of filler, while 10%vol series shows a substantially stress-independent behaviour similar to the base bitumen. Moreover, in the case of 10%vol mastics, no clear differences among the mineral fillers used were outlined. For the sake of brevity, Figure 4.27 displays only the results recorded for T = 70°C since similar trends were found also for T = 50°C and 60°C.

a)

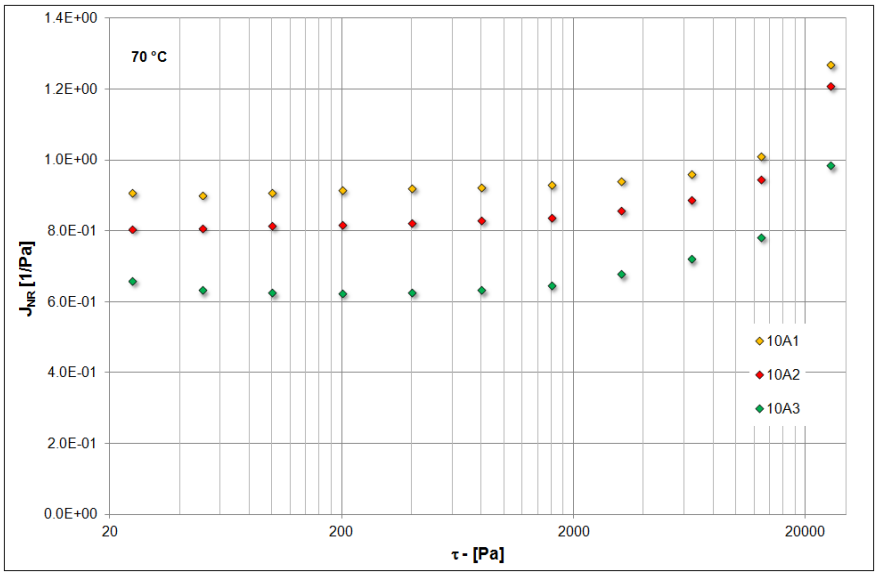
70 °C
1.4E+00
1.2E+00
1.0E+00
8.0E-01
6.0E-01
4.0E-01
2.0E-01
0.0E+00
J_{NR} [1/Pa]
20
200
2000
20000
τ - [Pa]
10A1
10A2
10A3

b)

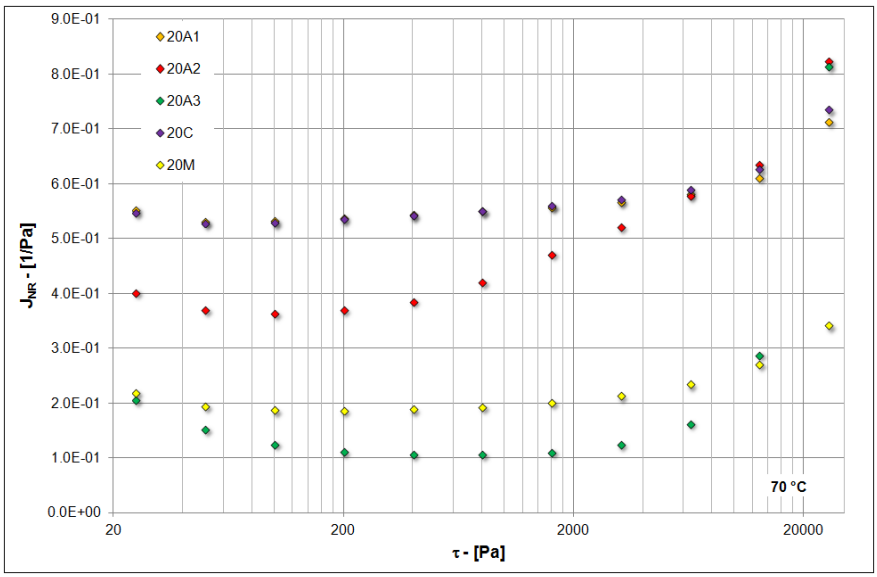
9.0E-01
8.0E-01
7.0E-01
6.0E-01
5.0E-01
4.0E-01
3.0E-01
2.0E-01
1.0E-01
0.0E+00
J_{NR} - [1/Pa]
20
200
2000
20000
τ - [Pa]
20A1
20A2
20A3
20C
20M
70 °C

c)

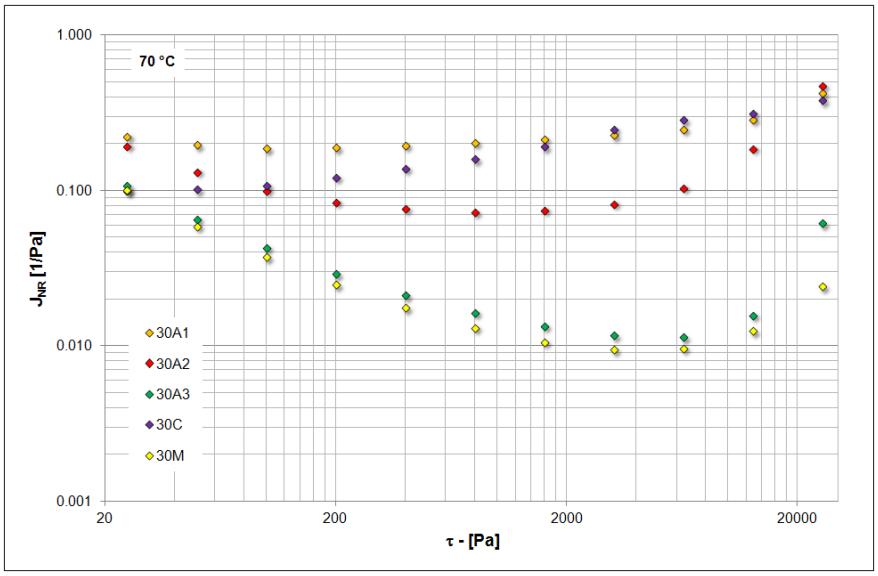

Figure 4.27 J_{NR} vs shear stress: a) mastic 10%vol, b) mastic 20&vol, c) mastic 30%vol. - 70°C.

References

[1] Jimenez-Mateos JM, Quintero LC, Rial C.. Characterization of petroleum bitumens and their fractions by thermogravimetric analysis and differential scanning calorimetry. Fuel 1996; 75:1691-1700.

[2] Kök Mv, Karacan Co. Behavior and effect of SARA fractions of oil during combustion. SPE Reservoir Evaluation & Engineering 2000; 3(5): 380-85.

[3] Xu T, Huang X. Study on combustion mechanism of asphalt binder by using TG-FTIR technique. Fuel 2010; 89: 2185-90.

[4] Donbavand J, Ball GFA, Patrick JE. A study of asphaltic cements and their fractions by thermogravimetry. Thermochim Acta 1986; 98: 99-109.

[5] Giuliani F, Merusi F, Filippi S, Biondi D, Finocchiaro M, Polacco G. Effects of polymer modification on the fuel resistance of asphalt binders. Fuel 2009; 88: 1539-46.

[6] Polacco G., Kriz P., Filippi S., Stastna J., Biondi D., Zanzotto L., “Rheological properties of asphalt/SBS/clay blends”, European Polymer Journal, Vol. 44, 2008, p. 3512-3521.

[7] Jahromi S.G., Khodaii A., “Effects of nanoclay on rheological properties of bitumen binder”, Construction and Building Materials, Vol. 23, 2009, p. 2894-2904.

[8] Zanetti M., Camino G., Thomann R., Mulhaupt R., “Synthesis and thermal behaviour of layered silicate – EVA nanocomposites”, Polymer, Vol. 42, 2001, p. 4501-4507.

[9] Gilman J.W., “Flammability and thermal stability studies of polymer layered-silicate (clay) nanocomposites”, Applied Clay Science, Vol. 15,1999, p.31-49.

[10] Lewin M., “Some comments on the modes of action of nanocomposites in the flame retardancy of polymers”, Fire and Materials, Vol. 27, 2003, p. 1-7.

[11] Liu G., Wu S., van der Ven M., Molenaar A., Besamusca J., “Characterization of organic surfactant on montmorillonite nanoclay to be used in bitumen”, Journal of Materials in Civil Engineering, Vol. 22, 2010, p. 794-799.

[12] Bartholmai M., Schartel B., “Layered silicate polymer nanocomposites: new approach or illusion for fire retardancy? Investigation of the potentials and the tasks using a model system”, Polymers for Advanced Technologies, Vol. 15, 2004, p. 355-364.

[13] Schartel B., Bartholmai M., Knoll U., “Some comments on the use of cone calorimeter data”, Polymer Degradation and Stability, Vol. 88, 2005, p. 540-547.

[14] Hull TR, Witkowski A, Hollingbery L. Fire retardant action of mineral fillers. Polym Degrad Stability 2011; 96: 1462-69.

[15] Heukelom W. (1965) The role of filler in bituminous mixes. Journal of the Association of Asphalt Paving Technologists, Vol. 34, USA. 1965.

[16] Heukelom W. Wijga PWO. (1971) Viscosity of dispersion as governed by concentration and rate of shear. Journal of the Association of Asphalt Paving Technologists, Vol. 40, USA. 1971.

[17] Faheem AF, Bahia HU (2009) Conceptual phenomenological model for interaction of asphalt binders with mineral fillers. Journal of the Association of Asphalt Paving Technologists, Vol. 78, USA. 2009.

[18] Ahmed F. Faheem & Hussain U. Bahia (2010): Modelling of Asphalt Mastic in Terms of Filler-Bitumen Interaction, Road Materials and Pavement Design, 11:sup1, 281-303.

[19] Ferry JD (1980) Viscoelastic properties of polymers. Wiley, New York.

[20] Gordon D. Airey (2002): Use of Black Diagrams to Identify Inconsistencies in Rheological Data, Road Materials and Pavement Design, 3:4, 403-424.

[21] Lesueur D., Gerard JF, Claudy P., Letoffe JM., Planche JP, Martin D, “A Structure-Related Model to Describe Bitumen Linear Viscoelasticity”, Proceedings of the Eurasphalt & Eurobitume Congress, Session 5, Binders-Functional Properties and Performance Testing, E&E.5.114, Strasbourg, 1996.

[22] Planche JP., Lesueur D, Hines ML., King GN, “Evaluation of Elastomer Modified Bitumens using SHRP Binder Specifications”, Proceedings of the Eurasphalt & Eurobitume Congress, Session 5: Binders-Functional Properties and Performance Testing, E&E.5.121, Strasbourg, 1996.

[23] Experimental evaluation of asphalt binders high specification temperatures based on the low shear viscosity concept, Proceedings of the 4th Euroasphalt and Eurobitume Congress, Copenhagen, Denmark.

[24] Salomon D, Zhai H (2004), Asphalt binder flow activation energy and its significance for compaction effort. Proceedings of the 3rd Euroasphalt and Eurobitume Congress, Vienna, Austria.

[25] ASTM International, “Standard Test Method for Multiple Stress Creep and Recovery (MSCR) of Asphalt Binder Using a Dynamic Shear Rheometer” in D7405-10a.

5 Asphalt mixtures

The asphalt mixtures fire behaviour was analysed by means of a cone calorimeter (Standard ISO 5660-1 [1]) made by Fire Testing Technology Limited, under fully ventilated conditions.

For each asphalt mixture, three cylindrical samples with 100 mm diameter were subjected to the radiant heat flux. All the asphalt mixtures were tested at an irradiance level of 70 kWm^{-2}. Dense and open graded mixtures produced with natural porphyry aggregates (D-BC and O-BC) were tested also at two other radiant heat fluxes: 35 and 50 kWm^{-2}, with the aim of characterizing the overall fire behaviour in a wider range of heat exposure.

Before testing, samples were conditioned to constant mass at 23 ± 2°C and relative humidity equal to 50% following the requirements of ISO 554 [2]. A single layer of aluminium foil was then used to wrap the bottom and sides of the specimen to avoid mass-transfer along all boundaries except the top burning surface. Finally, wrapped samples were adjusted in the specimen holder in horizontal position and covered by a stainless steel retainer frame. The distance between the top of the specimen and the bottom of the cone electric heater was set equal to 25 ± 1 mm. It is worth noting that the cut face coincided with the bottom of the sample, thus exposing to the heat flux the same black surface of highway pavement.

An electric spark was placed on top surface of the sample up to ignition, and removed thereafter, thus all the tests were performed in flaming condition. The experiments were stopped manually if no ignition occurred within 30 minutes of exposure. During the investigation, the fan volumetric flow rate was maintained equal to 0.024 ± 0.002 m^3s^{-1}. When ignition occurred, the operator measured the surface temperature of the sample by applying a wire Type k thermocouple (1 mm diameter) in contact with the top of the sample. The fire properties were then described in terms of heat and smoke release parameters, by means of their averaged values based on three independent replications.

5.1 Fire behaviour of dense and open graded mixtures

The first purpose of the cone calorimeter investigation was the characterization of conventional dense and open graded mixtures produced with natural aggregates. Asphalt mixture D-BC and O-BC were tested at three distinct

irradiance levels, equal to 35, 50, and 70 kWm^{-2}. Results were then discussed in order to identify the ignition parameters of mixtures. More specifically, the critical heat flux (CHF) and the theoretical ignition temperature (T_{ig}) were determined. To this aim, a typical ignitability analysis based on a simplified heat conduction model was adopted. The non-steady state 1-D heat conduction problem is governed by the Fourier equation Eq. 2.4, where $\alpha = k/\rho c$ represents the thermal diffusivity of materials.

In modelling the ignition of solid fuels, it is generally adopted a closed solution of Eq. 2.4 that can be derived by considering the transient pyrolysis of a semi-infinite charring solid subject to a constant radiant heat flux [1]. This approach, known as semi-infinite solid assumption, holds for the early transient regime and it is well known that it can accurately approximate the real behaviour of a plane wall of thickness 2δ provided the Fourier Number $Fo= \alpha t/\delta^2 < 0.2$ [3].

This assumption entails that during the pre-heating period up to ignition, the heat perturbation penetrates into the material by affecting a heated layer smaller than the actual thickness of the specimen. Furthermore, the initial and boundary conditions were that the initial temperature at t = 0 s was T_0 uniform inside the sample; the top surface was exposed to a constant heat flux $\dot{q}''_{ext}$, while the heat losses from the top surface were assumed to be negligible. Under such conditions, the time to ignition can then be calculated by Eq. (4.1), which is described and extensively detailed in Refs. [4-6].

$$t_{ig} = \pi/4\, k\rho c \left(T_{ig} - T_0\right)^2 / \dot{q}''^{\,2}_{ext} \tag{5.1}$$

By plotting $t_{ig}^{-1/2}$ as a function of the external radiant heat flux, a linear trend can be identified whose slope allows the computation of the theoretical critical heat flux (CHF). Indeed, the CHF is defined as the minimum value of the imposed heat flux at which ignition is theoretically possible, i.e. $t_{ig} = \infty$. Figure 5.1 shows the evolution of the square root of the inverse of the ignition temperature as a function of the external radiant heat flux referred to the dense graded mixture D-POR. The critical flux for ignition (CHF) was obtained by extrapolating ignition data to zero and resulted equal to 22.5 kWm^{-2}.

The slope of the line in Figure 5.1, along with Eq. (4.1), allows the assessment of the equivalent thermal inertia ($k\rho c$) of asphalt mixture as illustrated by Eq.(5.2).

$$k\rho c = \frac{4}{\pi}\left(\frac{\varepsilon}{Slope\ (T_{ig} - T_0)}\right)^2 \tag{5.2}$$

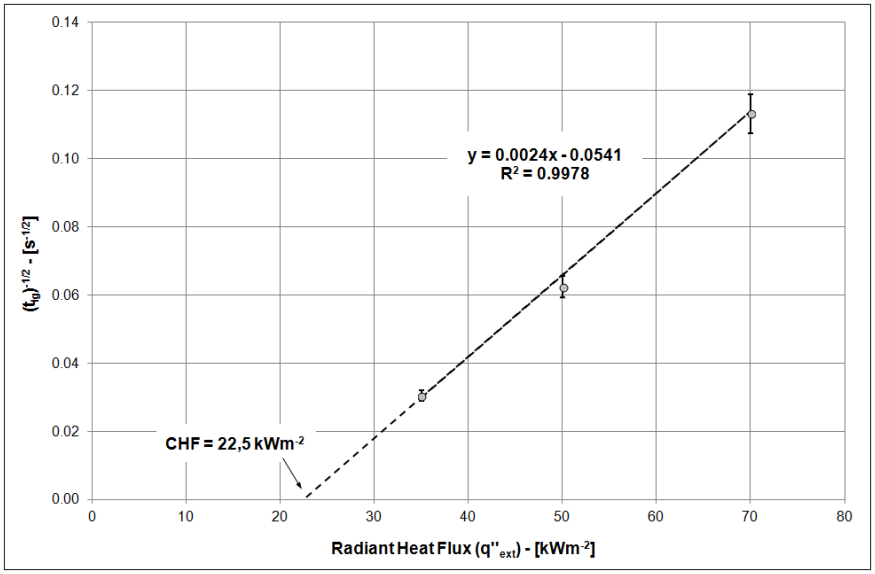

Figure 5.1 Square root of the inverse of ignition time as a function of radiant heat flux. Dense graded mixture.

Obviously, this is an equivalent value, which is a representative value averaged over the temperature range between T_0 and T_{ig}. The ignition temperature T_{ig} is calculated by iteratively solving Eq. (5.3), representing the boundary condition of the thermal problem at the exposed surface at the ignition [7].

$$\dot{q}''_{ext} = 1/\varepsilon \left[h_c\left(T_{ig} - T_0\right) + \varepsilon\sigma\left(T_{ig}^4 - T_0^4\right)\right] = CHF \tag{5.3}$$

To this aim, the emissivity coefficient ε was assumed equal to 0.91 [8], T_0 equal to 293.15 K, and CHF equal to 22.5 kWm^{-2}. The convective heat transfer coefficient, h_c, was calculated according to the empirical relation outlined by Dietenberger [9], specifically developed for the cone calorimeter apparatus: horizontal surface in natural convection with buoyancy forces depending on the cone irradiance and the cone heater itself. A mean value of 21.2 $Wm^{-2}K^{-1}$ was derived, in agreement with the correlation outlined by Staggs [10], as a function of the exposed surface temperature.

The theoretical T_{ig} found for dense graded mixture resulted 422 °C, which is in good agreement with the experimental value measured by means of the k-thermocouple positioned in contact with the top surface of the sample. Indeed, the experimental T_{ig} was found equal to 405 ± 21 °C, determined as an average of nine independent measurements (one for each sample). The equivalent thermal inertia resulted equal to 1.152 $kJ^2\ m^{-4}s^{-1}\ K^{-2}$.

In order to verify the adequateness of the semi-infinite solid hypothesis, the thermal diffusivity (α) was then calculated. To this aim, the density value reported in Table 3.6 was adopted (2275 kg m^{-3}) while the specific heat capacity was assumed constant and equal to 0.880 $kJkg^{-1}K^{-1}$[11].

Starting from the equivalent thermal inertia previously derived, the equivalent thermal conductivity resulted 0.563 $Wm^{-1}K^{-1}$ and the thermal diffusivity $2.8 \cdot 10^{-7}$ m^2s^{-1}. The length of the heated layer due to the heat wave penetrating inside the sample can then be calculated as L = $4\sqrt{\alpha t}$ [12], along with the Fourier number, at the time to ignition. Table 5.1 summarizes the obtained results considering the different irradiance levels.

Table 5.1 Verification of the semi-infinite solid hypothesis for dense graded mixture.

Asphalt Mixture ID	Heat flux	t_{ig}	Thickness δ	Heated Layer L= $4\sqrt{\alpha t}$	Fo
	[kWm^{-2}]	[s]	[cm]	[cm]	[-]
D-BC	70	66±4	4.0	1.7	0.01
D-BC	50	241±6	4.0	3.3	0.03
D-BC	35	1211±130	4.0	7.4	0.17

Focusing on the dimensionless number, the semi-infinite solid condition (Fo < 0.2) was verified at all the irradiance levels considered, although some criticality are expected for the lowest radiant heat flux values (Fo=0.17). Due to these approximations at lower heat fluxes and to the poor agreement of experimental data to Eq (4.1), the theoretical CHF resulted slightly underestimated. Previous studies [13,14] quantified such underestimation around the 64÷76% of the real CHF. Moreover, the CHF cannot be considered as an intrinsic thermal property, being highly influenced by the heat transfer conditions in the cone calorimeter apparatus. Nevertheless, it represents a useful indicator of the ignition properties of materials for ranking purposes, while the application to real fire scenarios would imply a thorough knowledge of the likely heat transfer boundary conditions. The same considerations are valid for the thermal properties previously outlined, due to their significant temperature-dependence.

Completely different outcomes were obtained when open graded mixture was tested. Indeed, the heat fluxes of 35 kWm^{-2} and 50 kWm^{-2} were found not sufficient for igniting the samples within 30 minutes of exposure prescribed by the specifications. Therefore, only a rough estimation of the critical heat flux could be inferred, resulting between 50 kWm^{-2} and 70 kWm^{-2}.

Such significant gap in t_{ig} values is mainly ascribable to the different air voids content characterizing the mixtures. Indeed, high air voids content results in a more uneven top surface. Consequently, the radiant heat flux of 70 kWm^{-2} is not equally applied to the whole surface of the sample and this delays the achievement of the critical mass loss rate required for ignition. As well as the CHF for open graded mixture, the theoretical temperature of ignition T_{ig} could not

be calculated, while an experimental value was measured during tests at 70 kWm^{-2} radiant heat flux, resulting equal to 580 ± 9 °C.

After ignition, steady flames established on the top surface of the samples, as shown in Figure 5.2.

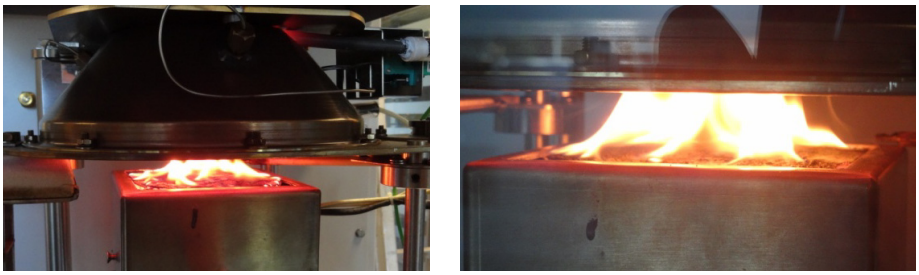

Figure 5.2 Dense graded mixture after ignition.

In this phase, the burning behaviour of materials is governed by the release rate of flammable volatiles due to thermal degradation, i.e. the burning rate $\dot{m}''$.

Assuming constant the heat feedback from the flames to the surface of the sample, and the heat flux from the external radiant heater, the steady state burning rate is determined as the ratio between the net heat flux applied to the surface and the heat of gasification *L*, as shown in Eq (5.4). The net heat flux is in turn obtained as a balance between the external heat of exposure ($\dot{q}''_{ext}$), the heat feedback from the flames (*FHF*, composed of the radiative and convective components), and the radiative heat flux loss from the sample surface ($\varepsilon\sigma T_V^4$).

$$\dot{m}'' = \frac{\dot{q}''_{ext} + FHF - \varepsilon\sigma T_V^4}{L} \tag{5.4}$$

In this stage, both the convective and the conductive losses are assumed negligible compared to the radiative one, while they should be taken into account if an analysis of transient burning rate would have been performed [4]. Heat of mass gasification, *L*, represents the heat required to gasify, or to produce volatiles, from a unit weight of combustible solid at temperature T_0.

The radiative heat loss from the surface of the sample should be calculated considering the temperature of vaporization T_V, defined as the temperature of the moving vaporizing surface penetrating into the sample [4,5]. The average burning rates measured over the whole duration of the test are represented in Figure 5.3 as function of the external radiant heat flux.

Mass loss rate increased with increasing irradiance levels, showing a linear trend in agreement with Eq.(5.4). Theoretical heat of gasification *L* can then be deduced from the slope of the fit line, resulting equal to 58.8 MJ kg^{-1}.

The heat feedback from the flames can also be approximately estimated by assuming the temperature of vaporization to be equal to the ignition temperature T_{ig} [4]. Under these conditions, the heat feedback from flames results 24.5 kWm^{-2}.

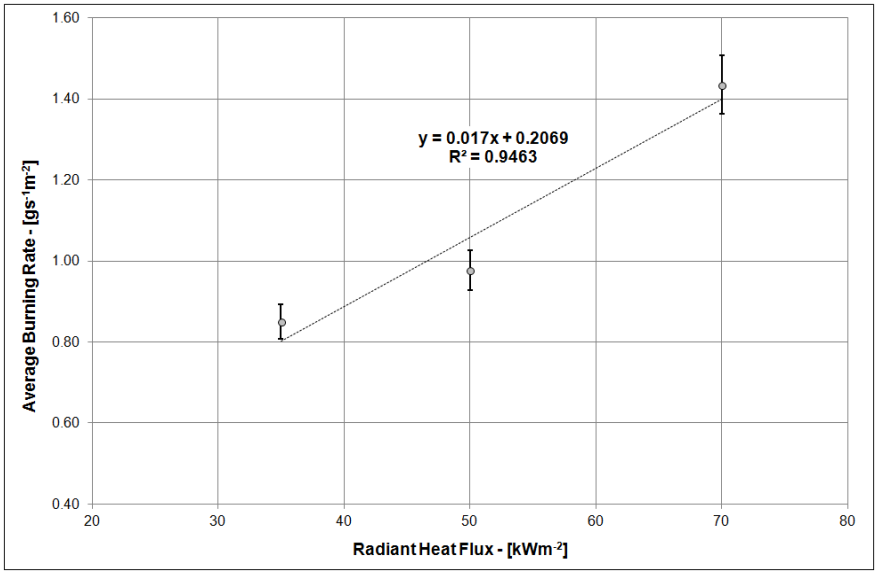

Figure 5.3 Average burning rate as a function of radiant heat flux. Dense graded mixture.

The characterization of the fire behaviour of asphalt mixture develops with the description of the evolution of the heat release rate (HRR) during the test. HRR was determined through the oxygen consumption method by measuring the flow rate of the exhaust gases through the duct system and the oxygen depletion in this flow [15]. This parameter is considered the most important factor affecting the fire hazard of materials [15,16], since it controls the rate of growth in fire, as well as the amount of smoke and toxic gases generated.

HRR curves found for dense graded mixture (D-BC) at different radiant heat fluxes are depicted in Figure 5.4 and show a typical trend of semi-infinite char-forming solid [17], coherently with the hypothesis formulated in the previous section.

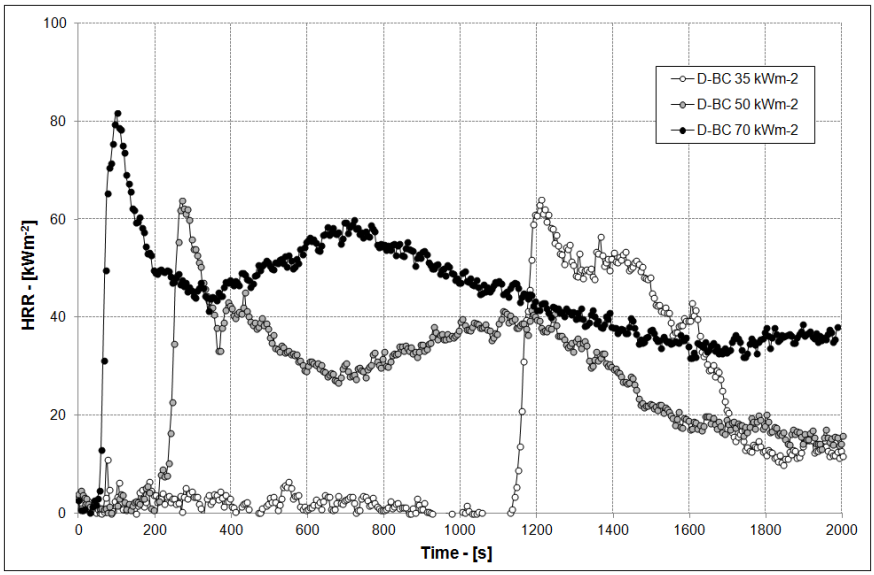

Figure 5.4 HRR curves as functions of different radiant heat fluxes - Dense graded mixture.

Conversely, the HRR curves found for open graded mixtures (O-POR) are characterised by significantly postponed ignition, with a t_{ig} almost equal to 30 min when subjected to 70 kWm^{-2} (see Figure 5.5), and a unique peak. Due to the extended period of pre-heating before ignition, the hypothesis of semi-infinite solid became implausible, as the heated length most likely exceeded the sample thickness and led to negligible temperature gradients inside the sample. The more intense and sharp peak in HRR curve supported this hypothesis, as it could be considered the result of the whole pyrolyzation of the sample once the ignition temperature had been achieved.

Focusing on the D-POR mixture, the peak in heat release rate (PHRR) raised with increasing irradiance levels, following almost the same trend of the burning rate. The ratio between the average HRR and the average burning rate represents the effective heat of combustion (EHC), corresponding to the actual heat released from the volatile fraction during solid material combustion.

Table 5.2 summarizes the burning rate, HRR, EHC and the total heat release (THR) found for conventional open and dense graded mixtures. For O-POR mixture, only results referred to 70 kWm^{-2} of irradiance level were reported.

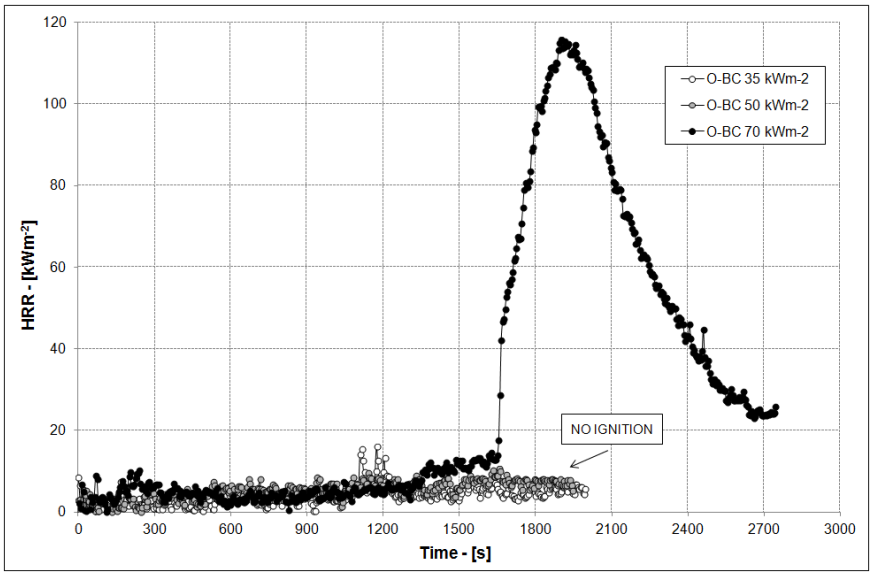

Figure 5.5 HRR curves as functions of different radiant heat fluxes. Open graded mixture.

The effective heat of combustion (EHC) was found independent of the radiant heat flux, as well as of the aggregate gradation of the mixture. This fact was somewhat expected, being the EHC dependent on the combustible portion of the mixture, i.e. the asphalt binder, which is present in the same amount in all the tested mixtures. Moreover, the EHC found for asphalt mixtures was quite comparable with the values found by Schartel et al. [18] (25.8-27.7 $MJkg^{-1}$) for asphalt mixtures with slightly different aggregate gradations and bitumen contents.

Table 5.2 Fire response parameters: peak of heat release rate (PHRR); average heat release rate (Av. HRR); total heat release (THR); effective heat of combustion (EHC); average burning rate ($\dot{m}''$).

Asphalt Mixture	Heat Flux	PHRR	Av. HRR	THR	EHC	$\dot{m}''$
	$[kWm^{-2}]$	$[kWm^{-2}]$	$[kWm^{-2}]$	$[MJm^{-2}]$	$[MJkg^{-1}]$	$[gs^{-1}m^{-2}]$
D-BC	35	52±7	26±4	20±3	34±6	0.85±0.01
D-BC	50	69±8	35±6	62±11	33±7	0.98±0.14
D-BC	70	83±4	57±3	84±2	35±5	1.43±0.11
O-BC	70	102±19	35±5	68±6	34±4	1.69±0.13

5.2 Influence of the physical properties of aggregates on fire behaviour

Previous experimental results highlighted the significant role of the aggregate gradation in the fire behaviour of asphalt mixtures. Open graded mixtures actually ignited only at relevant irradiance levels (higher than 50 kWm^{-2}). Therefore, the investigation developed focusing on the role of aggregates nature only considering the dense graded structure, which was found ignitable for irradiance levels theoretically higher than 22.5 kWm^{-2}. The analysis was based on the HRR curves, depicted in Figure 5.6, along with other significant test results synthetically reported in Table 5.3.

Table 5.3 Fire response parameters: time to ignition (t_{ig}); peak of heat release rate (PHRR); average heat release rate (Av. HRR); total heat release (THR); effective heat of combustion (EHC); average burning rate ($\dot{m}''$).

Asphalt Mixture	Heat Flux	t_{ig}	PHRR	Av. HRR	THR	EHC	$\dot{m}''$
	[kWm^{-2}]	[s]	[kWm^{-2}]	[kWm^{-2}]	[MJm^{-2}]	[$MJkg^{-1}$]	[$gs^{-1}m^{-2}$]
D-BC	70	66±4	83±2	57±3	84±2	35±5	1.43±0.11
D-EAF	70	104±10	72±7	46±4	82±7	36±2	1.35±0.18
D-LECA	70	42±4	112±4	51±3	92±5	35±5	1.48±0.22

Physical properties of coarse aggregates played an important role only in governing the ignition phase of asphalt mixtures. In fact, asphalt mixtures with EAF aggregates postponed ignition of approximately 40 s thanks to their higher density while D-LECA mixture reaches the ignition only after 40 s, 20 s earlier than conventional aggregates. So, in agreement with previous Eq.(4.1), the lower the density, the shorter the time to ignition t_{ig}.

Once ignited, D-LECA mixtures showed an overall burning behaviour quite similar to the conventional one but slightly accelerated in time and more intense. Indeed, due to an overall raise of the flammable volatile release, the peak in heat release rate (PHRR) increased by approximately 35%, along with the THR that exhibited a 10% growth.

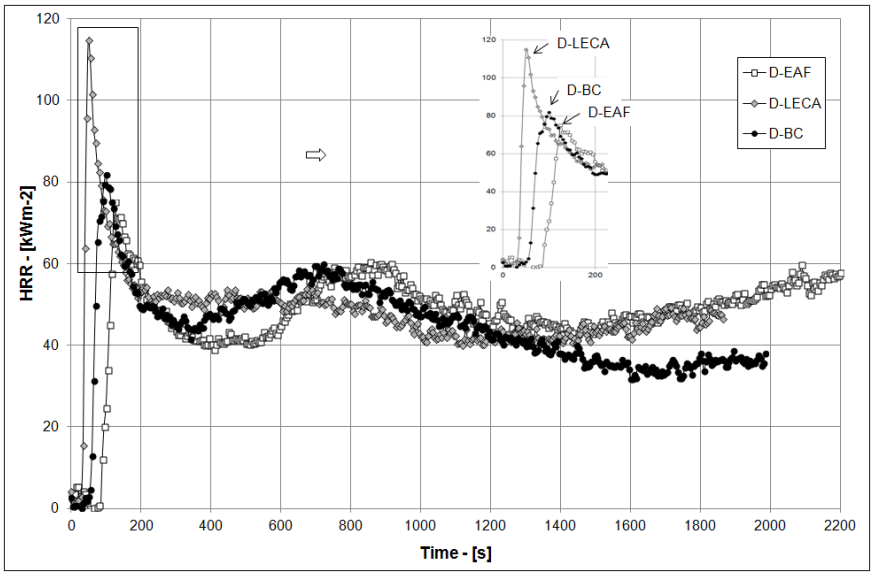

Figure 5.6 Effect of different aggregates on HRR curves. Exposure 70 kWm^{-2}.

Conversely, D-EAF mixture showed a HRR curve quite similar to D-POR mixture, also in terms of PHRR, but postponed in time due to an overall delaying of the asphalt combustion. Nevertheless, the EHC value remained constant because the combustible portion was present in the same quality and quantity for all the tested mixtures. Moreover, the average burning rate ($\dot{m}''$) exhibited a slight increasing trend with lowering density, consistent with the PHRR values, but with not remarkable differences among the tested mixtures. Thus, physical properties of coarse aggregates significantly affected only the first phase of the burning behaviour of mixtures, with weaker effect after the ignition of the samples.

Finally, by means of a gas sampling apparatus, cone calorimeter test also allowed to quantify the emission yields of CO and CO_2 as the ratio between the exhaust product mass flow rate and the mass loss rate of the whole sample. Furthermore, smoke production was assessed basing on the theory of the attenuation of a beam of light by suspended aerosol particulates.

The amount of smoke was detected during all the duration of the test and the total smoke production (TSP) was referred to the entire testing period. The TSR was then calculated as the ratio of TSP to the exposed surface area. Table 5.4 shows the results obtained for all mixtures.

Table 5.4 Influence of aggregates on fire response parameters: CO and CO_2 yields; total smoke release (TSR).

Asphalt Mixture ID	Heat flux	CO	CO_2	CO/CO_2	TSR
	[kWm^{-2}]	[g_{CO}/g_{SAMPLE}]	[g_{CO2}/g_{SAMPLE}]	[%]	[m^2/m^2]
D-BC	70	0.044±0.006	1.920±0.141	2.3	248±63
D-EAF	70	0.037±0.009	2.298±0.138	1.6	353±77
D-LECA	70	0.030±0.006	2.278±0.274	1.3	391±12
O-BC	70	0.050±0.003	2.075±0.092	2.4	1145±224

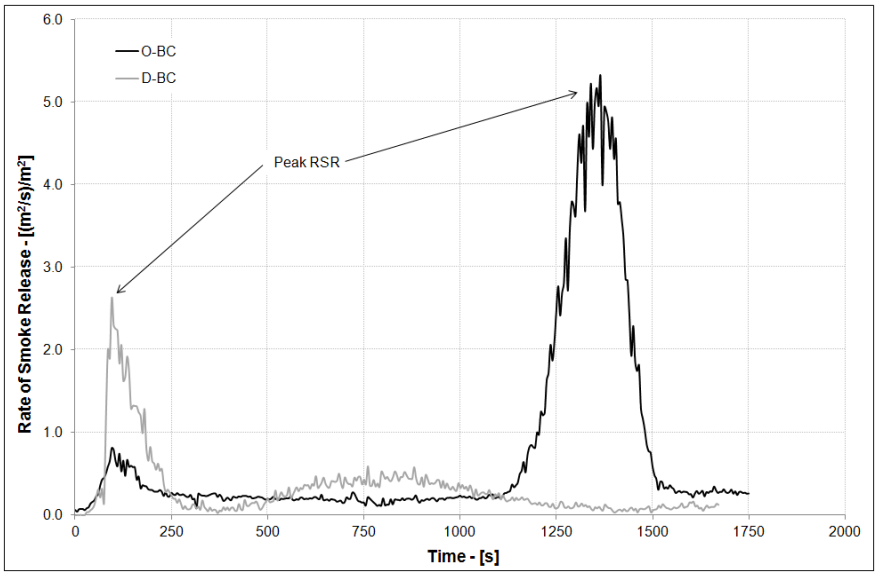

Figure 5.7 Rate of Smoke Release (RSR) of O-BC and D-BC mixtures.

Figure 5.7 shows the overall RSR trends recorded for O-BC and D-BC mixtures: the TSR is evaluated as the area under the RSR curve.

Comparing D-BC and O-BC mixtures, no significant differences in terms of CO and CO_2 yields could be identified, although remarkable smoke production was highlighted in the case of the open graded mixture. The effect of aggregates was found not considerably relevant, being the CO and CO_2, along with the smoke production, characterized by not remarkable variations.

A final interesting consideration can be drawn by the observation of the samples after the test. O-BC mixtures simply resulted in a mass of completely loose aggregates, as it can be observed in Figure 5.8, with the asphalt binder totally burnt. Conversely, D-BC mixtures showed an even and compact superficial residue as expected from the analysis of the HRR curve. This carbonaceous layer actually plays an effective shielding action on the fuel

beneath since the asphalt mixtures directly affected by the combustion process is limited to the upper 15÷20 mm layer, as can be observed by cutting the burnt sample (see Figure 5.8).

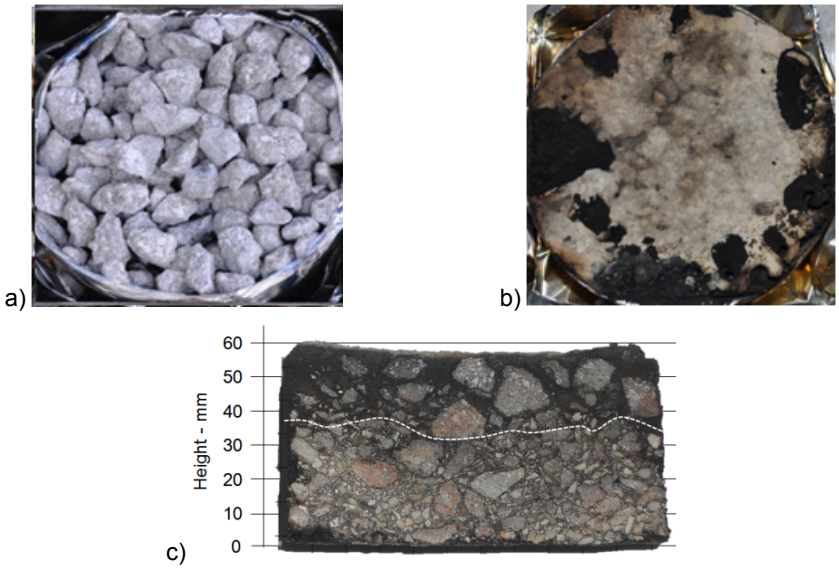

Figure 5.8 a) Residue of O-BC sample and b) D-BC sample. c) Section of D-BC sample.

5.3 FR-asphalt mixtures

5.3.1 Effect of FR-fillers

The present section reports the analysis of cone calorimeter tests performed on open graded mixtures containing base bitumen B50 combined with limestone, ATH and MH fillers. As usual, the HRR and RSR curves obtained for each asphalt mixtures are reported in Figure 5.9 a) and b) respectively (each curve is referred to one of the three specimens for each asphalt mixture) while Table 5.5 and Table 5.6 synthetically summarizes all the fire properties of the mixtures.

a)

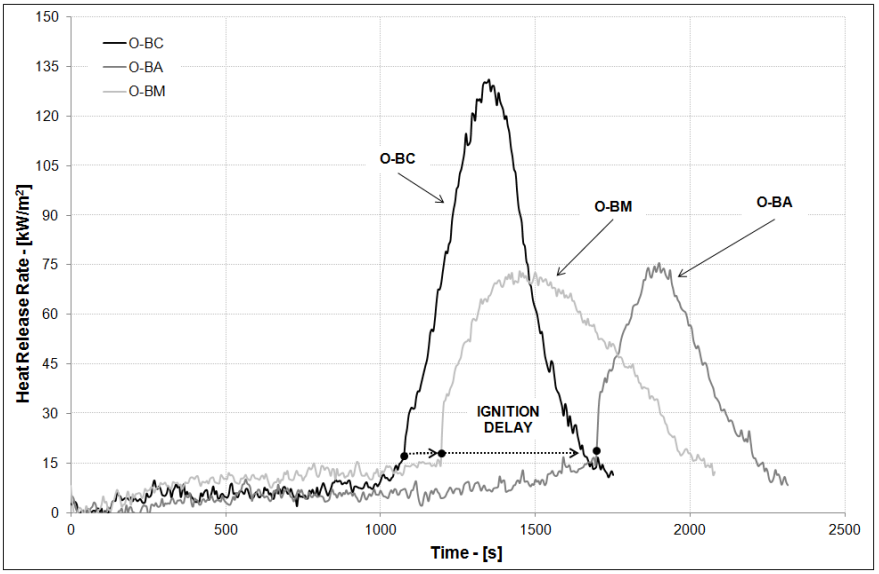

b)

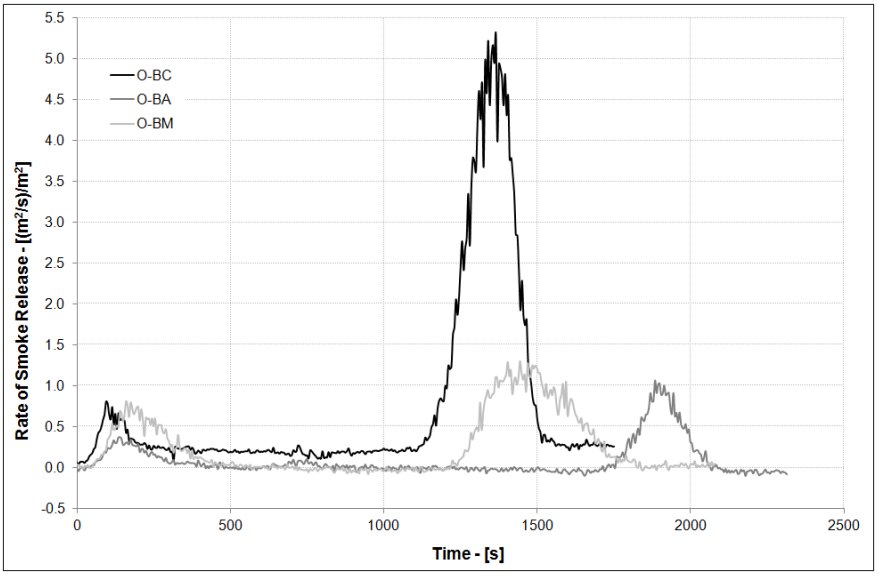

Figure 5.9 HRR (a) and RSR (b) curves for open graded mixtures with FR fillers.

Table 5.5 Fire response parameters of mixtures with base bitumen B50: time to ignition (t_{ig}); time to flame-out (t_{fo}); peak of heat release rate (PHRR); total heat evolved (THE); average effective heat of combustion (EHC).

Asphalt Mixture	t_{ig}	t_{fo}	PHRR	THE	EHC
	[s]	[s]	[kW/m^2]	[MJ/m^2]	[MJ/kg]
O-BC	1079±157	1613±9	122±14	37±4	31.8±1.6
O-BM	1157±72	1992±53	69±5	45±4	32.5±1.7
O-BA	1654±79	2180±103	75±2	28±3	30.4±5.0

Table 5.6 Fire response parameters of mixtures with base bitumen B50: CO yield; total smoke release (TSR); peak of Mass Loss Rate (MLR).

Asphalt Mixture ID	CO	TSR	Peak of MLR
	[g_{CO2}/g_{SAMPLE}]	[m^2/m^2]	[g/s]
O-BC	0.050±0.003	1145±224	0.284±0.054
O-BM	0.029±0.003	424±142	0.041±0.005
O-BA	0.058±0.002	309±84	0.040±0.010

All the asphalt mixtures show similar HRR curves, characterized by only one peak of heat and smoke releases occurring in the final part of the test. Thus, an overall burning behaviour quite comparable could be initially identified. Nevertheless, the introduction of FR fillers, such as ATH-3 and MH, in place of conventional limestone filler leads to several significant differences in the fire response parameters.

The first relevant dissimilarity concerns the time to ignition. Indeed, all the asphalt mixtures show t_{ig} higher than 1000 s but following a specific trend: t_{ig}(O-BC) < t_{ig}(O-BM) < t_{ig}(O-BA). If we consider the flammability analysis performed on the corresponding asphalt mastics, LOI results referred to asphalt mastics prepared with the same base bitumen of the present work and mineral filler at 1/1 ratio (w/w) were: 27%, 31% and 48% referring to limestone C, magnesium hydroxide MH, and aluminium hydroxide ATH-3 respectively. Thus LOI(C) < LOI(M) < LOI(A), as well as the t_{ig} found for the corresponding open graded mixtures. Therefore, even if LOI and t_{ig} could not be directly correlated, the results obtained in this research confirm that FR fillers play an important role in enhancing the ignitability of asphalt mixtures.

This result can be explained keeping in mind how these FR-fillers work. In fact, both ATH and MH start decomposing at 200°C and 300°C respectively to aluminium or magnesium oxide and water. This decomposition leads to several beneficial effects on asphalt binder thermal degradation which have been widely analysed in previous chapters. More specifically, the endothermic reaction basically acts as a heat sink mechanism resulting in a significant slowing down of

bitumen pyrolysis which in turn reduces the flammable volatiles release. In this way, the achievement of the above-cited critical mass loss rate is postponed, thus the time to ignition is delayed and the LOI increased.

A more clear explanation of this FR mechanism can be outlined by focusing on the terms characterizing Eq.(5.5) which describes how the HRR is determined during cone calorimeter test.

$$HRR = EHC \cdot MLR = (1-\mu)\left(\frac{EHC}{h_g}\right) q_{net} \qquad (5.5)$$
$$= (1-\mu)\left(\frac{EHC}{h_g}\right)\left(aq_{ext} + aq_{flame} - q_{rerad}\right)$$

Indeed, the heat release rate is evaluated through the oxygen consumption method by measuring the flow rate of the exhaust gases through the duct system and the oxygen depletion in this flow [15]. Moreover, by means of a weighing device it is possible to register the mass of the sample during the whole test, thus outlining the mass loss rate (MLR) of the material. HRR and MLR are strictly correlated, since the heat release rate is evaluated as the mass loss rate in kg/s multiplied by the effective heat of combustion EHC in kJ/kg (see Eq. (5.5)) [3, 5]. The mass loss rate is in turn controlled by the net heat flux applied to the surface (q_{net}) and the heat of gasification (h_g). The former results from the heat balance between the in-coming fluxes, such as the external applied flux (aq_{ext}) and the flux radiated from flames (aq_{flame}), and the heat flux reradiated to the environment, according to the Stefan-Boltzmann equation [3]. On the other hand, the heat of gasification (h_g) represents the heat required to produce the volatiles and it is a specific property of the burning material. Finally, μ represents the char yield.

The EHC values reported in Table 5.5 are almost identical for all the mineral fillers, thus indicating that both A and M filler do not change the nature of the fuel gases. More precisely, FR fillers simply act as inert filler toward asphalt binder without achieving any kind of chemical interaction, as already outlined by means of TGA analyses on the corresponding asphalt mastics.

The main result attained with the introduction of the FR fillers is a dramatic decrease in mass loss rate, almost reaching a reduction of 85% compared with mixtures containing limestone filler.

This beneficial outcome is achieved by different concurring mechanisms which can be all ascribed to the endothermic decomposition of the FR filler. Indeed, the heat required by ATH and MH to decompose, equal to 1,300 and 1,450 kJ/g respectively, significantly increases the heat of gasification h_g, which is the energy required to gasify the unit mass of solid fuel originally at ambient temperature, including the heat of melting, decomposition, crosslinking, and vaporization [16]. Moreover, the Al_2O_3 and MgO residue (identified by μ coefficient) produced after the decomposition performs as a high heat capacity barrier for the condensed phase. Thus, instead of decreasing the heat of complete combustion of the fuel gases, the heat of gasification per unit mass of

volatiles is increased in accordance with the increase of char yield. Therefore, both the dilution of combustible volatiles and residue formation inhibit the rates of heat transfer from the flame to the underlying matrix (q_{flame}). This reduction in the applied heat flux is combined with increased surface heat losses (q_{rerad}) due to the capability of fine particles to reach high temperatures, consequently acting as effective radiation shields.

All these factors result in a significant decrease in PHRR values, with ATH and MH fillers found almost equally effective in reducing this fire hazard related to flame spread. However, ATH filler also leads to the most effective delay of asphalt mixtures' ignition. This specific performance is mainly ascribable to the different onset decomposition temperatures of the FR fillers. Indeed, ATH starts decomposing at 200°C anticipating the onset of bitumen decomposition occurring at approximately 250°C. Conversely, MH begins its decomposition at 300°C, when the bitumen pyrolysis is in action, as outlined in previous chapters. It is then evident that even if the overall FR mechanism is the same for both A and M, as highlighted by the same effectiveness in reducing the PHRR, the onset decomposition temperature of FR filler is the leading factor in controlling the time to ignition.

Focusing on the Total Heat Evolved THE, O-BA results the asphalt mixture producing the lower heat release during the combustion process while O-BM reached the highest value. This outcome is somewhat contrasting with the above-cited observations. Anyway, it is worth noting that the cone calorimeter test is based on the oxygen depletion calorimetry, which evaluates the heat release assuming that 13.1 kJ of heat is released per gram of oxygen consumed [38]. So, only the effects produced by the endothermic process, such as delay in t_{ig} and decrease in PHRR, can be directly highlighted by using oxygen depletion calorimetry, while the endothermic process itself can be observed only by means of a thermometric device, such as DSC.

Figure 5.9 displays the Rate of Smoke Release (RSR) curves recorded during the development of the combustion process.

The RSR curves substantially follow the same trend of HRR curves. Peak in RSR is reached immediately after ignition and both ATH and MH were found to be effective smoke suppressant. Both CO and smoke yields are due to incomplete combustion which is generally increased when FR additives acting in the gas phase, such as halogenated FRs, are used [19].

Conversely, the asphalt mixtures containing ATH and MH fillers show completely different behaviours. Indeed, MH leads to the lowest CO yield while ATH dramatically decreases the peak of RSR and the consequent Total Smoke Release (TSR). These beneficial effects are mainly due to the inorganic MgO and Al_2O_3 residue. In fact, the oxide residue acts as a physical barrier in the condensed phase which not only limits the flammable volatile release but also the yield of incomplete combustion by-products. Moreover, in case of polymers, freshly formed oxides are characterised by high surface areas and catalytic properties which promote the deposition of carbon and subsequent oxidation processes. Thus, the volatilization of carbonaceous residue as carbon oxides occurs and the obscuration effects of the smoke release consequently decrease.

In addition, a small further contribution can be provided by the water evolved from hydroxide decomposition, being known to oxidise carbon.

Finally, it is worth noting that even traditional limestone filler mainly composed of calcium carbonate decomposes into CaO and CO_2 in an endothermic reaction. Nevertheless, the same outcome of FR fillers cannot be reached because of the high onset decomposition temperature of calcium carbonate, approximately equal to 700 °C. Thus, limestone can only play the role of inert filler which partially reduces the amount of fuel in volume without playing an active and effective role in hindering bitumen thermal degradation.

5.3.2 Effect of organoclay-modified bitumen

Open and dense graded mixtures with nanocomposite binder modified with 3.33wt% organomodified-montmorillonite (OMMT) were tested and results are synthetically reported in Table 5.7 and Table 5.8.

Table 5.7 Fire response parameters of mixtures with base bitumen B50: time to ignition (t_{ig}); time to flame-out (t_{fo}); peak of heat release rate (PHRR); total heat evolved (THE); average effective heat of combustion (EHC).

Asphalt Mixture	t_{ig}	t_{fo}	PHRR	THE	EHC
	[s]	[s]	[kW/m^2]	[MJ/m^2]	[MJ/kg]
O-NBC	158±48	210±37	95±11	46±5	24.0±2.0
O-NBM	76±8	1565±85	61±6	62±3	25.7±0.7
O-NBA	78±1	552±35	45±8	28±1	17.5±0.3
D-NBC	84±3	1917±68	90±4	100±15	31.9±1.0
D-NBM	95±11	2666±145	75±8	94±1	25.4±3.6
D-NBA	105±5	1483±54	79±2	85±4	22.0±2.7

Table 5.8 Fire response parameters of mixtures with base bitumen B50: CO yield; total smoke release (TSR); peak of Mass Loss Rate (MLR).

Asphalt Mixture	CO	TSR	Peak of MLR
	[g_{CO2}/g_{SAMPLE}]	[m^2/m^2]	[g/s]
O-NBC	0.082±0.007	558±95	0.095±0.013
O-NBM	0.036±0.003	273±21	0.103±0.028
O-NBA	0.046±0.001	184±79	0.116±0.018
D-NBC	0.030±0.008	1412±68	0.081±0.019
D-NBM	0.034±0.004	913±12	0.083±0.017
D-NBA	0.032±0.002	664±40	0.091±0.016

The selected criteria for comparison reside within the HRR curves which are depicted for each mineral filler in Figure 5.10, Figure 5.11 and Figure 5.12.

As usual, a first significant outcome can be highlighted by comparing the time to ignition (t_{ig}) reported in Table 5.5 and Table 5.7. Indeed, irrespective of the mineral filler used, all the O-NB mixtures show early ignition compared with the corresponding O-B series. This fact was already observed in case of nanocomposite polymers [19], and it is mainly ascribable to the degradation of the organic content in the OMMT [20], which exhibits scarce thermal stability [21,22] and starts decomposing at about 250°C, thus favouring an increase in flammable volatile release and consequent early ignition.

Nevertheless, the sustained flaming combustion was actually anticipated in case of mixtures containing FR fillers but a somewhat peculiar behaviour was highlighted for O-NBC mixtures. Indeed, all the three samples of O-NBC series show a first ignition occurring at approximately 150÷200 s followed by a brief flaming combustion which rapidly extinguishes in 60 s. Then, a second ignition is reached after 950 s from the beginning of the test resulting in a second sustained flaming combustion which lasts approximately 600 s before the flame-out occurs. Conversely, both O-NBM and O-NBA show only a single ignition and a flaming combustion phase but with different durations. The former reached approximately 1500 s while the latter reached the best performance in terms of flaming combustion duration since the flame out occurs after 500 s (see Table 5.7). For the sake of clarity, the t_{ig} and t_{fo} reported in Table 5.7 for O-NBC are referred only to the first ignition while the second ignition and flame-out are only pointed out in Figure 5.10. It is also worth noting that in case of limestone filler C, the nano-modification of asphalt binder does not change the overall burning behaviour (thick charring/thick non-charring) of mixtures which remains strictly related to the aggregate gradation (compare Figure 5.4, Figure 5.5 and Figure 5.10).

The most significant enhancements due to nano-modification of asphalt are achieved in case of open graded mixtures where the PHRR and TSR decreased by 22% and 51% respectively. Conversely, the PHRR of D-NBC and D-BC are almost equal while the TSR is reduced by 70%. Nevertheless, irrespective of the aggregate gradation, nanocomposite binder leads to lower peaks in mass loss rate and effective heat of combustion, as already observed in previous chapters.

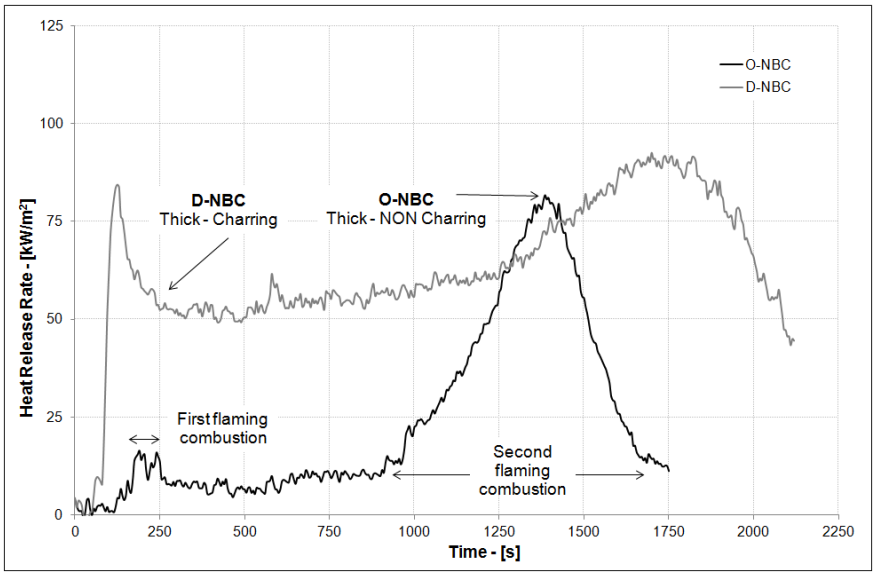

Figure 5.10 HRR curves of asphalt mixtures with binder 3.33BC and filler C.

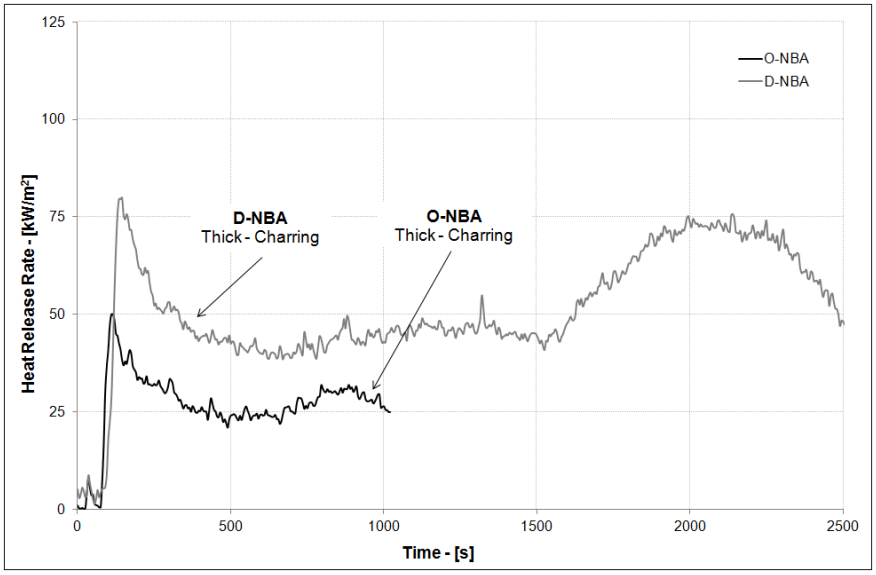

Figure 5.11 HRR curves of asphalt mixtures with binder 3.33BC and filler ATH-3.

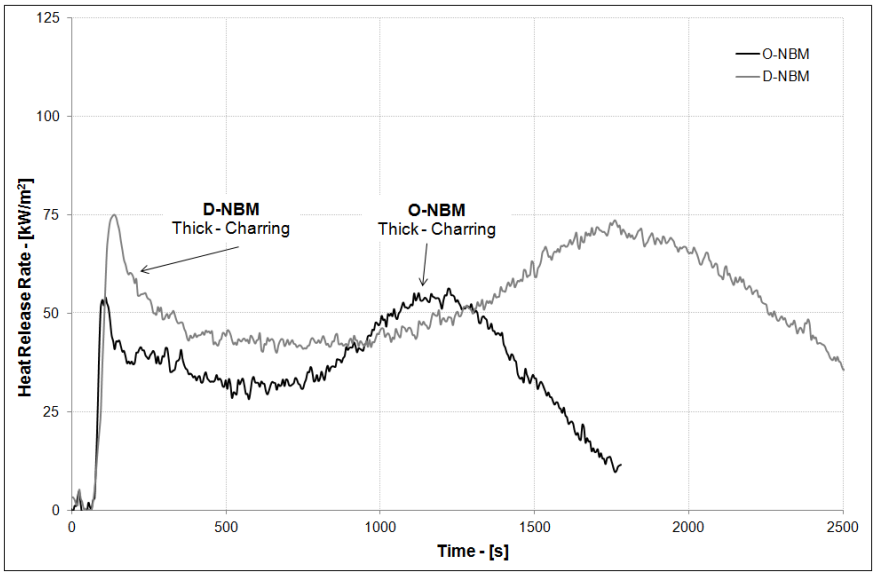

Figure 5.12 HRR curves of asphalt mixtures with binder 3.33BC and filler MH.

Further important outcomes are reached when the nano-modification is coupled with the addition of FR fillers. Indeed, by comparing the HRR curves of open graded mixtures with ATH and MH fillers, a synergism between FR filler and OMMT can be highlighted by the achievement of an effective shifting of the fire behaviour of asphalt mixture from a thick-non charring (O-B series) to a thick char forming material (O-NB series).

This fact is even more evident if we compare the HRR curves of open and dense grade mixtures containing FR fillers and 3.33BC bitumen and the superficial residues observed after the cone calorimeter test (Figure 5.13) where O-NBA and O-NBM are characterized by the presence of bubbles and thin slivers in the film covering the coarse aggregates.

Thus, the combination of FR fillers and nanocomposite bitumen actually changes the fire response of asphalt mixtures and somehow eliminates the differences due to distinct aggregate gradations. Conversely, asphalt binder in O-NBC mixtures (which do not include the FR fillers) is totally burnt and O-NBC samples substantially behave as O-BC, thus resulting in a mass of completely loose aggregates.

Furthermore, not only the HRR curves are significantly influenced by the simultaneous presence of FR fillers and OMMT but also the fire response parameters are dramatically changed. It is therefore evident that the beneficial effects due to the endothermic decomposition of FR fillers are still valid but now they are coupled with other mechanisms related to the nano-modification of the asphalt binder. More specifically, the contribution of nanocomposite has been recently analysed in case of polymer nanocomposites [23] and it is generally recognized that it is due to the mechanism of barrier formation during

combustion, thus excluding any FR action in the gas phase. When the surface temperature of the samples reaches 250÷300 °C, the quaternary alkilammonium compounds undergo a thermal degradation, thus leading the nanostructure to collapse and leaving the most superficial montmorillonite (MMT) stacks free to migrate. The MMT foils are subjected to driving forces of different kinds which lead to an ablative reassembly of the silicate layers on the surface of the sample.

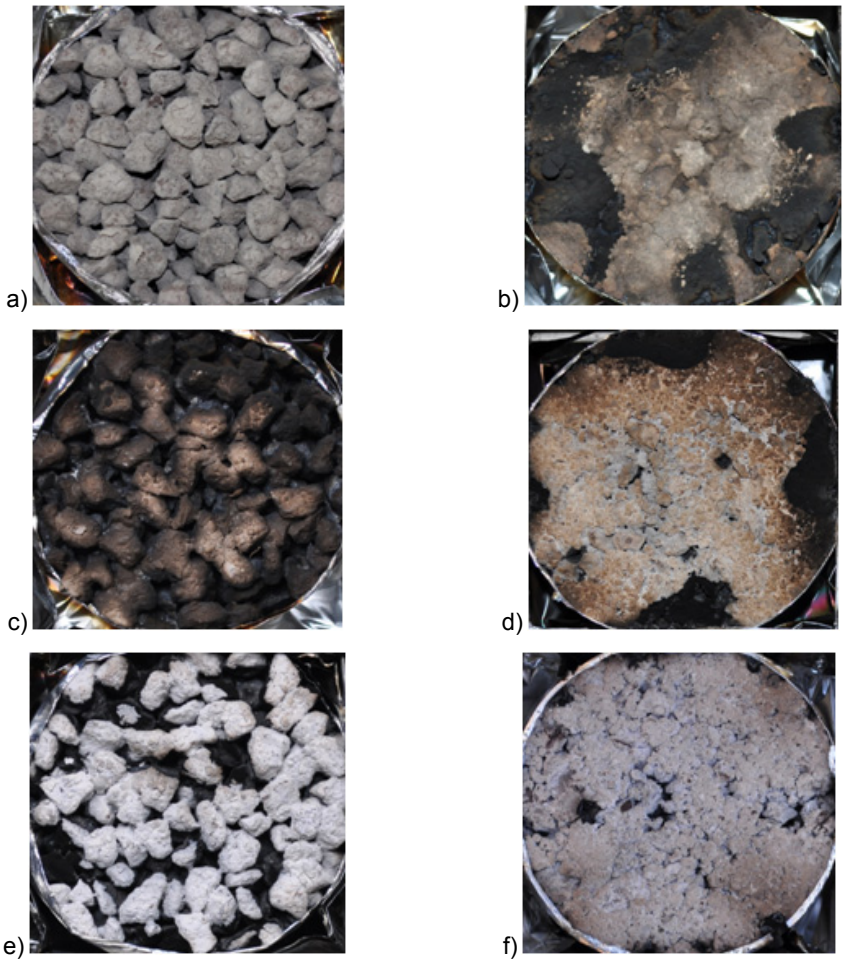

Figure 5.13 Residue after cone calorimeter test:
a) O-NBC; b) D-NBC; c) O-NBA; d) D-NBA; e) O-NBM; f) D-NBM.

Different mechanisms were proposed to explain the MMT surface accumulation in case of polymer nanocomposites [24] and some of them can be transferred to the asphalt binder nanocomposites. In fact, MMT is an alumina-silicate characterized by surface free energy lower than a carbon-based material,

such as bitumen. Therefore, MMT is alien to the bitumen host and with increasing temperatures it is driven towards the surface because of these different energies. Moreover, the migration is favoured by vapour or gas bubbles formed due to the degradation of the ammonium compounds and bitumen itself. Thus, even if the decay of the organically modified clay results in an anticipated ignition, it is certainly essential for flame-retarding purpose, being the first step for creating an effective superficial clay-rich barrier. When the nanocomposite is coupled with FR fillers, the barrier mechanism is significantly strengthened, as highlighted by the dramatic decrease in PHRR and TSR.

The best performance is achieved with ATH filler, being the PHRR reduced by 41%, the TSR by 41% and the CO yield by 20%. In addition, O-NBA reaches the flame-out before all the other mixtures, thus indicating that the char layer formed on the top of the sample acts as an insulator and mass transport barrier which leads to stop flaming because of fuel starvation. Moreover, the presence of intercalated layered silicates in the asphalt matrix beneath the superficial protective layer hinders the escape of flammable components as in a labyrinth effect [25], thus resulting in a significant decrease in flammable volatile release [26].

All these results are a clue of the actual nano-modification of the base asphalt binder. Indeed, the catalysis in charring can be effectively achieved only in the nanocomposite structure where the intimate contact between the asphaltic molecules and the inorganic silicate layers is so extensive that thermal bond scission is partially prevented.

Conversely, in microcomposites the volatilization usually prevails over charring because this contact is weak and inefficient and clay simply behaves as a inert filler. This interaction results in a modification of the fuel released, as clearly outlined by the decreased effective heat of combustion which in turn leads to a decrease in heat release rate (Eq. (5.5)).

References

[1] International Organization for Standardization. Reaction to fire tests - Heat release, smoke production and mass loss rate. Part 1: Heat release rate (cone calorimeter method). ISO 5660-1:2002; 2002.

[2] International Organization for Standardization. Standard atmospheres for condition and/or testing. Specifications. ISO 554:1976; 1976.

[3] Incropera FP, DeWitt D, Bergman TL Lavine AS. Fundamentals of heat and mass transfer. 6th ed. Chichester: John Wiley & Sons; 2006.

[4] Rhodes BT, Quintiere JG. Burning rate and flame heat flux for PMMA in a cone calorimeter. Fire Safety J 1996; 26:221–40.

[5] Hopkins Jr D, Quintiere JG. Material fire properties and predictions for thermoplastics. Fire Safety J 1996; 26:241–68.

[6] Delichatsios MA, Panagiotou Th, Kiley F. The use of time to ignition data for characterizing the thermal inertia and the minimum (critical) heat flux for ignition or pyrolysis. Combustion and Flame 1991; 84:323-32.

[7] Janssens M. A thermal model for piloted ignition of wood including variable thermophysical properties. Proc. Fire Safety Science – Proceedings 3rd International Symposium. Pp. 167-176. Edinburgh, 8-12 July 1991.

[8] Stempihar JJ, Pourshams-Manzouri T, Kaloush KE, Rodezno MC. Porous asphalt pavement temperature effects for urban heat island analysis. Transportation Research Record: Journal of the Transportation Research Board 2012; 2293:123-30.

[9] Dietenberger M, Ignitability analysis using the cone calorimeter and LIFT apparatus. 22nd International Conference on Fire Safety, Columbus, OH, 1996.

[10] Staggs JEJ. Convective heat transfer in the cone calorimeter. Fire Safety J. 2009; 44:469-74.

[11] Luca J, Mrawira D. New measurement of thermal properties of superpave asphalt concrete. J Mater Civil Eng 2005; 17:72-9.

[12] Drysdale, D., “An introduction to fire dynamics”; 2nd ed.; J. Wiley, Chichester, 1999.

[13] Delichatsios MA, Piloted ignition times, critical heat fluxes and mass loss rates at reduced oxygen atmospheres. Fire Safety J 2005; 40:197–212.

[14] Spearpoint MJ, Quintiere JG, Predicting the piloted ignition of wood in the cone calorimeter using an integral model - effect of species, grain orientation and heat flux. Fire Safety J 2001; 36:391–415.

[15] Babrauskas V, Peacock RD. Heat Release Rate: The Single Most Important Variable in Fire Hazard. Fire Safety J 1992;18:255-72.

[16] Tewarson A. Heat release rate in diffusion flames. Thermochim Acta 1996; 278:19-37.

[17] Schartel B, Hull TR. Development of fire-retarded materials. Interpretation of cone calorimeter data. Fire Mater 2007; 31:327-54.

[18] Schartel B, Bahr H, Braun U, Recknagel C. Fire risks of burning asphalt. Fire Mater. 2010; 34:333–340.

[19] Schartel B, Bartholmai M, Knoll U. Some comments on the main fire retardancy mechanisms in polymer nanocomposites. Polym Adv Tech 2006; 17:772-7.

[20] Gilman JW. Flammability and thermal stability studies of polymer layered-silicate (clay) nanocomposites. Appl Clay Sci 1999;15:31-49.

[21] Davis RD, Gilman JW, Sutto TE, Callahan JH, Trulove PC, De Long HC. Improved thermal stability of organically modified layered silicates. Clay Clay Minerals 2004;52(2):171-9.

[22] Leszczynska A, Njuguna J, Pielichowski K, Banerjee JR. Polymer/montmorillonite nanocomposites with improved thermal properties Part I. Factors influencing thermal stability and mechanisms of thermal stability improvement. Thermochim Acta 2007; 453:75-96.

[23] Kiliaris P, Papaspyrides CD. Polymer/layered silicate (clay) nanocomposites: An overview of flame retardancy. Progr Polym Sci 2010; 35:902–58.

[24] Bartholmai M, Schartel B. Layered silicate polymer nanocomposites: new approach or illusion for fire retardancy? Investigation of the potentials and the tasks using a model system. Polym Advanc Tech 2004;15:355-64.

[25] Zanetti M, Camino G, Thomann R, Mulhaupt R. Synthesis and thermal behaviour of layered silicate – EVA nanocomposites. Polymer 2001; 42:4501-7.

[26] Barral M, Garmendia P, Muñoz ME, Palmillas Z, Romera R, Santamaria A, Villanueva S. Novel bituminous mastics for pavements with improved fire performance. Constr Build Mater 2012; 30: 650-6.

6 FDS numerical simulation

6.1 Cone calorimeter numerical simulation

Fire burning behaviour of the conventional dense graded mixture in the cone calorimeter configuration was modelled by means of the NIST Fire Dynamics Simulator (FDS) v. 5.5, open-source software developed by the NIST (National Institute of Standards and Technology). The formulation of the equations along with the numerical algorithm used by the software can be extensively found in the FDS User's Guide and Technical Reference Guide [1,2].

FDS simulates thermally driven flows with relatively low speed compared to the speed of sound, i.e. low Mach number.

In turbulent flows, there are wide ranges of length and time scales involved in the dynamics of the flow. For the turbulence calculations in the gas phase the user can apply either the Direct Numerical Simulation (DNS) or the Large Eddy Simulation (LES) model within FDS. For DNS, all fluctuations within the flow are solved directly, which can be extremely time-consuming. In this study LES approach was chosen, thus approximating the sub-scale turbulence and directly calculates the swirls and fluctuations that have relatively large length scales compared to those used in DNS.

Combined with the turbulence model, FDS uses the mixture fraction approach to model combustion. The mixture fraction approach assumes that the combustion reaction depends on the mixing of fuel and oxygen. This assumption may not hold for cases where combustion does not take place, even with the proper mixing. One example is ventilation-limited conditions. FDS implements an empirical model for flame extinction to account for this phenomenon. The volume fraction of the oxygen and temperature of the volume near the fire is evaluated within the model to determine whether or not the flame is supported.

Simulations of cone calorimeter test were performed by both setting the heat release rate measured in the cone calorimeter tests, and by predicting the heat release rate by modelling the asphalt pyrolysis process. The FDS capacity for predicting fire growth in such a simple configuration was then assessed, as a first step to enable accurate and more realistic simulations of potential involvements of asphalt pavements in tunnel fire scenarios.

The FDS model for the cone calorimeter was developed by reproducing all the geometrical characteristics as close as possible to those of the real cone specified in ISO 5660-1.

The computational domain was 0.5 m long by 0.5 m wide by 0.5 m high. The bottom side was specified to be an open vent, i.e open to ambient, while the top side had a central 0.2 m long by 0.2 m wide exhaust surface with a specified volume flux (0.024 m^3s^{-1}). A numerical grid size of 40 by 40 by 40 cells was adopted, after performing grid sensitivity analysis. This choice was based on the criterion used by Hietaniemi et al. [3], in order to have a grid size proportional to the characteristic fire diameter D*, which is in turn function of the maximum HRR expected (considering the experimental results, a maximum HRR of 1 kW was considered).

The dimensions of the sample were specified according to the real size in cone calorimeter tests (0.1 m long by 0.1 m wide by 0.05 m high). Being the tested samples cylindrical (100 mm diameter), the comparison between experimental and numerical data was based on the heat release rate per unit area. The size and shape of the cone heater were set according to the conical heater in the cone calorimeter. The inner surface was a heater surface with a net heat flux specified according to the required incident heat flux level on the exposed surface of the sample. This value was calibrated by means of three heat flux gauge devices placed on the top surface of the sample at a distance of 0.025 m below the bottom surface of the cone heater. The environmental parameters were determined according to the actual test conditions (22°C, 53% relative humidity and ambient pressure of 99726 Pa). The simulation time was 2500 s for each simulation. Figure 6.1 shows a representative overview of the FDS cone calorimeter model.

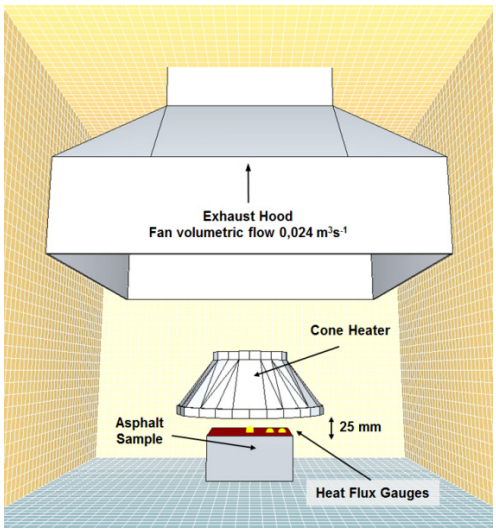

Figure 6.1 FDS cone calorimeter model.

The main purpose of the simulation was to check the reliability of the theoretically derived material properties and the consequent capacity of FDS to provide reasonable prediction of the experimental test results. Only dense graded mixture (D-BC) was considered in this analysis, with the aim of extending the fire simulation in subsequent work with further experimental investigation on the other mixtures. It is worth reminding that the properties derived cannot be considered as intrinsic to the material, but the result of the combined effect of material characteristics, environmental conditions, and combustion model of the test. Therefore, special caution should be used in using them in computations referred to different scenarios. Furthermore, the FDS simulation only focused on the pyrolysis process, i.e. on the solid phase processes leading to the production of the gas phase fuel, while the gas phase reaction was described using the default mixture fraction model.

FDS provides two main methods for modelling the burning behaviour of solids and liquids and the approach to choose depends mainly on the availability of material properties. In one case, the burning rate is prescribed, by means of the HRR curve per unit area, along with the ignition temperature T_{ig}. Thus, the surface burns like a burner at a specified mass loss rate, once the ignition temperature has been reached. Obviously, the bulk thermal properties must be specified in order to achieve the actual time to ignition t_{ig}. In the other approach, the burning rate of the fuel is predicted by the code according to the net heat feedback to the surface from the fire. In this case, not only the thermal properties, but also the kinetic properties governing the pyrolysis must be defined.

In this study, the simulation was initially performed according to the first approach, i.e. HRR-prescribed method, in order to first check the suitability of the geometric model. Furthermore, the reliability of the thermal properties derived from the analysis of the experimental results was assessed.

Asphalt sample was modelled as an obstruction with layered surfaces 0.05 m thick; physical and thermal properties were identified accordingly to the equivalent properties previously outlined. In fact, density was 2275 kgm^{-3}, the specific heat was 0.880 $kJkg^{-1}K^{-1}$, thermal conductivity was 0.563 $Wm^{-1}K^{-1}$, and emissivity was assumed equal to 0.91. The ignition temperature T_{ig} was set equal to 420 °C while the HRR was described referring to the experimental HRR found for one test sample.

FDS simulation was initially performed considering 70 kWm^{-2} external radiant heat flux. As expected from the HRR-imposed method, FDS was able to reproduce the identical shape of the experimental HRR curve. Nevertheless, the thermal properties derived from the theoretical analysis led to a slightly early ignition (approximately 10 s in advance), as can be clearly seen in Figure 6.2.

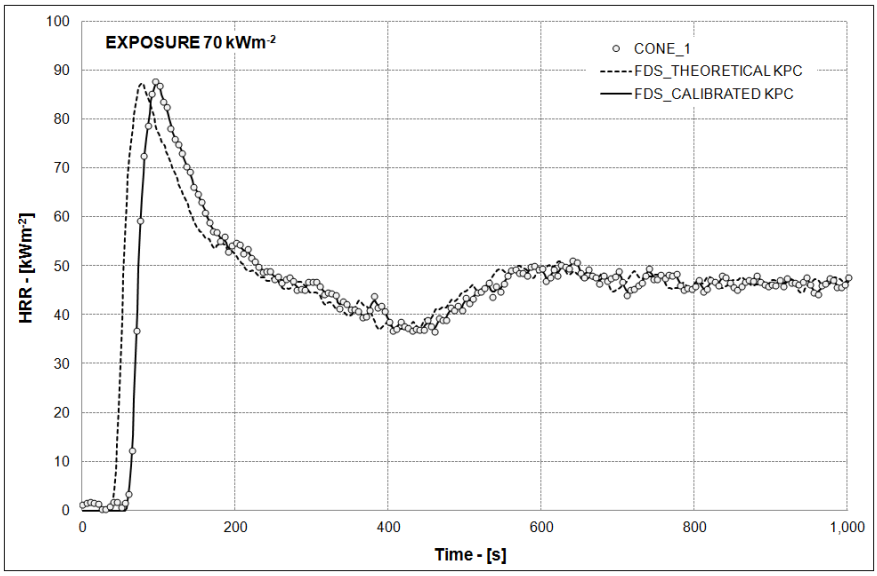

Figure 6.2 Experimental data compared with FDS predictions at 70 kWm^{-2}.

Repeating the FDS simulations at 50 and 35 kWm^{-2} heat fluxes of exposure, the gap between the predicted and the experimental t_{ig} values progressively increases with lowering irradiance levels, thus outlining the necessity to calibrate these values for a better prediction of the time to ignition.

It is worth reminding that ignition is mainly governed by thermal inertia and ignition temperature, but the latter was found approximately constant and independent of the heat flux [4,5], as also supported by the measurements of T_{ig} directly above the top surface of the sample.

Thus, only the thermal inertia was tuned, operating under a parameter estimation approach by minimising the squared errors of the prediction with respect to the experimentally measured values for t_{ig}. It is also worth noting that only the thermal inertia, as a product of three independent factors could be estimated, whereas the evaluation of the single parameters contributing to the product, i.e. the thermal conductivity, specific heat capacity and density, could not be possible. More specifically, the density of material was assumed constant and independent of the heat flux while the thermal conductivity and specific heat capacity were estimated. The calibration of thermal inertia was repeated for all the irradiance levels considered in the experimental tests.

a)

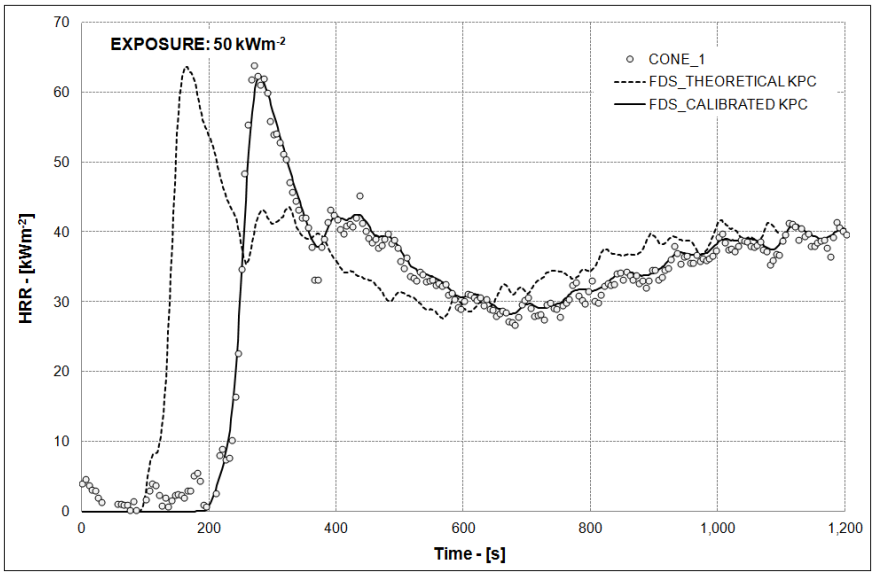

b)

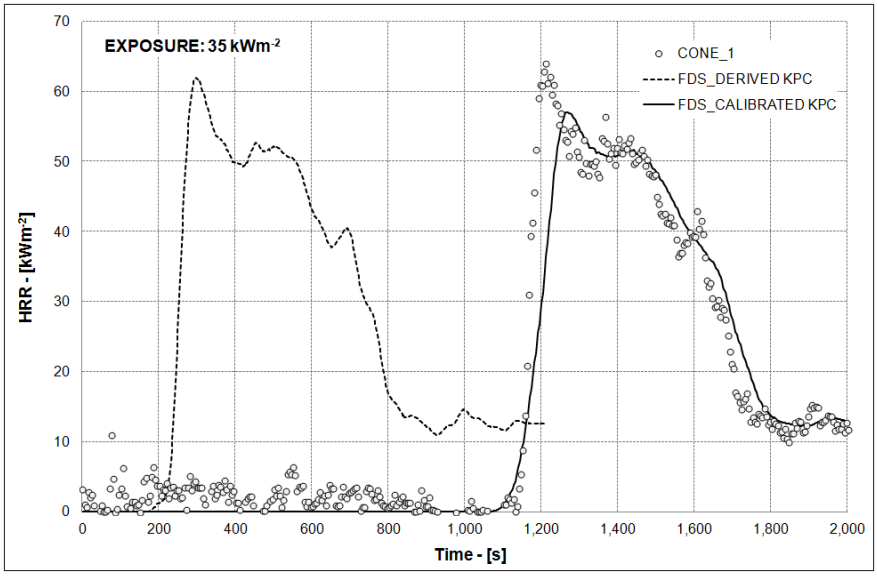

Figure 6.3 Experimental data compared with FDS predictions at 50 kWm^{-2} (a) and 35 kWm^{-2} (b).

The experimentally measured HRR data along with the results of the numerical simulation performed with the theoretical thermal inertia and the numerical prediction after tuning are shown in Figure 6.2 and Figure 6.3, while

the calibrated thermal inertia is plotted as a function of the exposure heat flux in Figure 6.4.

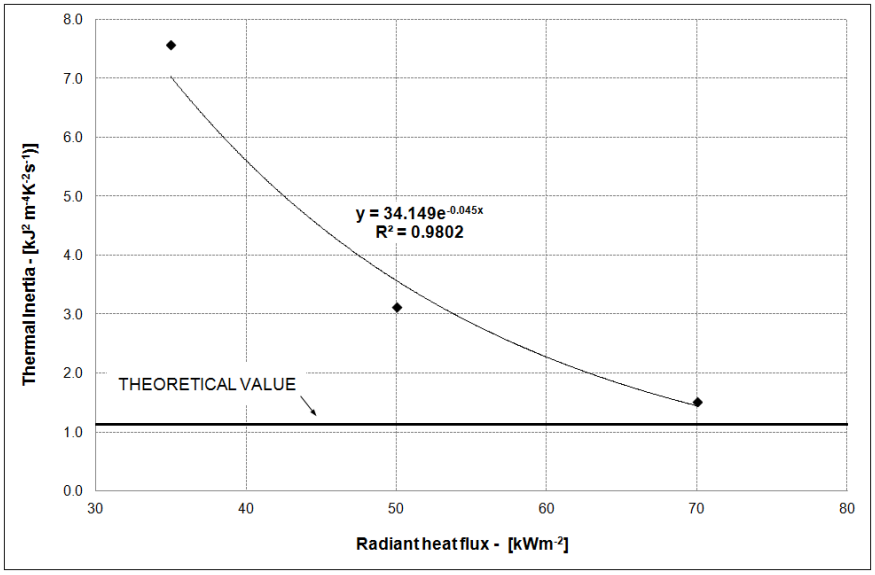

Figure 6.4 Calibrated thermal inertia at different irradiance levels.

Calibrated thermal inertia resulted strongly influenced by the irradiance level and showed the most significant gap from the theoretical value at lower heat fluxes. This fact is ascribable to the fundamental basis of the equation used to deduce the theoretical value, i.e. the semi-infinite solid hypothesis, which entails the heat wave perturbation has not yet reached the bottom of the sample at the time to ignition t_{ig}.

As already outlined in Table 5.1, with lowering heat fluxes the heated layer at ignition increased and finally exceeded the actual thickness of the sample at 35 kWm^{-2}, thus making inapplicable the above-mentioned hypothesis.

Actually, no single constant value of thermal inertia could be outlined to satisfactorily predict the ignition at different heat flux levels. Along with the aforementioned limitations outlined for testing apparatus-related properties, this fact must be taken into account if the objective of the simulation concerns the prediction of more complex fire scenarios, such as those characterizing vehicle fires in tunnels where the heat fluxes are significantly different depending on the distance from the fire source.

Finally, the second approach aimed at modelling the solid phase reactions that govern the pyrolysis of the solid fuel was applied. In FDS model, each material component can undergo different competing reactions, and each of these reactions may lead to some other solid component (residue), along with gaseous volatiles (fuel and water vapour) according to the yield coefficients specified by the user. The reaction rates are function of the local mass

concentration and temperature, and they are generally evaluated as a combination of Arrhenius and power functions. A thorough description of the hypothesis and equations used by FDS to describe such phenomena can be found in [1].

Combustion behaviour resembling that of charring solid emerged from the preliminary experimental phase. For this reason, the pyrolysis model of asphalt was initially outlined following a lumped-parameter kinetic model defined for simulating wood pyrolysis, which has been deeply investigated in previous works [6, 7].

The asphalt surface was defined as a layered surface composed of 15 vol% of combustible material (representing asphalt mastic, composed of asphalt bitumen and mineral filler), and 85 vol% of inert material (representing mineral aggregates). The thermal properties of the materials were established in order to implicitly take into account the presence of air voids in the mixture. In fact, density, thermal conductivity and specific heat were the same as previously found, when the mixture was modelled as a unique material. The corresponding thermal inertia changed with the exposure heat flux, as already described.

Asphalt mixture pyrolysis was then ascribed only to the thermal degradation undergone by the combustible material, with no contribution from the inert component. The thermal degradation of combustible material was reproduced by means of a two-stage reaction. First, the combustible material was totally transformed into active solid representing lower molecular weight products due to depolymerization processes in asphalt binder chemical components. Then, this active solid was in turn converted into char and fuel gases, as described in Figure 6.5.

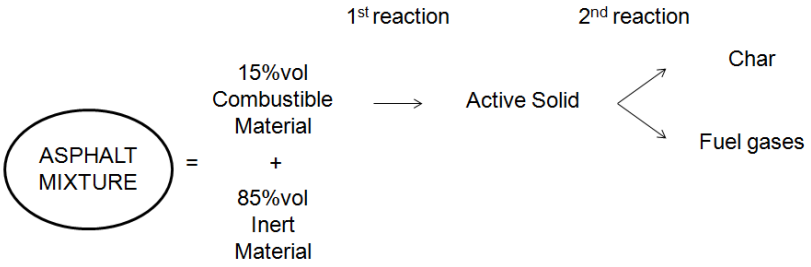

Figure 6.5 Schematic of asphalt mixture decomposition.

All reactions are endothermic and their rates are represented as first order in the mass of pyrolyzable material and with an Arrhenius type of temperature dependence (see § 2.2.1.1).

The heat of combustion of the flammable volatiles was set equal to 35 MJ kg^{-1} (see Table 5.2). Concerning the first reaction involving the transformation of the whole combustible portion into the active solid, the activation energy E and the pre-exponential factor A were tuned in order to reach the experimentally measured time to ignition.

Focusing on the reaction of the active solid into char and fuel, the activation energy E and the pre-exponential factor A characterizing the Arrhenius equation were set equal to 75 $kJmol^{-1}$ and $8 \cdot 10^{9}$ s^{-1} respectively, according to previous studies regarding the combustion kinetics parameters of asphalt binders [8].

This choice entailed a substantial simplification of the pyrolysis model of asphalt for two reasons. First, the reaction of binder was concentrated into only one stage, while previous TGA studies outlined three different stages of reaction during the thermal degradation of asphalt binder in air atmosphere. Second, the kinetic parameters are derived from pyrolysis reaction pathways, which are sensitive to the heating rate. The rates characterizing thermogravimetric analyses are an order of magnitude slower than the rates typical of fires, thus the constants should be obtained using multiple heating rates. No threshold temperature was specified in the FDS model. The calibration of the pyrolysis model was initially performed considering the 70 kWm^{-2} irradiance level.

The fuel vapour and the residue yields of the second reaction, along with the thickness of the layered surface were then estimated in order to minimise the squared errors of the prediction with respect to the experimentally measured values for the HRR curve. Figure 6.6 shows the HRR and the surface temperature obtained by the numerical prediction of the 70 kWm^{-2} exposure test.

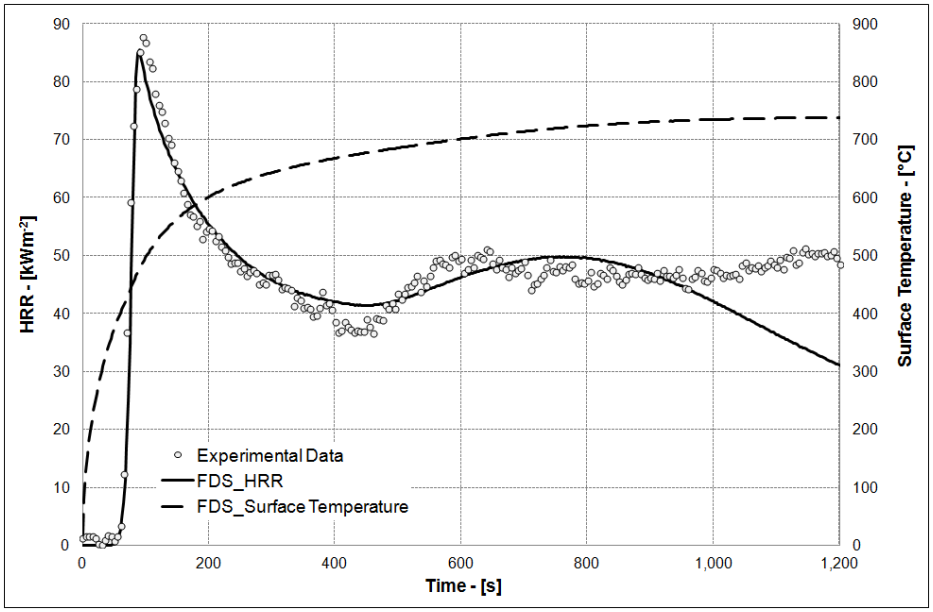

Figure 6.6 Experimental data compared with FDS prediction at 70 kWm^{-2} exposure heat flux. Pyrolysis model.

The FDS simulation successfully predicted the ignition and the HRR curve typical of char forming material, with the peak followed by an appreciable decrease of the burning rate. As can be observed by the surface temperature

curve, ignition occurred at approximately 400°C, accordingly with the experimentally measured values. Furthermore, the maximum and average burning rates were found respectively equal to 2.62 and 1.15 $gm^{-2}s^{-1}$, quite similar to the values experimentally assessed. The second peak in HRR was strictly dependent on the thickness of the layered surface, as highlighted in previous studies [9], where the "heat feedback" effect, due to the heat wave approaching the back end of the sample holder, was deeply discussed. In this case, no insulation was placed under the sample, and the boundary condition set in the FDS was the air gap condition.

In order to reproduce the second peak of the HRR in FDS prediction, the thickness of the surface layer was estimated equal to 2.5 cm, whereas a fuel yield of 23% was required for the prediction of the experimental first peak in HRR curve. With this parameter estimation, the FDS predicted curve overlaps the experimental values for 900 s, then the HRR significantly decreases due to the fuel lack.

The same set of parameters was then considered at 50 kWm^{-2} irradiance level. Time to ignition was again well predicted whereas the time to PHRR resulted postponed of 60 s and the peak value was underestimated by 10%. This result could be still considered acceptable, being included within the variability of the experimental results. Nevertheless, the 2.5 cm thickness layer led to significantly higher second peak and an overall overestimation of the total heat release. Better results could be achieved by increasing the fuel release to 25% and the layer thickness to 3.3 cm, as Figure 6.7 shows. The burning rate and the temperature of ignition still resulted quite similar to the measured values. Indeed, the average burning rate was found equal to 1.11 $gm^{-2}s^{-1}$ while the ignition temperature 394 °C.

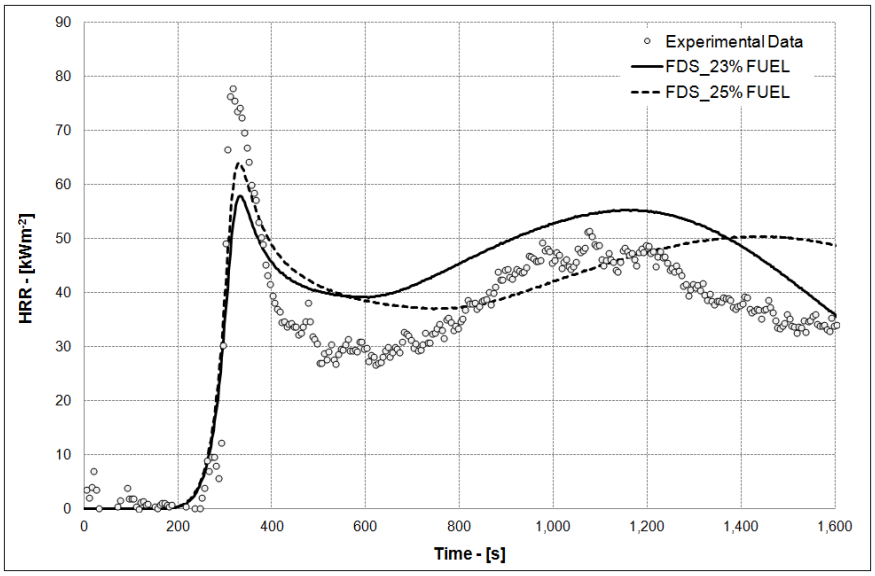

Figure 6.7 Experimental data compared with FDS prediction at 50 kWm^{-2} exposure heat flux. Pyrolysis model.

Finally, the simulation was performed considering 35 kWm^{-2} irradiance level. In this case, the parameters derived by the 70 kWm^{-2} configuration led to significantly earlier ignition. Moreover, the HRR curve was substantially different from the experimental one, which in turn differed from the HRR curves found at higher exposure levels. This fact could be ascribed to the different reaction mechanisms occurring at lower temperatures, as actually verified in case of wood [53]. Consequently, in addition to the parameters estimation related to the second reaction, the calibration of the activation energy and the exponential factor of the first reaction was also necessary in order to postpone the ignition and to best fit the HRR curve. The post calibration results are shown in Figure 6.8 where the HRR and the surface temperature curves are plotted.

This outcome was achieved by setting the fuel yield to 23% (as in the 70 kWm^{-2} irradiance level) and decreasing the layer thickness to 1.8 cm in order to reduce the duration of the flaming combustion. The average burning rate was found equal to 0.68 $gm^{-2}s^{-1}$, comparable with the experimental average burning rate reported in Table 5.2. However, the FDS predicted curve still slightly overestimated the total heat release, thus outlining actually different mechanisms governing the pyrolysis at lower heat fluxes.

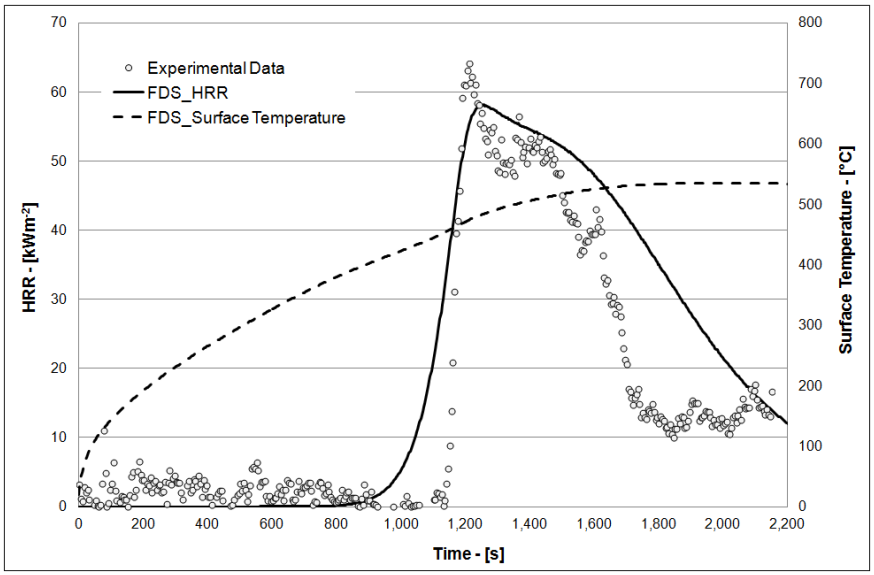

Figure 6.8 Experimental data compared with FDS prediction at 35 kWm^{-2} exposure heat flux. Pyrolysis model.

6.2 Tunnel fire simulation

Once the fire behavior of dense grade asphalt concrete had been assessed, the simulation of a tunnel fire was performed in order to verify the chance of igniting the asphalt pavement. It is evident that a great number of variables (for example: tunnel geometry and ventilation, number of vehicles involved in fire) can lead to completely different fire scenarios. Therefore, the results obtained in this final step should be considered only a partial description of the actual fire behavior of asphalt pavement in case of fire. Nevertheless, this can be considered as a first step in the tunnel fire risks analysis.

With the aim to validate the numerical predictions of the FDS model, the FDS simulation reproduced the Memorial tunnel in Boston, Massachusetts (USA). Memorial is a two-lane decommissioned tunnel 853 m long with 3.2% slope from south to north portal and a cross section of 60.4 m^2 (configuration without the ceiling). Figure 6.9 shows the cross section and the test instrumentation location.

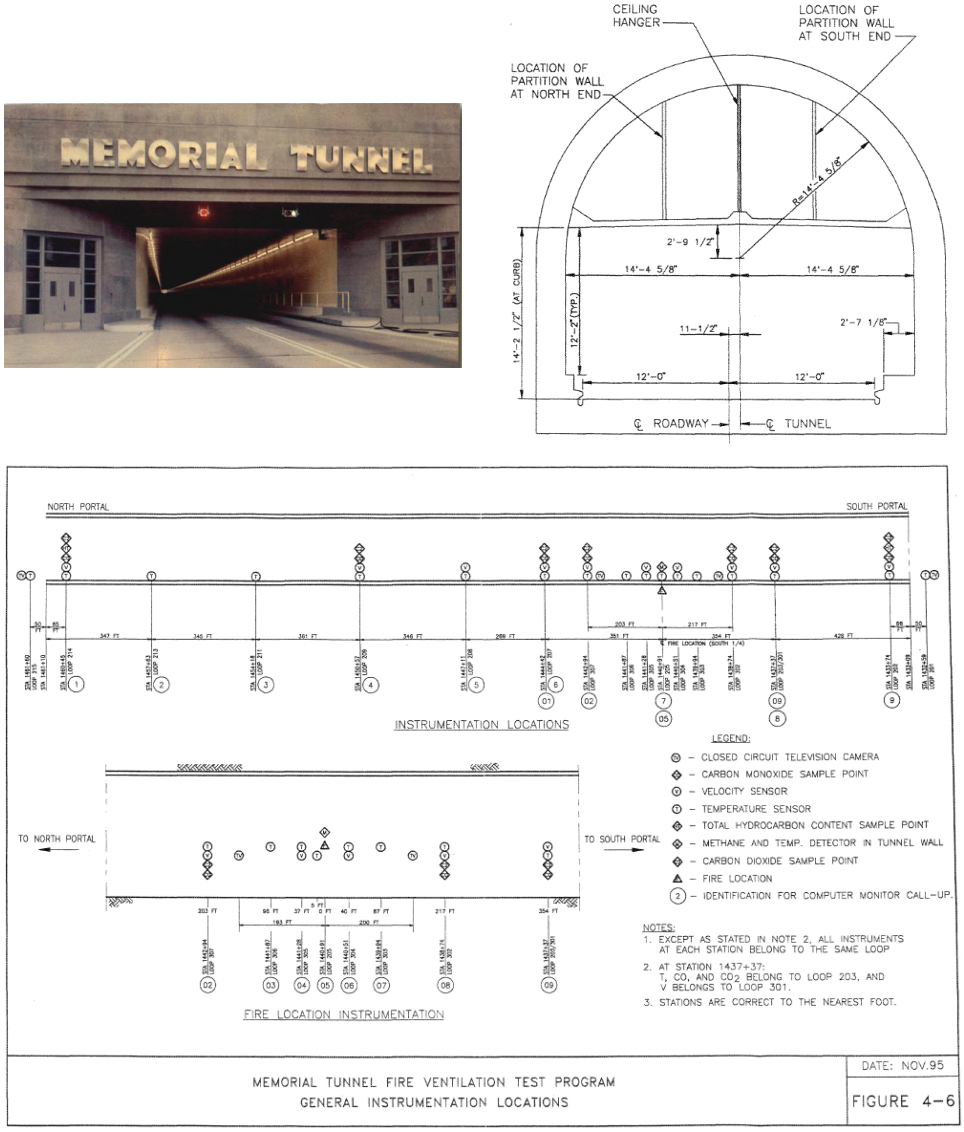

Figure 6.9 Schematic of the Memorial Tunnel Fire Ventilation Test Program (MTFVTP) – Cross Section and Instrumentation location.

From September 1993 through March 1995, 98 fire ventilation tests were undertaken in the Memorial Tunnel Fire Ventilation Test Program (MTFVTP) to provide full-scale fire test results. Tests were conducted with fire sizes of 10, 20, 50, and 100 MW in combination with a number of different ventilation configurations (full transverse ventilation, partial transverse ventilation, point

supply and point exhaust, natural ventilation, and longitudinal ventilation with jet fans). 1400 measurement locations in 12 cross section along the tunnel allows to gain measurements of air temperature, air velocity, CO and CO_2 concentrations collected in MTFVTP Report [10] which constitutes the most comprehensive database in road tunnel fires up to date.

In this study, Test n. 501 was reproduced, i.e.: 20 MW fire size, natural ventilation without ceiling. This fire size is comparable with those developed by 1 van, or 1 bus or 1 HGV with no hazardous goods transported [11]. The fuel used for the tests was No. 2 fuel oil poured on top of water in large pans. The fuel surface was about 0.6 m off the floor of the tunnel. The burning rate of fuel was not monitored during the tests. Instead, the pan size was chosen so that the burning rate would be approximately what was desired, based on previously measured burning rates of the fuel.

The entire length of tunnel was modeled in FDS and a longitudinal symmetry boundary condition was defined to reduce the computational effort.

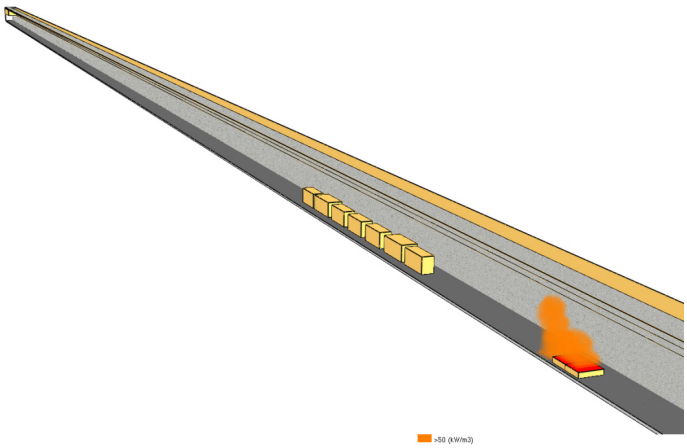

Figure 6.10 FDS model of Memorial tunnel.

In this model material properties were defined accordingly to the previous test results. More specifically, asphalt pavement was modeled as a burner surface with an asphalt superficial layer 5 cm thick. The thermo-physical properties of asphalt were defined according to the parameters found from cone calorimeter test performed at 70 kW/m^2 exposure (see §6.119). The HRR-prescribed method was chosen and the ignition temperature was set equal to 420 °C. Tunnel walls and ceiling were made of 50 cm thick concrete layer.

The burning surface was characterized by a t^2 curve, with a ramp-up time set to 20 s. The dimensions of the burning surface and the HRRPUA (Heat Release Rate Per Unit Area) were set in order to reach the 20 MW fire size, as shown in Figure 6.11.

The slope of the tunnel is not directly defined in the model but included in the body forces by means of the gravity direction (i.e. gravity acceleration

components g_z and g_y were defined, being y the longitudinal axis of the tunnel). The density of the outside air was used as a reference to estimate the change in the atmospheric pressure due to the altitude of the portals.

The time step imposed in the unsteady calculations was 1 s, though smaller values tested resulted in identical predictions. The time period simulated extended to 900 s. The numerical simulation was conducted with a numerical grid whose cells are on the order of 50 cm for covering a 100 m long section of the tunnel surrounding the fire pan, while approaching the south and north portal the cell size gradually increased to 1 m.

In order to simulate the presence of vehicles in tunnel, inert obstacles were also placed with the aim to reproduce the dimensions of passenger cars and vans used in the Memorial tunnel test.

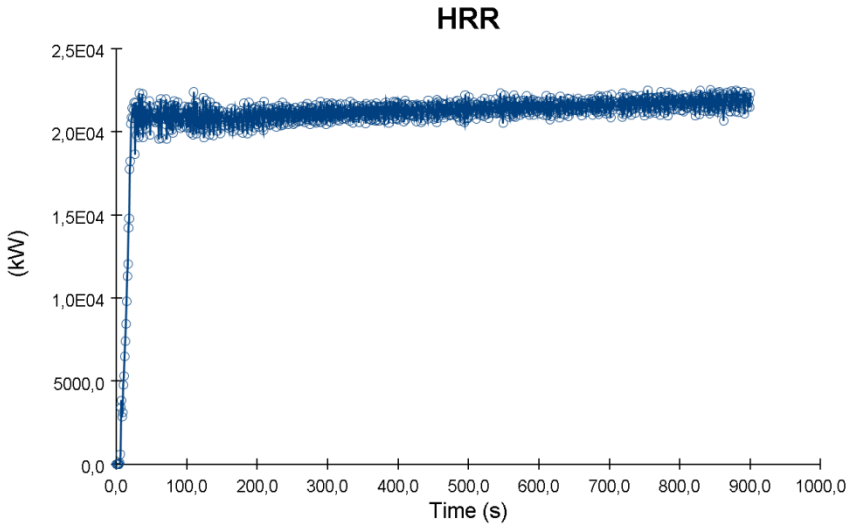

Figure 6.11 Fire size in FDS model.

The temperature recorded near the ceiling of the tunnel directly over the fire during the 20 MW test reached approximately 300°C. The peak temperature reached in the FDS simulation agreed within 50 °C, as can be observed in the subsequent Figure 6.12.

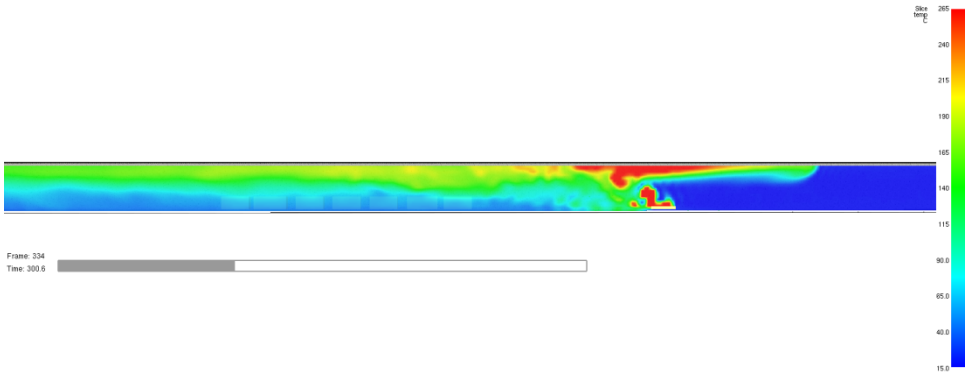

Figure 6.12 FDS simulation. 20 MW fire size – Temperature reached at t = 300 s.

Another important parameter to take into account for the safety of tunnel occupants is how fast the air temperature grows near the fire source. Figure 6.14 provides a description of the development of the high-temperature zone marked by isotherm surface T= 60 °C in the first five minutes of the simulation. After only 180 s, the isotherm surface at 60 °C reached the vehicle silhouettes, thus outlining a serious hazard for the escape of the tunnel occupants.

It is worth noting that tunnel slope (3.2% upgrade, from the right-hand side to the left-hand side) makes the smoke and heat moving to the left (uphill), thus pointing out the buoyancy-driven airflows.

Finally, the numerical simulation highlighted that the tunnel north of the fire filled with smoke for the entire height of the cross section, resulting in zero visibility within five minutes, as described by Figure 6.13.

Figure 6.13 FDS simulation. 20 MW fire size – Smoke spread at t = 300 s.

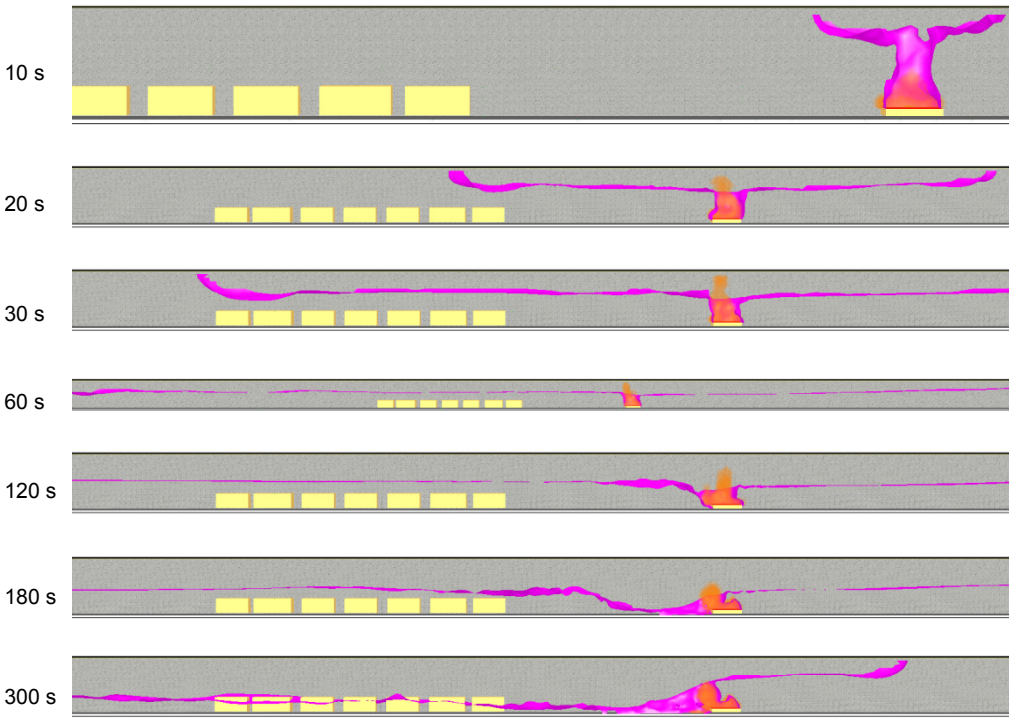

Figure 6.14 FDS simulation. 20 MW fire size – Isotherm T= 60°C.

Focusing on the fire behavior of asphalt pavement, the temperature was monitored by specific devices (thermocouples) positioned at the centerline of the tunnel (being (x;y) = (0;0) the fire source, temperature is monitored at y = +2.5 m, +5.0 m and +7.5 m) and to the side of the fire source (x = +3.0 m and +4.0 m from the centerline). Figure 6.15 shows the obtained results.

The most important outcome is the limited involvement of asphalt pavement in the overall fire. Indeed, only the upstream pavement actually reached the ignition temperature, while on the opposite side the temperature remained under the critical limit. Moreover a very limited portion of asphalt is involved, as the thermocouple positioned at + 5.0 m reached the ignition temperature almost at the end of the numerical simulation. The same result is achieved in the cross direction, being the main air stream parallel to the centerline of tunnel. So, in this specific geometry/ventilation configuration, asphalt pavement could actually ignite in case of 20 MW fire but the spread of fire was very limited, together with very scarce contribution to the overall heat release rate. Indeed, assuming that an area of 2.5x7 m^2 ignites, the maximum heat released by the asphalt material is approximately 1575 kW (with the hypothesis of an HRR per unit area of 90 kWm^{-2}) which is roughly only the 7.5% of the overall fire size.

Since a few European countries banned the use of asphalt pavement in highway tunnels in favor of cement concrete pavement due to its inorganic

nature, a simplified analysis of the thermal response of such material was also performed.

The FDS simulation of the 20 MW fire size was repeated with a pavement surface composed of conventional cement concrete pavement. The compressive strength was assumed equal to 35 MPa while the temperature-dependent thermal properties (thermal conductivity, density, specific heat, and Young modulus) were set according to Eurocode 2 [12], considering calcareous aggregates. The obtained temperature curves are displayed in Figure 6.16.

The time-temperature curve obtained at y = 2.5 m was then used as an input datum for the subsequent numerical simulation performed by means of Comsol Multiphysics ® v. 4.3 software. In this final phase a simple unsteady 1-D heat transfer problem was solved, with the aim to outline the temperature profile inside a 35 cm thick cement concrete slab, characterized by the same physical and thermal properties used in the FDS simulation. The initial temperature was set equal to 15°C while the boundary condition at the top surface was defined accordingly to the time-temperature curve obtained from the FDS simulation.

a)

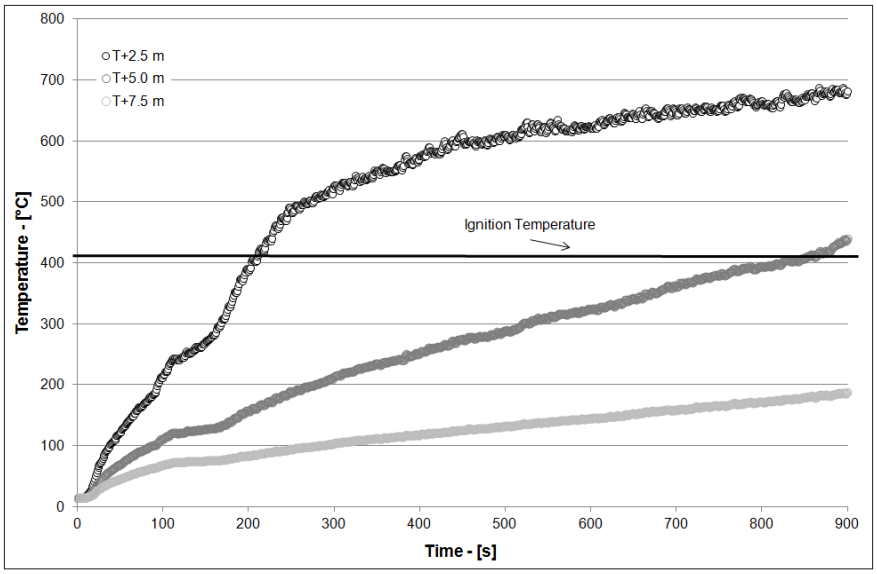

b)

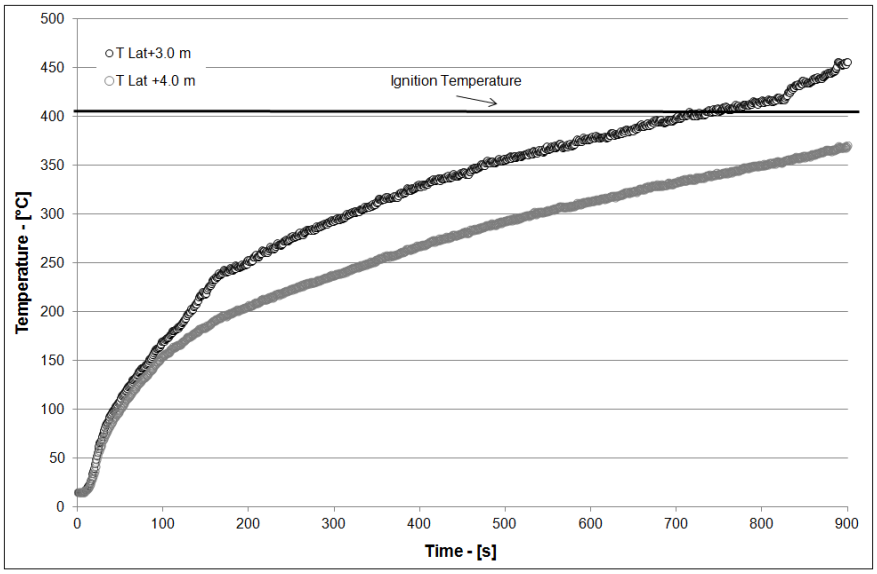

Figure 6.15 FDS simulation. 20 MW fire size – Temperature in asphalt pavement: a) Longitudinal section; b) Cross section.

a)

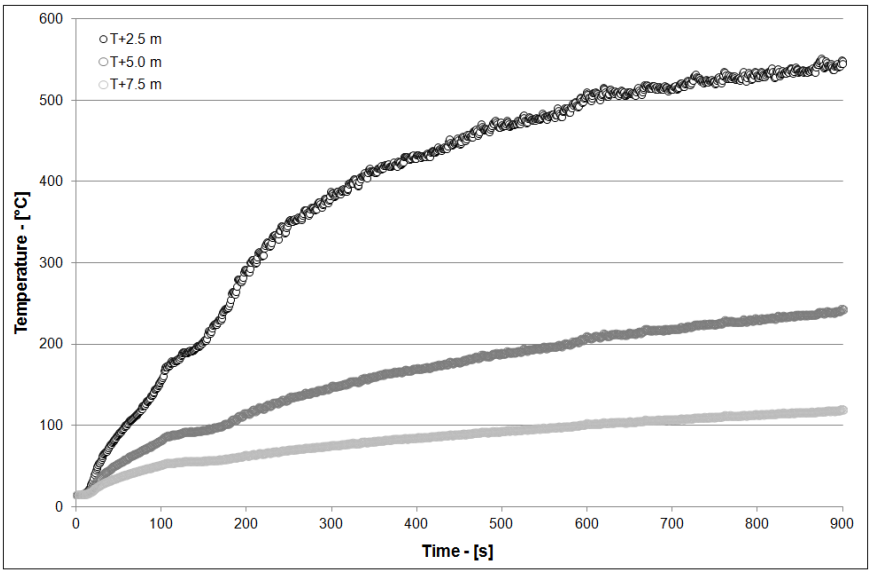

b)

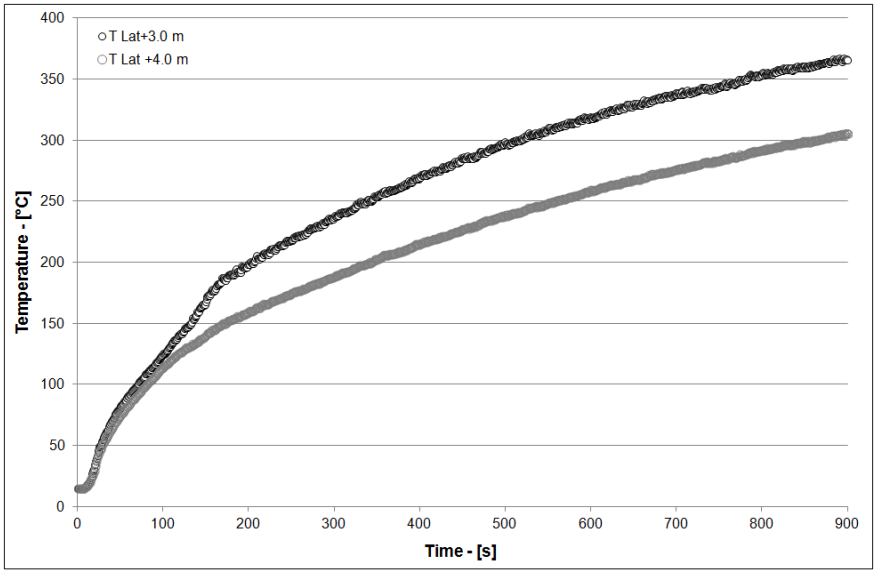

Figure 6.16 FDS simulation. 20 MW fire size – Temperature in cement concrete pavement: a) Longitudinal section; b) Cross section.

Heat transfer coupled with thermal stress analysis allows the evaluation of the eigenstresses due to the thermal gradients arisen in the concrete pavement. Of course, this is only a rough approximation of the complex phenomena occurring in such extreme conditions [13, 14], being those elements outside the

scope of the thesis. Nevertheless, this preliminary analysis can be useful to highlight possible criticality for the cement concrete technical solution. Figure 6.17 describes the temperature profiles obtained across the concrete slab for different periods of exposure. After only six minutes of exposure, the thermal wave involved 6 cm thick slab.

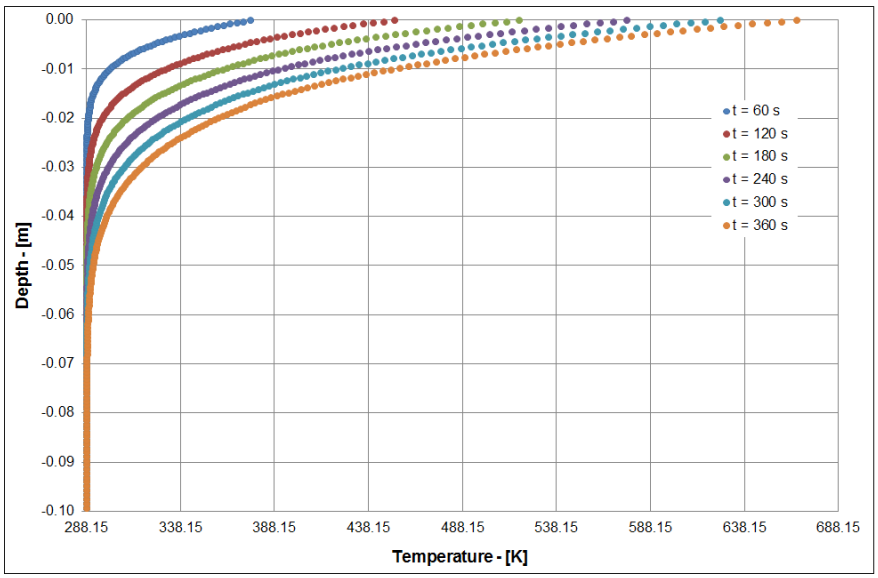

Figure 6.17 Time – temperature curves inside the concrete slab – Y=+2.5 m.

Figure 6.18 shows the radial stresses achieved after only 3 minutes of exposure. Even if the model is extremely simplified, it is reasonable to assume that ordinary cement concrete pavement is not able to maintain its integrity in case of such extremely high temperatures. Moreover, the high temperature gradients reached a significant depth in a few minutes, thus implying not negligible costs of rehabilitation.

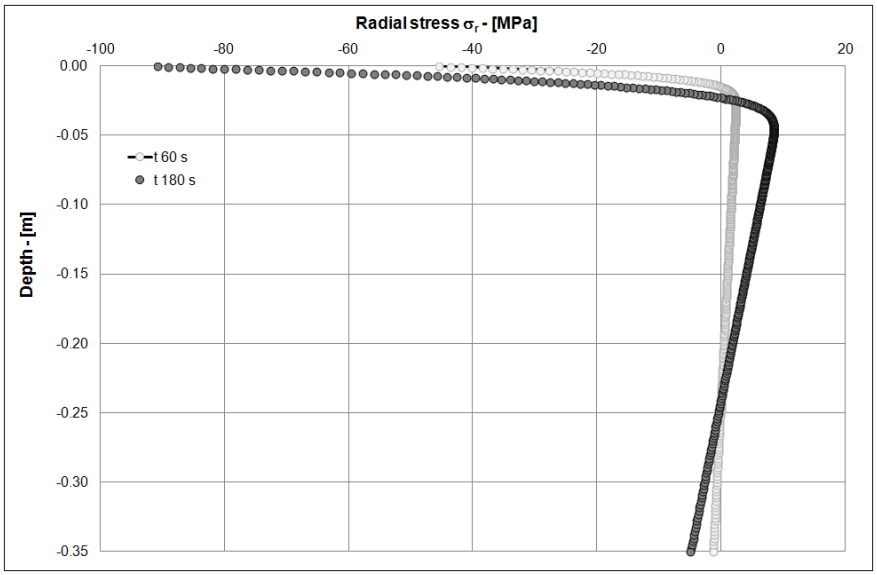

Figure 6.18 Radial stress at t = 60 and 180 s – Y=+2.5 m.

Clearly, the possible fire scenarios can be definitely different both in terms of vehicles involved (fire size) and ventilation configuration. Therefore, this experience should not be considered as an exhaustive description of the fire behavior of asphalt mixture but only a possible approach to investigate such critical aspect for the safety of tunnel occupants and rescue teams.

References

[1] McDermott R, McGrattan K, Hostikka S, Floyd J. Fire Dymanics Simulator (Version 5.5), Technical Reference Guide. NIST Special Publication 1018-5, National Institute of Standards and Technology, Gaithersburg, Maryland, October 2010.

[2] McGrattan K, McDermott R, Hostikka S, Floyd J. Fire Dymanics Simulator (Version 5.5), User's Guide. NIST Special Publication 1019-5, National Institute of Standards and Technology, Gaithersburg, Maryland, October 2010.

[3] Hietaniemi J, Hostikka S, and Vaari J. FDS Simulation of Fire Spread - Comparison of models results with experimental data. (2004) VTT-WORK-4, VTT Building and Transport, Kivimiehentie, Finland.

[4] Thomson HE, Drysdale DD, Beyler CL. An experimental evaluation of critical surface temperature as a criterion for piloted ignition of solid fuels. Fire Safety J 1988; 13(2):185-196.

[5] Thomson HE, Drysdale D. Flammability of plastics, I: Ignition Temperatures. Fire and Materials 1987; 11:163-72.

[6] Di Blasi C. Physico-chemical processes occurring inside a degrading two-dimensional anisotropic porous medium. Int. Journal of Heat Mass Transfer 1998;41:4139-50.

[7] Di Blasi C. Modeling and simulation of combustion processes of charring and non-charring solid fuels. Prog. Energy Combust Sci. 1993; 19:71-104.

[8] Xu T, Huang X. Combustion properties and multistage kinetics models of asphalt binder filled with flame retardant. Combustion Science and Technology 2011; 183(10):1027-38.

[9] Carvel R, Steinhaus T, Rein G, Torero JL. Determination of the flammability properties of polymeric materials: A novel method. Polymer Degradation and Stability 2011; 96:314-9

[10] Massachusetts Highway Department. (1995). Memorial Tunnel Fire Ventilation Test Program. *Test Report*, Boston, MA.

[11] Ingason H, Design fires curves for tunnels, Fire Safety Journal 44(2009) 259-265.

[12] UNI EN 1992-1-2:2005 Eurocode 2 – Design of concrete structures. Part 1-2 : General rules – Structural fire design.

[13] D. Gawin, F. Pesavento, “An Overview of Modeling Cement Based Materials at Elevated Temperatures with Mechanics of Multi-Phase Porous Media”, Fire Technology, 48, 2012, pp. 753–793.

[14] P. Bamonte, P.G. Gambarova, " Thermal and Mechanical Properties at High Temperature of a Very High-Strength Durable Concrete", Journal of materials in civil engineering, ASCE, 22 (6), 2010, pp. 545-555.

7 Conclusions and future research

The main aim of this work of thesis was to characterize the fire behaviour of asphalt mixture in order to evaluate its possible involvement in case of fires in highway tunnels.

Asphalt mixture is a complex material composed of different parts which were singularly analysed, focusing on the asphalt binder, the mineral filler and the mineral aggregates. Thermogravimetric analysis (TGA) and LOI tests were initially performed to investigate asphalt binders and mastics, while cone calorimeter test was used to describe the overall fire behaviour of asphalt mixture.

Focusing on the combustible portion of mixture, i.e. the asphalt binder, TGA performed under air atmosphere showed a typical trend in the TG curve, representing the decreasing mass of the sample with the growing temperature. Indeed, three distinct stages could be clearly outlined, mainly ascribable to the different S.A.R.A. fractions of the investigated binders. In this phase, the asphalt binder characterised by the lowest pen-grade and the lowest content of saturates and aromatics showed the highest thermal stability, especially in the lower range of temperatures.

LOI tests partially confirmed the TGA results, even if scarce differences among the neat asphalt binders were outlined. By adding the organo-modified clay (organo-modified montmorillonite - OMMT) to asphalt binder in order to obtain a sort of nanocomposite binder, the ignitability of binders dramatically worsened. This fact could be related to the thermal decomposition of the organic surfactants or to a postponed decomposition of the lightest fractions which is shifted to higher temperatures. Nevertheless, a significant slowdown of the early thermo-oxidative decomposition was also achieved.

The introduction of different mineral fillers led to important outcomes in terms of ignitability and thermal stability. The addition of conventional limestone filler could not modify the thermal decomposition of asphalt binder because the calcium carbonate simply acted as an inert diluting material due to its too high decomposition temperature (approximately 650°C). Conversely, Flame Retardant (FR) fillers such as aluminum hydroxide (ATH) and magnesium hydroxide (MH) actually retarded the thermal decomposition of asphalt binder, thanks to their endothermic decomposition occurring in a narrow range of temperatures corresponding to the onset of asphalt degradation (around 200°C in case of ATH

filler and 300°C in case of MH). Moreover, the effectiveness of the FR-fillers is enhanced by the lowest specific surface area. Indeed, the best performance in terms of smoke emission and highest LOI was achieved in case of ATH characterized by a median particle size of 0.99 μm.

The analysis of the fire behavior of asphalt mixtures by means of the cone calorimeter was organized in different steps, in order to investigate the roles of the aggregates gradation, the physical properties of aggregates, and the mineral filler.

Focusing on the aggregates gradation, dense-graded mixtures ignite at all the three radiant heat fluxes considered in this work, i.e. 35, 50, and 70 kW/m^2, showing time to ignition increasing with the incident flux. The results collected were then used to identify the critical heat flux by applying the semi-infinite solid assumption. In this way, a critical heat flux equal to 22.5 kW/m^2 was extrapolated and the corresponding temperature of ignition (around 400°C) was derived and successfully compared with the experimentally collected results.

Completely different outcomes were found in case of open-graded mixtures. In fact, the ignition was achieved only when exposed to the highest incident flux, thus showing a significant higher critical heat flux.

In closed environments, such as highway tunnels, dense graded mixtures are generally preferred to the open-graded ones, so the fire behaviour of dense-graded mixtures was deepened. The influence of the physical properties of coarse aggregates was then assessed by testing mixtures composed of light-expanded clay aggregates and electric-arc furnace slags, characterized by significantly different density. The main effect played by the different aggregates was the postponed ignition achieved in case of highest density aggregates. This fact confirmed the role played by the thermal inertia ($k\rho c$) in governing the ignition phase.

Finally, the role of mineral fillers and nano-modified asphalt binders was assessed. In this phase, both FR-fillers (ATH and MH) and organo-modified clay in asphalt binders were used in order to achieve a synergistic effect: FR-fillers governed the ignition phase while nano-modified binders slowed-down the overall combustion process. In case of dense-graded mixtures, an actual delay in ignition was achieved, as well as a reduction in peak of heat release rate; in case of open-graded mixtures, the overall fire behaviour was shifted from a thick-non charring (O-B series) to a thick char forming material (O-NB series).

The final phase of this work of thesis concerned the numerical simulation of the asphalt mixture fire behaviour by means of the NIST Fire Dynamics Simulator (FDS) v. 5.5, open-source software developed by the NIST (National Institute of Standards and Technology). Initially, the fire behaviour of the conventional dense-graded mixture in the cone calorimeter configuration was modelled. Simulations of cone calorimeter test were performed by both setting the heat release rate measured in the cone calorimeter tests, and by predicting the heat release rate by modelling the asphalt pyrolysis process. The collected results were then used for the simulation of a real scale experiment performed during

the Memorial Tunnel Fire Ventilation Test Program. Indeed, a 20 MW fire size in natural ventilation condition was reproduced in order to outline the possible involvement of asphalt pavement. The results of the FDS simulation of this specific fire scenario highlighted a limited involvement of the asphalt pavement which is strictly confined in the proximity of the fire source. Moreover, the heat released by the burning asphalt pavement was found a small percentage of the overall fire size, thus highlighting the limited contribution of asphalt pavement in worsening the safety of the occupants and the rescue team. Conversely, a simplified 1-D heat transfer problem applied to an ordinary cement concrete pavement outlined the possibility of severe damage after only a few minutes of exposure.

The present work showed that asphalt pavement is actually a combustible material which can ignite in case of fire in closed environments such as highway tunnels. The main physical and thermal properties governing the asphalt fire behavior were identified, thus providing specific mix-design criteria for improving the fire safety requirement. Indeed, dense-graded mixtures produced with high-density aggregates (high thermal inertia) and with FR-filler can reduce the ease of ignition of pavement material. Moreover, it has been shown that even if the ignition of conventional asphalt material should take place, the actual contribution to the overall fire size is limited. This fact is due to the relatively high critical heat flux, which is required to ignite the asphalt pavement and to the consequent limited spread of fire over the surface of asphalt pavement.

The analysis of the results collected from the rheological characterization of asphalt mastics highlighted some criticality, especially in viscosity, when fillers of smallest particle size were used. Therefore, a balance between effectiveness in flame retardancy, good mechanical properties and satisfying workability should be addressed in future research.

Furthermore, the present work achieved a deepened description of conventional dense-graded mixture fire behavior and provided some indications of the possible approaches which can be followed for improving the fire safety of asphalt pavements. Further analyses specifically addressed at the definition of the main physical and thermal properties of FR-asphalt pavements could be useful to achieve a thorough description of their fire behavior, especially in terms of critical heat flux and ignition temperature.

Finally, this work of thesis outlined a possible approach to identify the criticality in case of fires in highway tunnels and should not therefore be considered an exhaustive description of the fire safety performance of asphalt. Nevertheless, asphalt mixture should not be excluded a priori for applications in highway tunnels, being the fire behavior governed by different components and the fire scenarios extremely variable. Thus, depending on the risk analysis specific for a single highway tunnel (kind of vehicles, transported goods, tunnel ventilation, water-based fire suppression systems) the mix design of asphalt could be calibrated in order to minimize the risk of its possible involvement in fire.

Ringraziamenti

Al termine di questo percorso vorrei ringraziare chi ha contribuito a rendere possibile il presente lavoro di tesi. Ringrazio pertanto il Prof. Felice Giuliani per avermi dato la possibilità di intraprendere questa esperienza. Ringrazio il Prof. Giovanni Polacco e la Dott.ssa Sara Filippi per la grande disponibilità e il fondamentale supporto nel lavoro sperimentale condotto presso l'Università di Pisa. Ringrazio il team dei Laboratori di comportamento al fuoco dell'Istituto CNR–IVALSA: Dott.ssa Giovanna Bochicchio, Dott.ssa Barbara Tessadri e il Sig. Renato Leveghi per aver messo incondizionatamente a disposizione le loro strutture e il loro tempo. Ringrazio la Prof.ssa Sara Rainieri per avermi dato le basi su cui poggiare l'interpretazione dei risultati sperimentali, mostrando sempre grandissima disponibilità ed entusiasmo nell'accompagnarmi in questo percorso. Ringrazio i tesisti che con il loro lavoro hanno contribuito in modo determinante a concretizzare tutto questo: Emanuele Sciuto e Chiara Iacci. Ringrazio poi i miei compagni di viaggio, sempre al mio fianco e a disposizione per scambiare un parere: Dario Pecchini e Filippo Merusi.

Infine, ringrazio chi mi ha sempre supportato e spronato ad andare avanti: Federico, Sara e la mia famiglia.